A 21178 E

Biological Cybernetics

Volume 22 Number 3 1976

Indexed in Current Contents

Springer-Verlag Berlin Heidelberg New York

Biol. Cybernetics BICYAF 22 (3) 121-180 (1976) 20. 4. 1976

Lecture Notes in Biomathematics

Editorial Board: W. Bossert, H.J. Bremermann,, J.D. Cowan, H. Hirsch, S. Karlin, J.B. Keller, M. Kimura, S. Levin (Managing Editor), R.C. Lewontin, L. A. Segel

This series aims to report new developments in biomathematics research and teaching – quickly, informally and at a high level.
The type of material considered for publication includes:

1. Preliminary drafts of original papers and monographs,
2. Lectures on a new field, or presenting a new angle on a classical field,
3. Seminar work-outs,
4. Reports of meetings, provided they are
   a) of exeptional interest and
   b) devoted to a single topic

With the recent advances in the field of biomathematics, it is appropriate that a series "Lecture Notes in Biomathematics" be developed. Here, new and exciting applications and theories, including the construction and testing of mathematical models simulating complex biological mechanisms and their constructive and predictive views in experimental design can be published.
Publication of Lecture Notes is intended as a service to the international scientific community, in that a commercial publisher, Springer-Verlag, can offer a wider distribution of documents which would otherwise have a restricted readership.

Volume 1: P. WALTMAN
Deterministic Threshold Models in the Theory of Epidemics
15 figures. V, 101 pages. 1974
DM 16,–; US $6.60
ISBN 3-540-06652-7

These notes correspond to a set of lectures given at the University of Alberta during the spring semester, 1973. The first four sections present a systematic development of a deterministic, threshold model for the spread of an infection. Section 5 presents some computational results and attempts to tie the model with other mathematical concepts. In each of the last three sections a separate, specialized topic is presented.

Volume 2:
Mathematical Problems in Biology
Victoria Conference
Editor: P. van den Driessche
VI, 280 pages. 1974
DM 28,–; US $11.50
ISBN 3-540-06847-3

The papers in this proceedings volume deal with a wide variety of mathematical problems in biology, the emphasis of the conference being application of mathematical ideas and techniques to the bioscience. The reader can obtain an overview of current research as well as acquaint himself with some unsolved problems.

Volume 3: D. LUDWIG
Stochastic Population Theories
Notes by M. Levandowsky
VI, 108 pages. 1974
DM 18,–; US $7.40
ISBN 3-540-07010-9

These notes serve as an introduction to stochastic theories which are useful in population biology; they are based on a course given at the Courant Institute, New York, in the Spring of 1974. Only a slight acquaintance with probability theory and differential equations is assumed and the more sophisticated topics, such as the qualitative behaviour of nonlinear models, are approached through a succession of simpler problems. As emphasis is placed upon intuitive interpretations, rather than upon formal proofs, in most cases the reader is referred elsewhere for a rigorous development. Simple, useful models are, however, treated in some detail.

Volume 4:
Physics and Mathematics of the Nervous System
Proceedings of a Summer School, held at Trieste, August 21-31, 1973
Editors: M. Conrad, W. Güttinger, M. Dal Cin
159 figures. XI, 584 pages. 1974
DM 45,–; US $18.50
ISBN 3-540-07014-1

This important volume represents the record and product of a summer school devoted to exploring major theoretical ideas and methodologies applicable to brain function and related problems. Topics covered include fundamental ideas, methods, and applications of dynamical systems, automata, and information theory; molecular basis of nerve impulse and brain function; biophysics of nerve cells and sensory perception; neural networks, cerebellum, and cerebral cortex; artificial intelligence. It is hoped that the coverage, which is unique, will serve a much needed catalytic function in an area which is felt by many workers to be ready for both theoretical and experimental breakthroughs.

Volume 5:
Mathematical Analysis of Decision Problems in Ecology
Proceedings of the NATO Conference Held in Istanbul, Turkey, July 9-13, 1973
Editors: A. Charnes, W.R. Lynn
77 figures, 23 tables. VIII, 421 pages
1975. DM 35,–; US $14.40
ISBN 3-540-07188-1

This volume consists of a collection of edited and up-dated versions of papers presented at the NATO conference "Mathematical Analysis of Decision Problems in Ecology" held in Istanbul, July 9 - 13, 1973. The objective of the conference was to bring together leading researchers from the major sciences involved in ecological problems and to present the current state of progress in research of a mathematical nature which might assist in the solution of these problems.

Volume 6: H.T. BANKS
Modeling and Control in the Biomedical Sciences
22 figures. V, 114 pages. 1975
DM 18,–; US $7.40
ISBN 3-540-07395-7

Optimal control theory has been used fruitfully and extensively in recent years in other areas of application. This volume presents representative material of the recent applications of such techniques in the biomedical sciences. These notes cover modeling and control problems for various phenomena, including surveys and original work. A considerable bibliography is also included.

Volume 7: M.C. MACKEY
Ion Transport Through Biological Membranes
An Integrated Theoretical Approach
IX, 240 pages. 1975
DM 25,–; US $10.30
ISBN 3-540-07532-1

Prices are subject to change without notice

Springer-Verlag
Berlin
Heidelberg
New York

Biological Cybernetics

Communication and Control in Organisms and Automata

Nachrichtenübertragung, Nachrichtenverarbeitung, Steuerung und Regelung in Organismen und in Automaten

Editors

H. B. Barlow, Cambridge/Cambs. · J. D. Cowan, Chicago/Ill.
O. Creutzfeldt, Göttingen · B. Hassenstein, Freiburg i. Br.
W. D. Keidel, Erlangen · K. Küpfmüller, Darmstadt
D. M. MacKay, Keele/Staffs. · H. Mittelstaedt, Seewiesen/Obb.
W. Reichardt, Tübingen (Editor-in-Chief) · W. A. Rosenblith, Cambridge/Mass.
J. F. Schouten, Eindhoven · D. Varjú, Tübingen

Springer-Verlag Berlin Heidelberg New York

Biological Cybernetics

Communication and control in organisms and automata.
Continuation of „Kybernetik" (Volume 1—16)

Biological Cybernetics appears about every month.

Subscription information

Volumes 21—23 (4 issues each) will appear in 1976. The publisher reserves the right to issue additional volumes during the calendar year. Information about obtaining back volumes available upon request.

North America. Subscription rate: $ 187.10, including postage and handling. Subscriptions are entered with prepayment only. Orders should be sent to your bookdealer or subscription agency or directly to: Springer-Verlag New York Inc. 175 Fifth Avenue, New York, N. Y. 10010.

Outside North America. Subscription rate: DM 444,-- plus postage and handling. Orders can either be placed with your bookdealer or sent directly to: Springer-Verlag, Heidelberger Platz 3, D-1000 Berlin 33.

Manuscripts should be addressed to:
Prof. Dr. W. Reichardt
Max-Planck-Institut für biologische Kybernetik
Spemannstraße 38
D-7400 Tübingen, FRG

It is a fundamental condition that submitted manuscripts have not been, and will not simultaneously be submitted or published elsewhere. With the acceptance of a manuscript for publication, the publishers acquire full and exclusive copyright for all languages and countries.

The use of registered names, trademarks, etc. in this publication does not imply, even in the absence of a specific statement, that such names are exempt from the relevant protective laws and regulations and therefore free for general use.

Correspondence concerning advertisements should be sent to the Advertisement Department of the publishing firm in Berlin: Kurfürstendamm 237, D-1 Berlin 15, Tel. (0 30) 8 82 10 31, Telex 01-85 411.

Springer-Verlag

Heidelberger Platz 3
D-1 Berlin 33
Tel. (0 30) 82 20 01
Telex 01-83 319

Postfach 105 280
D-6900 Heidelberg 1
Tel. (0 62 21) 4 87-1
Telex 04-61 690

Springer-Verlag New York Inc.
175 Fifth Avenue
New York, N. Y. 10010
Tel. 2 12 (6 73-26 60)
Telex 00-23 22 235

The concepts of transmission of information, processing of information and automatic control engineering originated within technology and physics. Today, however, these concepts have also proved useful in the biological sciences where analogous processes of communication and control are encountered. Despite the differences between nonliving and living systems, many of the logical procedures, the experimental and theoretical approaches and the mathematical techniques applicable to the physical sciences also find natural applications in the realm of the life sciences. In particular, by adopting this approach to sensory and neurophysiological problems new insight has been gained into the principles by means of which organisms handle and utilize information. Conversely, physicists and engineers have shown increasing interest in natural mechanisms of communication and control, including genetic communication and the control of reproduction.

The aim of "Biological Cybernetics" is to promote the exchange of experimental and theoretical information in the following fields: Quantitative analysis of behaviour, in both vertebrates and invertebrates; quantitative micro- and macro-physiological studies of information-processing in receptors, neural systems and effectors; mathematical models of communication and control processes in organisms, including reproductive mechanisms; biologically relevant aspects of information theory, network theory, theory of automata, theory of control systems.

Contents of the next issue

Instructions to Authors*

Papers must be as short and concise as possible. 2½ double-spaced manuscript pages correspond to about 1 printed page. The papers are put straight into pages after typesetting. Authors are therefore requested to follow the instructions below exactly in preparing their manuscripts; form and content must be carefully checked to avoid any necessity for corrections in proof. Later corrections differing from the manuscript must be charged to the author. Two copies of the final page-proofs with provisional page-numbers and with figures and tables in their final position are sent to the author. Page references can, therefore, be inserted at page-proof stage. The final page references will be inserted by the publishers. The desired positions of figures and tables should be marked in the respective margins of the manuscript.

Manuscripts must be typed on one side of each sheet only, with double spacing and wide margins.

Each manuscript should include a separate sheet of "Instructions for the compositor" explaining markings and special types used.

Each paper should be preceded by a *summary* of the main points. Papers in German or French should also have the title and an exhaustive summary in English.

Words or sentences to be set in *italics* should be marked by wavy underlining. Those sections of the manuscript that may be printed in *smaller* (Petit) *type* are indicated by a vertical line and the letter "P" in the margin. Formulae, footnotes and tables are always printed in small type. *Tables* should be provided with captions and numbered consecutively.

Footnotes, other than those which refer to the title heading, should be numbered consecutively. They should be placed at the foot of each page (not at the end of the article).

Formulae should preferably be typewritten but in any case should leave no room for misinterpretation — remember, the compositor is a layman! The position of indices and exponents should be made quite clear; if necessary, they may be inserted by hand in a smaller size. Special alphabets or typefaces (see below) may also be normally typed and distinguished merely by underlining in different colours, the suggested colour code being: *Greek — red, Gothic — blue, Script — green*. Where handwritten characters are used, capital letters should be underlined twice; this applies to Roman as well, especially the frequently confused *c, C; k, K; o, O; p, P; s, S; u, U; v, V; w, W; x, X; z, Z*. In formulae, do not underline in ink or with the typewriter unless the underlining is also to be printed. Other sources of trouble are: *e, l; n, u; n, r; o, O* (zero), also v, ν; ε and ϵ. Please take care to distinguish them in some way.

The fact that many typewriters use the same key for small "el" and "one" and for capital "oh" and "zero" is a special difficulty. "One" should be written with a preceding hook, not just as a downward stroke, the latter being particularly unfortunate when it appears as a superscript. Manuscripts in English should distinguish small Roman *"a"* used as a symbol from the indefinite article by leaving two spaces each side.

Letters in formulae and single letters in the text are automatically set in italics and therefore require no underlining. On the other hand, abbreviations in Roman type (the type normally used for the text) that appear in formulae (except in the case of familiar abbreviations such as of the trigonometrical functions) must be specially marked (by underlining in yellow). Abbreviations to be marked: e.g. Ord, Op, Re, Im, grad, div, dim, codim, rang, id, lim, bound, sup. Vectors (written as letters with an arrow above) are always set in boldface without an arrow.

It is requested that all *diagrams and figures* be sent in on separate sheets and not incorporated into the text.

The figures should not extend beyond the column width (8,1 cm) or page width (16,8 cm). Print area: 16,8 cm x 22 cm. Several figures should bei grouped into a plate on one page. For *line drawings*, sharp glossy prints in the desired final size are preferred. The inscriptions should be clearly legible. Letters 2 mm high are recommended. For *half-tone illustrations*, well-contrasted photographic prints, trimmed at right angles and in the desired printing size are essential. Inscriptions should be about 3 mm high. All figures must have legends, which should be submitted on a separate sheet. Illustrations taken from other publications should be accompanied by full information as to their source.

References to the literature should be listed at the end of the manuscript. The following information should be provided for journal articles: namens and initials of all authors, full title of paper, name of journal, volumne number, first and last page numbers and year of publication.

Example:

Leibovic, K. N., Balslev, E., Mathieson, T. A.: Binocular vision and pattern recognition. Kybernetik **8**, 14—23 (1970)

* The instructions are printed alternatively in German and English.

References to books should include name(s) of author(s), full title, edition, place of publication, publisher and year of publication.

Example:

Landgraf, Chr., Schneider, G.: Elemente der Regelungstechnik. Berlin-Heidelberg-New York: Springer 1970

It is assumed that manuscripts are submitted in the form in which the authors wish them to appear in print and that, apart from the correction of typographical errors, no further changes or additions will be made. If absolutely necessary, new results may be given at the end of the paper in a "Note added in proof".

Offprints: 50 offprints of each paper will be supplied free of charge.

Manuscripts must be accompanied by the full address of the author. Should the author change his address before the manuscript appears in print, he should in his own interest notify us immediately.

Available Alphabets and Typefaces:

Italic* (the type normally used for formulae)
A, B, C, D, ..., Z; a, b, c, d, ..., z

Sanserif* (also available in italic)
A, B, C, D, ..., Z; a, b, c, d, ..., z

Gothic* $\mathfrak{A}, \mathfrak{B}, \mathfrak{C}, \mathfrak{D}, \ldots, \mathfrak{Z}$; $\mathfrak{a}, \mathfrak{b}, \mathfrak{c}, \mathfrak{d}, \ldots, \mathfrak{z}$

Script $\mathscr{A}, \mathscr{B}, \mathscr{C}, \mathscr{D}, \mathscr{E}, \mathscr{F}, \mathscr{G}, \mathscr{H}, \mathscr{I}, \mathscr{J}, \mathscr{K}, \mathscr{L}, \mathscr{M}, \mathscr{N}, \mathscr{O}, \mathscr{P}, \mathscr{Q}, \mathscr{R}, \mathscr{S}, \mathscr{T}, \mathscr{U}, \mathscr{V}, \mathscr{W}, \mathscr{X}, \mathscr{Y}, \mathscr{Z}$

Greek* A, B, $\Gamma, \Delta, \ldots, \Omega$; $\alpha, \beta, \gamma, \delta, \ldots, \omega$

* Also available in boldface.

Biol. Cybernetics 22, 121—128 (1976)
© by Springer-Verlag 1976

A Model for the Mechanisms of Sensitivity Control in the Submammalian Vertebrate Retina

Ken-Ichi Hara and Munehiro Kurose

Department of Electronic Engineering, Toyama University, Toyama, Japan

Received: July 16, 1975

Abstract

A model is proposed for the mechanisms of sensitivity control at the outer and inner plexiform layers in the submammalian vertebrate retina on the basis of Werblin's results and other physiological results. The model is especially based on the following suggestions: The signal that acts to shift the bipolar curves is probably carried by horizontal cell processes extending from the surround to the center of the receptive field. Furthermore, amacrine cells carry a lateral antagonistic signal across the inner plexiform layer that affects the response properties of ganglion cells. The simulations of the model were made and the results of the ones considerably coincided with the experimental results of Werblin.

1. Introduction

The vertebrate retina can operate over an extremely broad range of luminances by changing sensitivity. Physiological results, however, have not been sufficiently obtained to elucidate the mechanisms of sensitivity control.

Recently, Werblin *et al.* studied the effects of background illumination upon the response characteristics of the receptors, bipolars, and ganglion cells (Norman and Werblin, 1974; Werblin, 1974; Werblin and Copenhagen, 1974): The intensity-response relation for both rods and cones is affected by steady background illumination. The receptor activity is carried to bipolar cells by antagonistic pathways that are concentrically organized at the outer plexiform layer. Since bipolar activity is modified by surround backgrounds, the outer plexiform layer seems to mediate sensitivity change. Furthermore, they characterized the effects of lateral interactions at the inner plexiform layer upon the signal transmitted from bipolar to ganglion cells. It was suggested that amacrine cells carried a lateral antagonistic signal across the inner plexiform layer, and affected the response properties and sensitivity of ganglion cells. Some results of their studies are as follows: (1) As the background intensity is increased, the operating range of the cone shifts along the log-test intensity domain so that it spans new regions around such new background intensity. (2) The entire log intensity-response curve for the bipolar is shifted without change of slope along the log intensity axis by surround illumination. (3) Steady backgrounds tend to shift the position of the intensity-response curves to the right, and changing backgrounds shift the curves still further and compress the response.

In a previous study (Hara and Kurose, 1975), a model is proposed for the functional mechanisms of light and dark adaptation of vertebrate cones, especially for the mechanisms of operating curve shifting during light and dark adaptation of the cones.

In this paper, on the basis of Werblin's results and other physiological results, we propose a model for the mechanisms of sensitivity control at the outer and inner plexiform layers in the submammalian vertebrate retina.

2. Model

2.1. The Mechanism of Sensitivity Control at the Outer Plexiform Layer

2.1.1. Responses of Bipolar Cells. Two types of bipolar cells have been found in certain vertebrate retinas, namely on-center bipolar cells and off-center bipolar cells. With on-center bipolar cells, central illumination presented to the center of the bipolar receptive field evokes a sustained depolarizing potential. With off-center bipolar cells, central illumination evokes a sustained hyperpolarizing potential.

According to the physiological results of Toyoda (Toyoda, 1973), the depolarizing responses were accompanied by a resistance decrease. On the other hand, the hyperpolarizing responses were accompanied by a resistance increase.

As a model of bipolar cell membrane, an equivalent circuit is shown in Fig. 1 (Takabayashi and Hara, 1974). In Fig. 1, E_i and R_i $(i=B)$ represent the fixed battery and resistance of bipolar cell membrane

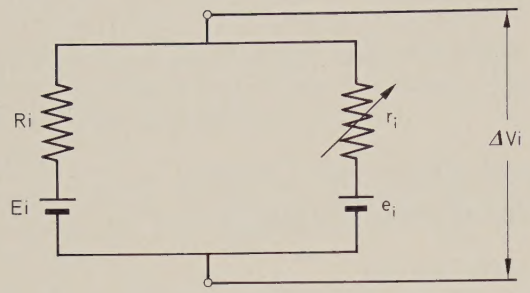

Fig. 1. Equivalent circuit of retinal cell membrane. Suffix i denotes B, AT, AS, GT, or GS

without active sites, respectively. e_i and r_i represent the battery and resistance of bipolar cell membrane containing active sites, respectively.

Suppose that r_B in the dark is equal to r_{B0} and is increased by Δr_B by light stimulation. From the equivalent circuit a potential increment from some resting potential level is given by

$$\Delta V_B = M_B \Delta r_B / (R_B + r_{B0} - \Delta r_B) \tag{1}$$

where

$$M_B = R_B(E_B - e_B)/(R_B + r_{B0}) .$$

According to Hodgkin and Huxley (1952), the mechanisms underlying the changes in sodium and potassium conductances of the membrane of a giant nerve fibre are assumed as follows: Sodium conductance is proportional to the number of sites on the inside of the membrane which are occupied simultaneously by three activating molecules but are not blocked by an inactivating molecule. Potassium ions can only cross the membrane when four similar particles occupy a certain region of the membrane.

In this paper, the process of change of membrane potential is assumed as follows: there are a number of receptor sites on the postsynaptic membrane of bipolar cells. A receptor site, X_B, receives some average number, β, of synaptic transmitters. We call the β synaptic transmitters an activating molecule. A receptor site may be complexed with an activating molecule. $[X_B]$ and $\Delta[C_R]$ represent the concentrations of active receptor sites and activating molecules, respectively. $[\Delta C_R X_B]$ represents the concentration of the receptor sites complexed with ΔC_R. Suppose that $[\Delta C_R X_B]$ follows a first order reaction:

$$d[\Delta C_R X_B] = k_2 \Delta[C_R][X_B] - k_1[\Delta C_R X_B] . \tag{2}$$

$$[X_B] + [\Delta C_R X_B] = [X_B]_0 , \tag{3}$$

where k_1, k_2 = constants, $[X_B]_0$ = concentration of active receptor sites in the dark.

When $d[\Delta C_R X_B]/dt = 0$, $[X_B]$ can be expressed by

$$[X_B] = \frac{k_1[X_B]_0}{k_2 \Delta[C_R] + k_1} . \tag{4}$$

From Eq. (4), the amount of variation of $[X_B]$, $\Delta[X_B]$, is given by

$$\Delta[X_B] = [X_B]_0 - [X_B] = \frac{[X_B]_0 \Delta[C_R]}{k_3 + \Delta[C_R]} , \tag{5}$$

where k_3 = constant.

The change of membrane resistance can be calculated as follows: Suppose that the increment of admittance of bipolar cell membrane is proportional to $\Delta[X_B]$. The total resistance $r_B^{(1)}$ is given by

$$1/r_B^{(1)} = 1/r_{B0} + n_1 \Delta[X_B] = (1 + n_1 r_{B0} \Delta[X_B])/r_{B0} . \tag{6}$$

Consequently, the decrement of membrane resistence, Δr_B, becomes

$$\Delta r_B = r_{B0} - r_{B0}/(1 + n_1 r_{B0} \Delta[X_B]) = n_1 r_{B0}^2 \Delta[X_B]/(1 + n_1 r_{B0} \Delta[X_B]) , \tag{7}$$

where n_1 = constant.

Annular illumination presented to the surround of on-center bipolar receptive fields evokes a sustained hyperpolarizing potential. Furthermore, when the central region is illuminated, annular illumination antagonizes the sustained potential produced by the central illumination. According to anatomical evidences, the bipolar receptive-field center matches closely in area the dendritic spread of bipolar cells, while the surround area approximates the lateral spread of horizontal cells.

The correlation between the response of horizontal cells and the steady response decrement after the initial peak in bipolar cells was examined (Werblin, 1974): As shown in Fig. 2, the response of horizontal cells was well correlated with the magnitude of decrement in bipolar cell response for all test disk diameters over about 2 mm. Thus, it is suggested that the weighting of the bipolar cell surround and the weighting of the horizontal cell response may both decrease with distance by a similar function.

From the above-mentioned physiological and anatomical results, the antagonistic surround response of bipolar cells appears to be mediated by horizontal-bipolar contacts. Furthermore, the bipolar cells are polarized in a graded, sustained manner by direct receptor-bipolar cell contacts. Sustained bipolar cell polarization is antagonized by horizontal-bipolar

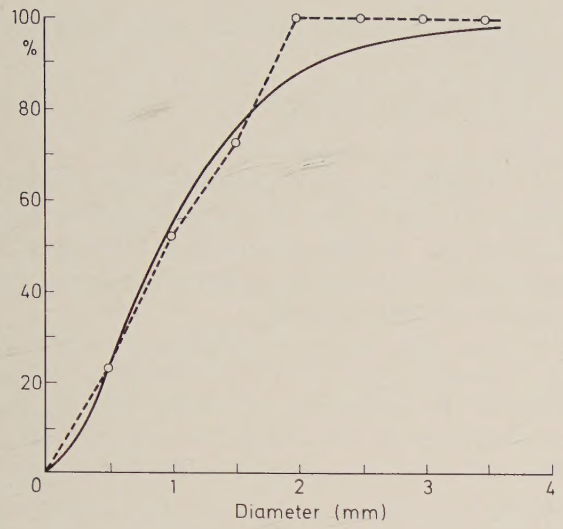

Fig. 2. Open circles show percent of maximum response in a horizontal cell and percent of maximum decrement of response in a bipolar cell for different size test disks. The solid curve shows the predicted values of response weighted by the function $W(x)=A\exp(-3.7x)$ where x is distance from the center of the field in mm and A is an arbitrary constant

contacts. It was suggested that surround antagonism in the bipolar cells subtracted from the center.

ΔQ_C and ΔQ_H represent the amounts of synaptic transmitters released from receptor terminals and horizontal cell processes, respectively. The equivalent amount of transmitter change that relates to the change of membrane resistance of on-center bipolar cells is given by

$$\Delta Q_T = q_1 \Delta Q_C - q_2 \Delta Q_H , \tag{8}$$

where q_1, q_2 = constants.

We assume that ΔQ_C and ΔQ_H are proportional to the equivalent potentials of receptors and horizontal cells, respectively. Consequently, Eq. (8) becomes

$$\Delta Q_T = q_3 \Delta V_C - q_4 \Delta V_H , \tag{9}$$

where q_3, q_4 = constants.

Suppose that the probability that a receptor site receives a synaptic transmitter is p, and that p is proportional to the amount of synaptic transmitters, ΔQ_T. Furthermore, $\Delta[C_R]$ is assumed to be proportional to p^β.

$$\Delta[C_R] \propto p^\beta \propto \Delta Q_T^\beta . \tag{10}$$

From Eqs. (9) and (10), $\Delta[C_R]$ is expressed by

$$\Delta[C_R] = q_5 \Delta Q_T^\beta = h_1 \| \Delta V_C - h_2 \Delta V_H \|^\beta , \tag{11}$$

where h_1, h_2, q_5 = constants, $\|A\|^\beta = A^\beta$ $(A \geqq 0)$, $\|A\|^\beta = -(-A)^\beta$ $(A < 0)$.

From Eqs. (1), (5), (7), and (11), ΔV_B is expressed as follows:

$$\Delta V_B = P_B \frac{\| \Delta V_C - h_2 \Delta V_H \|^\beta}{\| \Delta V_C - h_2 \Delta V_H \|^\beta + \sigma_B^\beta} \tag{12}$$

where P_B, σ_B = constants.

Central illumination presented to the center of off-center bipolar cells evokes a sustained hyperpolarizing potential. The hyperpolarizing potential is accompanied by a resistance increase. An equivalent circuit of off-center bipolar cell membrane is also shown in Fig. 1. From Fig. 1, the peak response of off-center bipolar cells, $\Delta V'_B$, is expressed by

$$\Delta V'_B = -M_B \Delta r'_B / (R_B + r_{B0} + \Delta r'_B) , \tag{13}$$

where $\Delta r'_B$ = the increment of membrane resistance.

For off-center bipolar cells, suppose that the decrement of admittance of bipolar cell membrane is proportional to $\Delta[X_B]$. The total resistance $r_B^{(2)}$ is given by

$$1/r_B^{(2)} = 1/r_{B0} - n_2 \Delta[X_B] = (1 - n_2 r_{B0} \Delta[X_B])/r_{B0} , \tag{14}$$

where n_2 = constant.

The increment of membrane resistance, $\Delta r'_B$, becomes

$$\begin{aligned} \Delta r'_B &= r_{B0}/(1 - n_2 r_{B0} \Delta[X_B]) - r_{B0} \\ &= n_2 r_{B0}^2 \Delta[X_B]/(1 - n_2 r_{B0} \Delta[X_B]) . \end{aligned} \tag{15}$$

On reference to Eq. (12), $\Delta V'_B$ can be expressed as follows:

$$\Delta V'_B = -P'_B \frac{\| \Delta V_C - h_2 \Delta V_H \|^\beta}{\| \Delta V_C - h_2 \Delta V_H \|^\beta + \sigma'^\beta_B} , \tag{16}$$

where P'_B, σ'_B = constants.

2.2. The Mechanism of Sensitivity Control at the Inner Plexiform Layer

2.2.1. Responses of Amacrine Cells. In certain vertebrate retinas, a major class of ganglion cell responds best to movement. According to anatomical studies, those retinas have inner plexiform layers with an abundance of amacrine-to-amacrine and amacrine-to-ganglion cell conventional synapses. Amacrine cells extend laterally across the inner plexiform layer. It has been suggested that motion and direction selective responses of ganglion cells are mediated at the inner plexiform layer by amacrine cells.

Two types of amacrine cells have been found in the vertebrate retina. One type gives a transient depolarizing response at the onset and/or cessation of stimulation. The other type gives a sustained hyperpolarizing or depolarizing response. The sustained

response of bipolar cells are converted to transient responses by transient-type amacrine cells. How the sustained responses are converted to transient responses at the level of amacrine cells is not known. However, a local feedback interaction between bipolar terminals and amacrine processes near the bipolar ribbon synapses could make amacrine cells respond transiently.

According to the physiological results of Toyoda (Toyoda, 1973), the transient depolarizing response of amacrine cells is accompanied by a decrease in the membrane resistance. An equivalent circuit of amacrine cell membrane is also shown in Fig. 1. e_{AT}, r_{AT}, E_{AT}, and R_{AT} correspond to e_B, r_B, E_B, and R_B, respectively. Suppose that with retinal illumination r_{AT} is decreased by Δr_{AT}. The amacrine cell response, ΔV_{AT}, is expressed by

$$\Delta V_{AT} = M_{AT} \Delta r_{AT} / (N_{AT} - \Delta r_{AT}) , \tag{17}$$

where r_{AT0} = membrane resistance in the dark,

$$M_{AT} = R_{AT}(E_{AT} - e_{AT})/(R_{AT} + r_{AT0})$$

$$N_{AT} = R_{AT} + r_{AT0} .$$

We assume that the mechanism of bipolar-amacrine is similar to the one of receptor-bipolar or horizontal-bipolar contacts. X_{AT} represents a receptor site of transient-type amacrine cell membrane and ΔC_B represents the activating molecules of a bipolar cell. On reference to Eqs. (2) and (3), the concentration of the receptor sites completed with ΔC_B respectively, $\Delta[C_B X_{AT}]$, becomes

$$\Delta[C_B X_{AT}] = \frac{K_2 [X_{AT}]_0 \Delta[C_B]}{K_1 + K_2 \Delta[C_B]} , \tag{18}$$

where K_1, K_2 = constants, $[X_{AT}]_0$ = concentration of active receptor sites of transient-type amacrine cell membrane in the dark, $\Delta[C_B]$ = concentration of the activating molecules of a bipolar cell.

On reference to Eq. (10), $\Delta[C_B]$ is expressed as follows:

$$\Delta[C_B] = q_6 [\![\Delta V_B]\!]^{\gamma_2} , \tag{19}$$

where q_6 = constant, $[\![X]\!] = X\ (X \geqq 0)$, $[\![X]\!] = 0\ (X < 0)$.

On reference to the case of off-center bipolar cells, the change of membrane resistance can be obtained as follows: Suppose that the increment of admittance of amacrine cell membrane is proportional to $\Delta[C_B X_{AT}]$. Consequently, the decrement of membrane resistance, Δr_{AT}, becomes

$$\Delta r_{AT} = r_{AT}^2 m_1 \Delta[C_B X_{AT}] / (1 + r_{AT0} m_1 \Delta[C_B X_{AT}]) , \tag{20}$$

where m_1 = constant.

Therefore, from Eq. (17)–(20), ΔV_{AT} is expressed as follows

$$\Delta V_{AT} = P_{AT} [\![\Delta V_B]\!]^{\gamma_2} / ([\![\Delta V_B]\!]^{\gamma_2} + \sigma_3^{\gamma_2}) , \tag{21}$$

where P_{AT}, σ_3 = constants.

2.2.2. On-Off Ganglion Cell Responses to Central Illumination. One type of ganglion cell responds transiently to retinal illumination. This type of ganglion cell presumably receives its input from transient-type amacrine cells.

An equivalent circuit of ganglion cell membrane is also shown in Fig. 1. $\Delta[C_{AT}]$ represents the concentration of activating molecules of transient-type amacrine cell. On reference to Eq. (10), $\Delta[C_{AT}]$ is assumed to be proportional to the γ_3-th γ_3 power of ΔV_{AT}:

$$\Delta[C_{AT}] = q_7 \Delta V_{AT}^{\gamma_3} , \tag{22}$$

where q_7 = constant.

On reference to the case of transient-type amacrine cells, the transient-type ganglion cell response, ΔV_{GT}, is expressed by

$$\Delta V_{GT} = P'_{GT} \Delta V_{AT}^{\gamma_3} / (\Delta V_{AT}^{\gamma_3} + \sigma_4^{\gamma_3}) , \tag{23}$$

where P'_{GT}, σ_4 = constants.

We assume that the number of spikes evoked in the transient-type ganglion cell is proportional to the difference between ΔV_{GT} and T_{GT}:

$$N_{GT} = P_{GT} [\![\Delta V_{GT} - T_{GT}]\!] \tag{24}$$

where P_{GT} = constant, T_{GT} = threshold in ganglion cells.

2.2.3. Effects of Background on On-Off Ganglion Cells. Bipolar activity is not affected by flashes and moving stimuli in the surround. On the other hand, change in the surround of the receptive field of on-off ganglion cells elicits activity in transient-type amacrine cells. The amacrine cells in turn hyperpolarize the ganglion cell membrane and limit the ganglion cell responses to central stimuli. The lateral antagonistic effects elicited by flashes and moving stimuli are probably carried across the inner plexiform layer by amacrine cells. Differential action in the surround of on-off ganglion cells is mediated by the synaptic pathways from bipolar to sustained-type amacrine cells to on-off ganglion cells. The differential action antagonizes the direct input from transient-type amacrine cells to on-off ganglion cells. From the above considerations, a scheme of synaptic contacts at the inner plexiform layer in this model is shown in Fig. 3.

Retinal cells can respond only to some range of frequencies. For example, the gain characteristic of

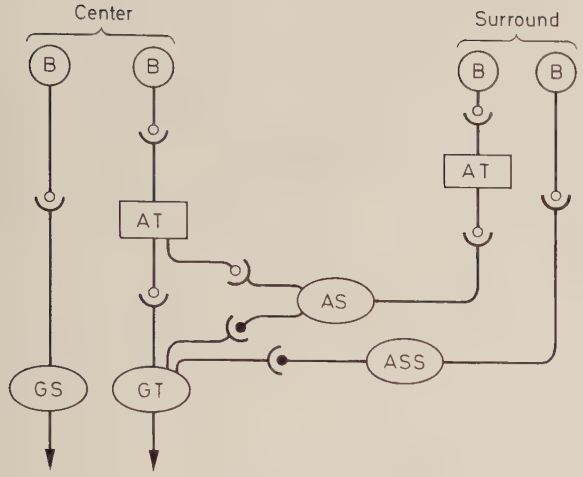

Fig. 3. Scheme of synaptic contacts at the inner plexiform layer in this model. *B*: bipolar cells; *AT*: transient-type amacrine cells; *AS*: *ASS*: sustained-type amacrine cells; *GT*: transient-type ganglion cells; *GS*: sustained-type ganglion cells; ○, excitatory synapse; ●, inhibitory synapse

a transfer function of certain horizontal cells in the carp is as follows: The gain is constant up to 6 Hz and decreases at a rate of 24 dB/octave above 15 Hz. The transfer function can be sufficiently described by fourth order (Fukurotani and Hara, 1975). We assume that the synaptic transmitters released from each bipolar cell are decreased in inverse proportion to the γ_5-th power of W/W_0 for speeds above a critical speed W_0, where W denotes the speed of a spinning windmill.

Consequently, Eq. (18) is modified as follows:

$$\Delta[C'_B] = q_7 [\![\Delta V_B]\!]^{\gamma_2} / (W/W_0)^{\gamma_7}, \tag{25}$$

where q_7 = constant, $W/W_0 = 1$ for $W \leqq W_0$, $\gamma_7 = \gamma_2 \cdot \gamma_5$.

By a spinning windmill transient-type amacrine cells elicit a depolarizing response, $\Delta V'_{AT}$, and Eq. (21) is revised as follows:

$$\Delta V'_{AT} = P_{AT} \frac{[\![\Delta V_B]\!]^{\gamma_2}}{[\![\Delta V_B]\!]^{\gamma_2} + \sigma_3^{\gamma_2} (W/W_0)^{\gamma_7}}. \tag{26}$$

On the other hand, $\Delta[C'_{AT}]$ is the concentration of activating molecules of a transient-type amacrine cell. On reference to Eq. (10), we assume that $\Delta[C'_{AT}]$ is proportional to the product of the speed of the spinning windmill and the γ_4-th power of $\Delta V'_{AT}$:

$$\Delta[C'_{AT}] = q_8 \cdot W \cdot \Delta V'^{\gamma_4}_{AT}, \tag{27}$$

where q_8 = constant.

On reference to Eqs. (2) and (3), the concentration of receptor sites complexed with $\Delta[C'_{AT}]$, $\Delta[C'_{AT} X_{AS}]$, is given by

$$\Delta[C'_{AT} X_{AS}] = \frac{K_4 [X_{AS}]_0 \Delta[C'_{AT}]}{K_3 + K_4 \Delta[C'_{AT}]}, \tag{28}$$

where K_3, K_4 = constants, $[X_{AS}]_0$ = concentration of active receptor sites of sustained-type amacrine cell membrane in the dark.

On reference to the case of on-off ganglion cells, the decrement of sustained-type amacrine cell membrane resistance, Δr_{AS}, becomes

$$\Delta r_{AS} = r^2_{AS0} n_5 \Delta[C'_{AT} X_{AS}] / (1 + r_{AS0} n_5 \Delta[C'_{AT} X_{AS}]), \tag{29}$$

where n_5 = constant, r_{AS0} = membrane resistance of sustained-type amacrine cell in the dark.

Furthermore, an equivalent circuit of sustained-type amacrine cell membrane is also shown in Fig. 1. The response of sustained-type amacrine cells is given by

$$\begin{aligned} \Delta V_{AS} &= M_{AS} \Delta r_{AS} / (N_{AS} - \Delta r_{AS}) \\ &= P_{AS} \frac{q_8 W \Delta V'^{\gamma_4}_{AT}}{q_8 W \Delta V'^{\gamma_4}_{AT} + \sigma_5^{\gamma_4}}, \end{aligned} \tag{30}$$

where M_{AS}, N_{AS}, P_{AS}, σ_5 = constants.

The sustained-type amacrine cells which receive direct input from bipolar cells elicit a sustained slow potential, ΔV_{ASS}. On reference to Eq. (23), ΔV_{ASS} is given by

$$\Delta V_{ASS} = P_{AS} \frac{\|\Delta V_B\|^{\gamma_4}}{\|\Delta V_B\|^{\gamma_4} + \sigma_5^{\gamma_4}}. \tag{31}$$

Depolarizing activity of sustained-type amacrine cells hyperpolarizes transient-type ganglion cell membrane and apparent threshold in transient-type ganglion cells is elevated. Suppose that threshold in transient-type ganglion cells, T_{GT}, is increased in proportion to ΔV_{AS} and ΔV_{ASS}:

$$T_{GT} = T_{GT0} + t_1 \Delta V_{AS} + t_2 \Delta V_{ASS}, \tag{32}$$

where t_1, t_2 = constants, T_{GT0} = threshold in transient-type ganglion cells in the dark.

Consequently, Eq. (24) is revised as follows:

$$N_{GT} = P_{GT} [\![\Delta V_{GT} - (T_{GT0} + t_1 \Delta V_{AS} + t_2 \Delta V_{ASS})]\!]. \tag{33}$$

2.2.4. Responses of Sustained-Type Ganglion Cells. With central illumination, a sustained slow potential and steady discharge of spikes are evoked in sustained-type ganglion cells. The sustained-type ganglion cells appear to receive direct input from bipolar cells. An equivalent circuit of sustained-type ganglion cell

membrane is also shown in Fig. 1. The decrement of membrane resistance of sustained-type ganglion cell, Δr_{GS}, produces the response of the sustained-type ganglion cell, ΔV_{GS}:

$$\Delta V_{GS} = M_{GS}\Delta r_{GS}/(N_{GS} - \Delta r_{GS}) . \tag{34}$$

On reference to Eq. (23), ΔV_{GS} is expressed as follows:

$$\Delta V_{GS} = M'_{GS}[\![\Delta V_B]\!]^{\gamma_6}/([\![\Delta V_B]\!]^{\gamma_6} + \sigma_6^{\gamma_6}) , \tag{35}$$

where N_{GS}, M_{GS}, M'_{GS}, σ_6 = constants.

Consequently, the number of spikes discharged from a sustained-type ganglion cell is given by

$$N_{GS} = P_{GS}[\![\Delta V_{GS} - T_{GS}]\!] , \tag{36}$$

where P_{GS} = constant, T_{GS} = threshold in the sustained-type ganglion cell.

3. Simulated Results

Figure 4 shows three curves relating peak bipolar activity to peak receptor activity for three different levels of background illumination.

Figure 5 shows the intensity-response curves for the bipolar taken at three surround backgrounds.

Figure 6 shows the intensity-response curves for the transient-type amacrine cell and the sustained-type amacrine cell.

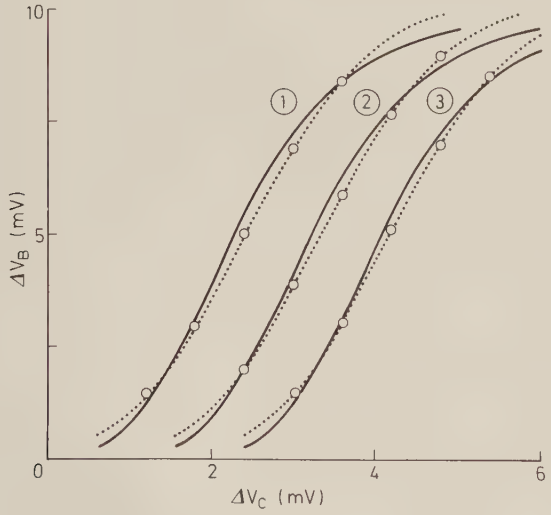

Fig. 4. Plot of the bipolar response versus receptor activity for three backgrounds. The dotted curves show the experimental results of Werblin *et al.* The solid curves show simulated results. The values of parameters are as follows: Curve *1*: $P_B = 10$, $\beta_1 = 4.5$, $h_2 = 10$, $\sigma_B = 2.93$, $\Delta V_H = 0.0$; Curve *2*: $P_B = 10$, $\beta_1 = 4.5$, $h_2 = 10$, $\sigma_B = 2.93$, $\Delta V_H = 0.108$; Curve *3*: $P_B = 10$, $\beta_1 = 4.5$, $h_2 = 10$, $\sigma_B = 2.93$, $\Delta V_H = 0.216$

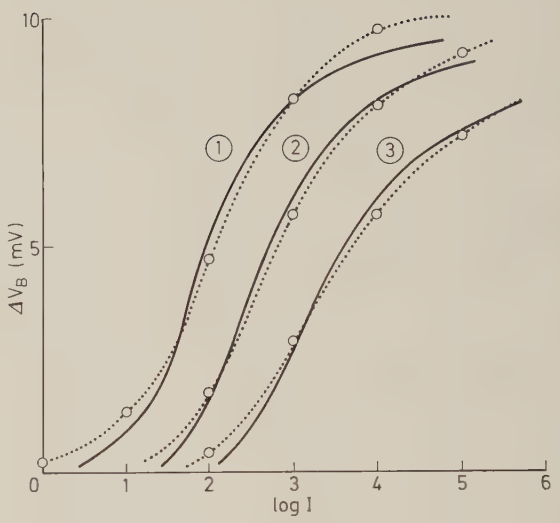

Fig. 5. Intensity-response curves for a bipolar cell at three different backgrounds. The dotted curves show the experimental results of Werblin *et al.* The solid curves show simulated results. ΔV_C is expressed as follows: $\Delta V_C = -P_1 I^{\alpha}/(I^{\alpha} + \sigma_1^{\alpha})$ (Takabayashi and Hara, 1974). The values of parameters are as follows: $P_1 = 6.0$, $\alpha = 0.7$, $\sigma_1 = 2.0$

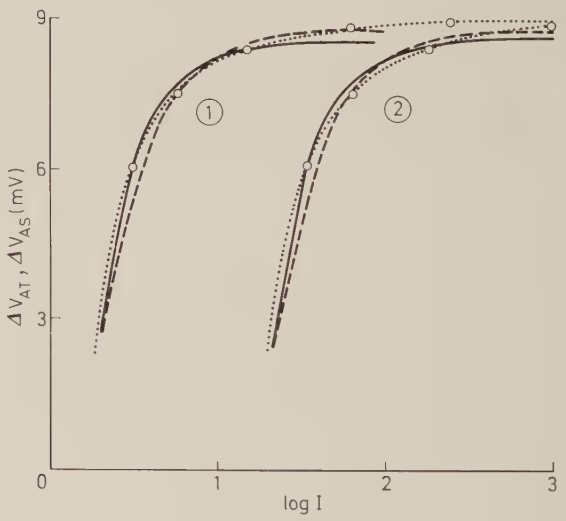

Fig. 6. Intensity-response curves for an amacrine cell at two different backgrounds. The dotted curves show the experimental results of Werblin *et al.* The broken curves show simulated results for a transient-type amacrine cell. The solid curves show simulated results for a sustained-type amacrine cell. The values of parameters are as follows: $P_{AT} = 10.0$, $\gamma_2 = 1.5$, $\sigma_3 = 2.7$, $P_{AS} = 16.0$, $\gamma_4 = 1.4$, $\sigma_5 = 8.0$, $q_8 = 1.0$, Curve *1*: $\sigma_4 = 2.0$, Curve *2*: $\sigma_1 = 3.0$

Figure 7 shows the intensity-response curves for the transient-type ganglion cell.

Figure 8 shows the intensity-response curves for the sustained-type ganglion cell.

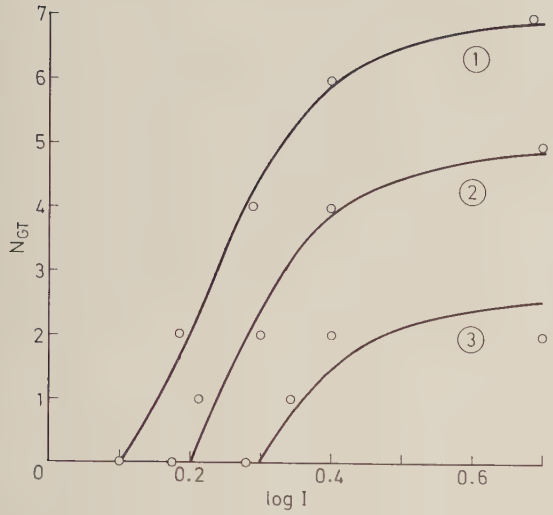

Fig. 7. Effect of the windmill on the transient-type ganglion cell response curves. Open circles show the experimental results of Werblin *et al.* The solid curves show simulated results. The values of parameters are as follows: $P_{GT}=8.3$, $\gamma_3=2.3$, $\sigma_4=2.2$, $P_{GT}=1.0$, $T_{GT0}=0.1$, $t_1=t_2=1.0$, Curve *1*: $\Delta V_{AS}=\Delta V_{ASS}=0$, Curve *2*: $\Delta V_{AS}=0.0$, $\Delta V_{ASS}=0.25$, Curve *3*: $\Delta V_{AS}=0.28$, $\Delta V_{ASS}=0.25$

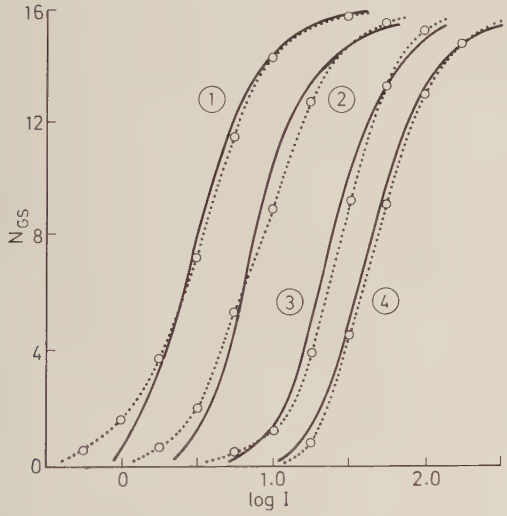

Fig. 8. Intensity-response curves for a sustained-type ganglion cell at four different backgrounds. The dotted curves show the experimental results of Werblin *et al.* The solid curves show simulated results. The values of parameters are as follows: Curve *1*: $\sigma_1=2.0$, $\Delta V_H=0.0$, Curve *2*: $\sigma_1=2.0$, $\Delta V_H=0.15$, Curve *3*: $\sigma_1=2.9$, $\Delta V_H=0.0$, Curve *4*: $\sigma_1=2.9$, $\Delta V_H=0.1$, $M'_{GS}=24.2$, $\gamma_6=1.2$, $\sigma_6=5.5$, $P_{GS}=1.0$, $T_{GS}=0.0$

Figure 9 shows the comparison of the intensity-response curves of retinal cells.

4. Conclusion

We proposed a model for the mechanisms of sensitivity control at the outer and inner plexiform layers in the submammalian vertebrate retina. In this model, the following physiological suggestions are especially taken into account: Horizontal cells mediate lateral antagonistic interactions that effect upon a second stage of sensitivity. Amacrine cells carry a lateral antagonistic signal across the inner plexiform layer that effects upon the sensitivity of ganglion cells.

The simulated results considerably coincided with the experimental results of Werblin.

This model suggests some of the mechanisms of sensitivity control in the submammalian vertebrate retina.

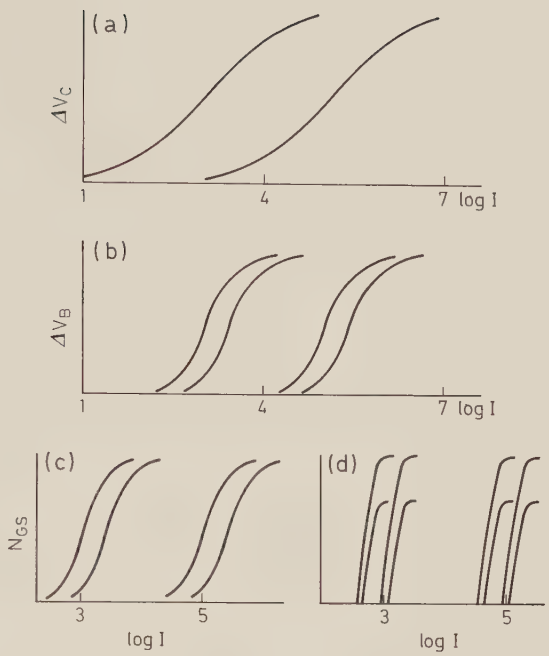

Fig. 9a–d. Comparison of the shifts in response range along the log-intensity axis by background. (a) The intensity-response curves for an photo-receptor at different backgrounds. (b) The intensity-response curves for a bipolar cell at different backgrounds. (c) The intensity-response curves for a sustained-type ganglion cell at different backgrounds. (d) The intensity-response curves for a transient-type ganglion cell at different backgrounds

References

Fukurotani, K., Hara, K.-I.: A dynamic model of the receptive field of *L*-cells in the carp retina. Biol. Cybernetics **20**, 1–8 (1975)

Hara, K.-I., Kurose, M.: A model for the mechanism of light and dark adaptation of vertebrate cones. Biol. Cybernetics **18**, 119–122 (1975)

Hodgkin, A. L., Huxley, A. F.: A quantitative description of membrane current and its application to conduction and excitation in nerve. J. Physiol. (Lond.) **117**, 500–544 (1952)

Marmarelis, P.Z., Naka, K.-I.: Nonlinear analysis and synthesis of receptive-field responses in the catfish retina. II. One-input white-noise analysis. J. Neurophysiol. **36**, 619–633 (1975)

Normann, R.A., Werblin, F.S.: Control of retinal sensitivity. I. J. gen. Physiol. **63**, 37–61 (1974)

Takabayashi, A., Hara, K.-I.: A model of photoreceptor cell for response to light through synaptic connection. Kybernetik **14**, 151–153 (1974)

Toyoda, J.: Membrane resistance changes underlying the bipolar cell response in the carp retina. Vision Res. **13**, 283–294 (1973)

Werblin, F.S.: Control of retinal sensitivity. II. Lateral interactions at the outer plexiform layer. J. gen. Physiol. **63**, 62–87 (1974)

Werblin, F.S., Copenhagen, D.A.: Control of retinal sensitivity. III. Lateral interactions at the inner plexiform layer. J. gen. Physiol. **63**, 88–110 (1974)

Dr. Ken-Ichi Hara
Department of Electronic Eng.
Toyama University
Takaoka-shi
Toyama, 933 Japan

Biol. Cybernetics 22, 129—137 (1976)
© by Springer-Verlag 1976

Effects of Elastic Loads on the Contractions of Cat Muscles

P. Bawa*, A. Mannard**, and R. B. Stein
Department of Physiology, University of Alberta, Edmonton, Canada

Received: September 5, 1975

Abstract

The nerves to plantaris and soleus muscles in the cat were stimulated with maximal single shocks and with random stimulus trains which produced partially fused contractions. In order to obtain information on the mechanism of muscular contraction, the effects of allowing the muscles to shorten against various elastic loads were studied in the time domain and in the frequency domain. When springs of increasing stiffness were placed in series with the muscle, the twitch tension increased greatly. The gain of the frequency response curve was also much greater with stiffer springs. The shape of the frequency response curve for plantaris muscle could usually be described by that expected for a second-order system with two real time constants or rate constants. The rate constants changed in qualitatively similar ways in response to increased stiffness of an elastic load, increased muscle length and increased mean rate of nerve stimulation. These results are in agreement with the hypothesis that the linear responses of muscles working against elastic loads are determined by the values of two rate constants. Thus, of the many processes associated with contraction, only two are rate-limiting: one associated with the viscoelastic properties of muscle and the second associated with the reuptake of Ca into the sarcoplasmic reticulum. Non-linear aspects of muscular contraction are also discussed. These are more prominent in soleus muscle than in plantaris muscle.

Introduction

The partially fused contractile responses resulting from random nerve stimulation resemble the natural activity of muscle more closely than do isolated twitches or fused tetani. We have been interested in describing the tension fluctuations of muscles under conditions of random activation and in drawing inferences from such a description about the underlying contractile mechanism.

Mannard and Stein (1973) showed that, with random stimulation, the partly fused responses of an isometric muscle of the cat were similar to those of a simple, linear, second-order system; i.e. the relationship between nerve stimuli and tension fluctuations, under various conditions of mean stimulation rate and muscle length, conformed to a family of second-order frequency response curves. A frequency response curve describes the ability of a system to respond to inputs of various frequencies. This curve measures both the gain and phase changes we would expect muscles to contribute to the cyclic activity found in natural movements such as walking, running and tremor. A second-order frequency response curve is conveniently described by the values of three parameters. One represents the low-frequency gain of the muscle while the other parameters are, under specified conditions, the *time constants* or the *rate constants* of the system (Milsum, 1966). Since normally functioning muscles are often free to shorten appreciably, we extended these experiments to muscles which were free to contract against elastic loads. As will be described, the second-order model still holds for muscles contracting against springs with widely different stiffnesses.

Models of force generation in muscle generally contain a contractile element which has kinetic properties that determine the time course of force generation. This force is then modified by the viscous and elastic properties of the muscle and its loads. One might expect that several variables would be needed to describe the behaviour of such a system, but the fact that a second-order model holds for both isometric and elastic loading implies that *only two variables are rate-limiting.*

Theoretical studies (Stein and Wong, 1974) were undertaken using a model for contraction based on the sliding filament theory (Huxley, 1957) as expanded by Julian (1969) to include the kinetics of activation mediated by Ca ions. These studies suggested that one of the rate-limiting processes was the reuptake of Ca by the sarcoplasmic reticulum. This process determined the relaxation phase of an isometric

* Graduate student of the Medical Research Council of Canada.

** Present Address: Department of Physiology, McGill University, Montreal, Quebec, Canada. Formerly a Post-doctoral Fellow of the Muscular Dystrophy Association of Canada.

twitch. However, it was not clear whether the second process which determined the contractile phase of a twitch involved the rate of making and breaking cross-bridges between actin and myosin molecules, or depended on the visco-elastic properties of muscle. Earlier models of muscle (Hill, 1938; Houk, Cornew and Stark, 1966) tended to assume that the increase in tension during a twitch was mainly limited by visco-elastic properties. However, in isolated single fibres of the frog in which tendon compliance had largely been eliminated, Huxley and Simmons (1971) showed that the formation of cross-bridges limited the rate of rise of an isometric twitch. Other possible rate-limiting steps include the breaking of cross-bridges (Podolsky *et al.*, 1969), the movement of cross-bridges (Weber and Murray, 1973) or the binding of Ca ions (Ashley and Moisescu, 1973). Although studies on the dynamic properties of whole muscles are unlikely to distinguish conclusively between these various possibilities, we felt we could test the visco-elastic hypothesis by varying the loading conditions.

Under isometric conditions both plantaris and soleus muscles behaved according to the predictions of the second-order model, although the natural frequency of soleus muscle (a mainly slow twitch muscle; Henneman and Olson, 1965) was much lower than for plantaris muscle (a mainly fast twitch muscle; Binkhorst, 1969). For plantaris muscle with elastic loads one rate constant increased systematically when increasingly stiff springs were added in series with the muscle. This supports the hypothesis that the visco-elastic properties of the muscle limit the rate of contraction. A quantitative model of contraction based on this hypothesis is introduced in a second paper (Bawa *et al.*, 1976). This model can predict the results of experiments when a muscle contracts, not only against elastic loads, but also against various inertial loads.

When elastic loads were applied to soleus muscle, certain properties were observed which would not be expected from a linear, second-order system. These are described qualitatively in the Results and are discussed in relation to recent studies of this muscle (Joyce, Rack and Westbury, 1969; Burke *et al.*, 1970; Nichols and Houk, 1973).

Methods

The experimental arrangements for this and the following paper (Bawa *et al.*, 1976) are shown schematically in Fig. 1. Random trains of supramaximal stimuli usually at a mean rate of either 5/sec or 10/sec were applied for 1 min to the nerve to either plantaris or soleus muscles (details in Mannard and Stein, 1973). The trains of pulses used were prerecorded on a tape recorder so that the rate

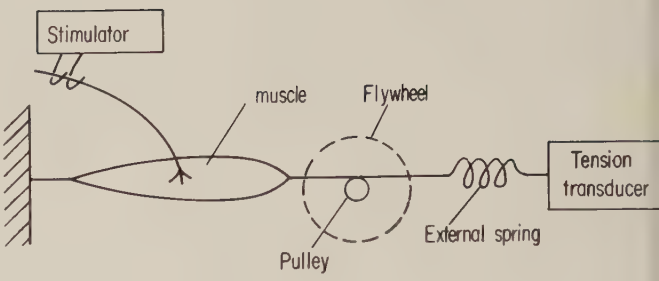

Fig. 1. Schematic diagram of the system used to apply varying elastic and inertial loads to a muscle. The pulley and flywheels for inertial loading (interrupted lines) were not connected except for experiments described in the following paper (Bawa *et al.*, 1975). They were included, when required, by passing the thread from the muscle around the pulley. The thread was knotted and attached tightly at one point on the circumference of the pulley so that no slippage could occur. The fixation point was selected with care so as not to interfere with the conversion of muscle displacement into rotation. The pulley had a sufficiently large diameter (6 cm) that only a fraction of a revolution occured with a maximal contraction

could be changed over an eight-fold range without altering the other statistical properties of the train. The two heads of gastrocnemius were divided and either plantaris or soleus muscle was freed. The Achilles tendon was divided to separate the tendon of the muscle to be studied. A non-compliant thread tied to the tendon was then attached either to

(1) a stiff tension transducer (stiffness = 10 kg/mm) – *isometric loading*;

(2) an external spring of varying stiffness (8 g/mm to 570 g/mm) – *elastic loading*;

(3) an external spring, after being wound around a pulley to which varying inertial loads could be added – *inertial loading.*

Under conditions (2) and (3) the tension transducer was connected to the end of the external spring remote from the tendon. Except when the effect of length was being studied, the muscle was kept at the length which produced the largest twitch tension. The passive tension corresponding to this optimal length was noted and when elastic loads were changed, each spring was stretched to produce the same level of passive tension. Different flywheels, mounted coaxial with the pulley, constituted inertial loads in the range 4–1500 g. After each experiment the viscosity of the system was measured by replacing the muscle with a spring and observing the damped oscillations that resulted from brief displacements of the various inertial loads. The damping of the pulley system was small compared to the probable damping introduced by the normal antagonistic muscles, but the range of elastic and inertial loads probably included most of the physiological range (A. Mannard and R. B. Stein, unpublished observations).

Values of tension are given in grams weight in this paper because these are easily comprehended and are consistent with much of the previous literature. These values can be easily converted to the more widely accepted MKS units of force, Newtons, by dividing by 1000 (to convert grams to kilograms) and multiplying the results by the acceleration of gravity, 9.8 m/sec^2. Similarly, the values of stiffness can be easily converted to N/m.

Analysis

The methods of spectral analysis used to determine the frequency response of the muscle have been described previously (Mannard and Stein, 1973). These methods have been further

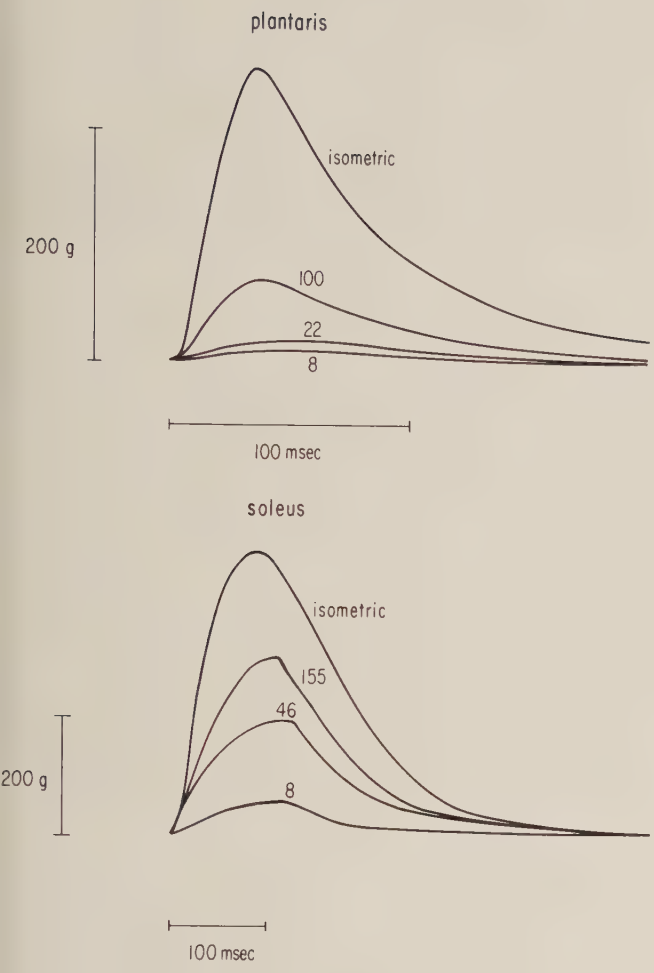

Fig. 2. Effect on twitch tension of adding springs in series with plantaris and soleus muscles. The values indicated give the stiffness of the springs in g/mm. The superposition was carried out by tracing the twitches from the original photographs

automated (French, 1973). Checks for the stationarity of the mean and standard deviation of the tension fluctuations have been introduced through use of a hot-stylus recorder during the experiment, and a short computer program during the analysis. In addition, a number of twitches were recorded once every 2 sec before and after a period of random stimulation to check for stationarity. If there were marked non-stationarities (systematic changes $>20\%$ in one or more parameters), this period or portion of a period of stimulation was not used in the analysis. Non-stationarity may be a limiting factor in the application of these techniques, but spectral analysis has been applied successfully to cat, amphibian (Wong, 1972) and human muscles (Aaron and Stein, 1976).

When the data were stationary and from later analysis appeared to be well-fitted by the frequency response function of a second-order system (see Results), a short computer program was used to determine the best-fitting parameters of low frequency gain, natural frequency and damping ratio. Initial values of the parameters were chosen, and each parameter was varied in turn by a preset percentage. The change which produced the greatest reduction in the least mean square error of the data points from the predicted gain curve was accepted, and the process was repeated until no further reduction in error could be obtained with that percentage of variation. The percentage was then reduced until the best-fitting parameters were obtained to the nearest 1%. This procedure was more accurate and reproducible than the curve-fitting by eye which had been used previously (Mannard and Stein, 1973). Using the values of parameters derived from the gain curve, the predictions for the phase as a function of frequency were examined. The phase is affected by the pure time delays involved in nervous conduction, neuromuscular transmission and excitation-contraction coupling. The best-fitting value of the total time delay could also be calculated so as to minimize the mean square error.

Altogether three criteria were available for checking the adequacy of a second-order model:

(1) the decline in gain at high frequencies according to the second power of frequency,

(2) no phase lags greater than approximately 180 after accounting for the pure time delays,

(3) the goodness of fit of the second-order curve. Standard deviations of the points from the fitted curve were typically less than $\pm 10\%$. Confidence intervals on the parameters characterizing the best-fitting curves are more difficult to calculate, but can be assessed empirically by repeating a given run several times (see Fig. 5). Details of all programs used in the analysis are available on request from Dr. Stein.

Results

Effect of Elastic Loads on the Twitch

Plantaris Muscle. Figure 2 shows a typical isometric twitch of plantaris muscle at its optimal length in response to supramaximal stimulation, together with the effects of placing increasingly compliant springs in series with the muscle. Note that the twitch tension is markedly reduced when more compliant springs are used, and the contraction time is lengthened somewhat. Similar results have been observed for frog sartorius muscle (Hill, 1951).

However, it is not obvious from Fig. 2 whether the relaxation phase of the twitch is similarly affected. To study this several twitches were averaged and various parameters were calculated from the average twitch. Twitches were applied before and after each period of random stimulation so the effect of random stimulation at 10 stimuli/sec for 60 sec could also be determined. These results are summarized in Fig. 3 for the same muscle as used in Fig. 2. The left half of Fig. 3 indicates that the half-relaxation time, as well as the contraction time, decreased when increasingly stiff springs were used. It was more difficult to measure changes in the final exponential decay of the twitch below the half-relaxation point (see also Jewell and Wilkie, 1960). Small increases or decreases in the rate of this decay were observed in different experiments after increasing the stiffness of external springs.

Much more dramatic than the changes in time course are the changes in twitch tension and the area

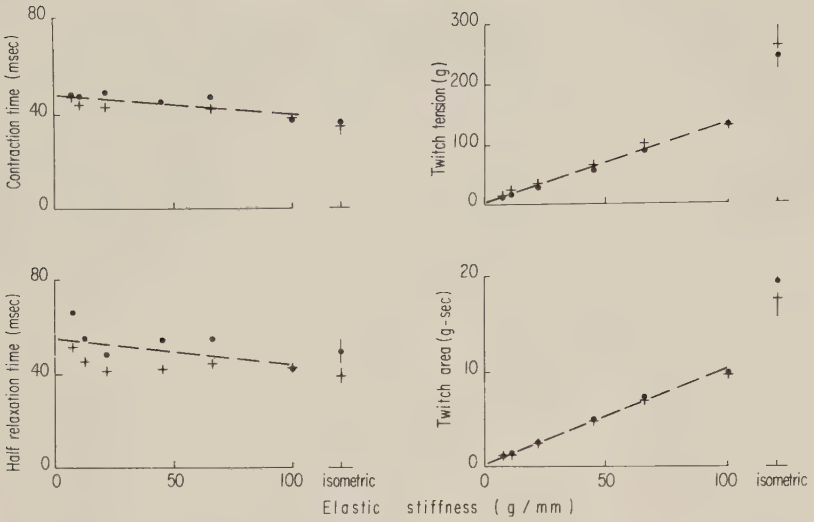

Fig. 3. Changes in parameters of twitches in plantaris muscle measured with series springs of different stiffnesses. Same muscle as in Fig. 2. The ·'s were values obtained before and the +'s were values obtained after a period of random stimulation. The straight lines were fitted to all the data except that from isometric trials. Several isometric trials were interposed between the trials using elastic loads and the vertical extent of the symbols for the isometric conditions gives the standard deviation of the values for each parameter

under the twitch shown on the right side of Fig. 3. The best-fitting straight lines have been computed for the data in each part of Fig. 3 to indicate the trends more clearly. The lines do not necessarily imply that these variables are all linearly related to series stiffness. The expected relations between some of these variables will be considered in the following paper (Bawa *et al.*, 1976).

By comparing the data points in Fig. 3 measured before (·) and after (+) a period of random stimulation, we see that a period of random stimulation slightly potentiated the twitch and shortened its time course. These two effects of stimulation cancelled in this experiment so that the area under a twitch (measured in g-sec) was little affected.

Soleus Muscle. The time course of the twitch in soleus was much longer than plantaris under isometric conditions and with all elastic loads. We also consistently observed that the twitch contractions of soleus muscle against weak springs increased toward a steady level, and then declined abruptly (Fig. 2). The contraction times were therefore longer with weak springs, as for plantaris, but the half-relaxation times were less. The unusual form of the twitch was presumably due to the formation of stable bonds during the contraction of this slow twitch muscle, the effects of which have been described previously (Joyce *et al.*, 1969; see also the Discussion).

Another probable effect of these stable bonds was that during the occasional long pauses in the random stimulation the mean level of tension would drop dramatically and only return to its previous level with a time course of a second or more (see also Burke *et al.*, 1970). These non-linear effects were much more prominent in the slow soleus muscle than in the faster plantaris, so that most of the subsequent linear analysis will deal with plantaris. However, comparisons with soleus will be included at several points in the Results and the Discussion.

A final difference between the two muscles was that the twitch tensions in soleus were generally somewhat depressed immediately after a period of random stimulation at a mean rate of 5 or 10/sec, when these periods were separated by a minute or so. Potentiation of the twitch was occasionally observed, particularly when higher, near-tetanic rates of stimulation were used.

Fatigue. Each period of random stimulation contained several hundred stimuli and during a long experiment 10000–20000 stimuli might be applied. Soleus muscle proved more stationary in that it fatigued less during a long experiment than did plantaris, presumably because of the higher percentage of slow twitch, slowly fatiguing fibres in soleus (Henneman and Olson, 1965). The twitch of plantaris muscle inevitably declined with time, and isometric runs were interposed between every few conditions with elastic loads to measure this decay. The vertical extent of the symbols for isometric loading in Fig. 3 gives the standard deviation of four runs over the period of this series. Thus, the vertical extent includes any systematic changes as well as random fluctuations. Long-term changes were minimized by randomizing the order of elastic loads and repeating the first couple of elastic loads at the end of the series. The values for 8 and 66 g/mm in Fig. 3 represent the average of two runs.

Results similar to those illustrated in Fig. 3 were observed consistently. They indicate that the interaction of an external elastic element with the internal

contractile visco-elastic elements of muscle markedly alters the twitch tension and affects the time course of a twitch to some extent. However, these results do not lend themselves easily to a quantitative analysis which could determine if the visco-elastic properties of muscle directly limit the rate of contraction. This is more easily done by analysis in the frequency domain rather than in the time domain.

The Frequency Response with Elastic Loads

Plantaris Muscle. Figure 4 shows the gain curves for the frequency response obtained by spectral analysis of the tension fluctuations using random stimulation and the same elastic loads as in Fig. 2. The gain curves have the same dimensions as the area under a twitch (g-sec/impulse), and in a linear system (Milsum, 1966) the gain at low frequency would be identical to the area under the twitches. Note that the low frequency gain, like the twitch area (Fig. 3) is much greater with stiffer springs.

Figure 4 also indicates that the responses decline as the second power of the frequency at high frequencies (a slope of -2 on these log-log plots). The transitions between the low frequency portions of these curves and the high frequency portions occur at about the same frequency, although the shapes of the curves vary somewhat with different elastic loads. This suggests that the plantaris muscle with various elastic loads behaves like a linear second-order system with about the same natural frequency, but with a damping ratio which may vary with the elastic load. The phase data for the responses as a function of frequency (not shown in Fig. 4) were consistent with the gain data. The coherence functions (a normalized measure of the linearity of the response; Bendat and Piersol, 1966) were uniformly high, typically between 0.6 and 0.9 for all springs over most of the frequency range shown. A coherence value of 1.0 would indicate a completely linear system.

The left-hand side of Fig. 5 shows the best fitting values of gain, natural frequency and damping ratio (see Methods) as a function of elastic stiffness for the same muscle as in Fig. 4 ($\cdot$) and another plantaris muscle ($+$). The gain increases steadily with stiffness, while the natural frequency showed no marked change. No consistent trends in natural frequency were observed in ten experiments. The relative constancy of the natural frequency implies that muscles should be able to follow oscillatory signals from the central nervous system of roughly the same bandwidth whether contracting isometrically or under quite light loads.

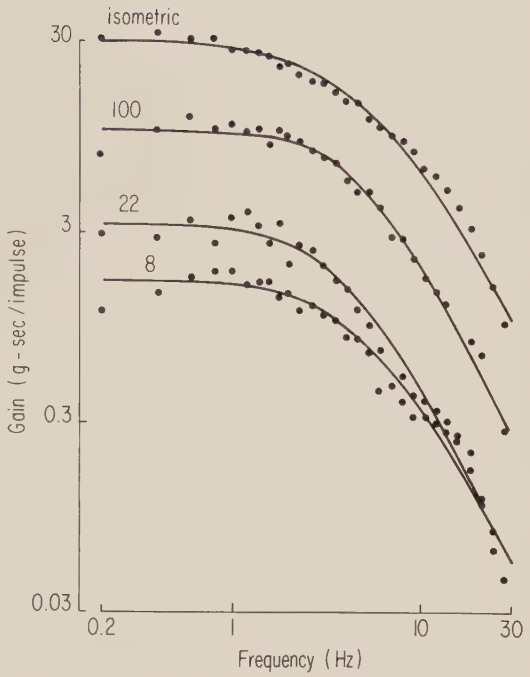

Fig. 4. Gain of a plantaris nerve-muscle preparation, measured during random stimulation, as a function of frequency under isometric conditions and with various elastic loads. The fitted curves for a second-order linear system were computed as described in the Methods. The values above the curves indicate the stiffnesses of the springs in g/mm. Both ordinate and abscissa are logarithmic scales. Different muscle from that used for Fig. 2 and Fig. 3

The damping ratio followed a U-shaped curve with a minimum at intermediate values of stiffness. This shape was observed in every experiment with plantaris muscle. The minimum value was always close to one (critical damping; Milsum, 1966) although slightly underdamped or overdamped values were obtained in some experiments.

The three parameters: low frequency gain (G_0), natural frequency (f_n) and damping ratio (ζ) are sufficient to completely describe a linear-order system. When the damping ratio is greater than or equal to one, an equivalent set of parameters is the low frequency gain and two rate constants or time constants (Milsum, 1966).

The relation between the two rate constants, r_1 and r_2, and the other parameters is given by

$$r_1, r_2 = 2\pi f_n(\zeta \pm \sqrt{[\zeta^2 - 1]}), \quad \zeta \geqq 1 . \tag{1}$$

Note that when $\zeta = 1$, $r_1 = r_2$. For $\zeta < 1$ the response is oscillatory but the envelope of the oscillation will decay exponentially with a rate constant r, where

$$r = 2\pi f_n \zeta . \tag{2}$$

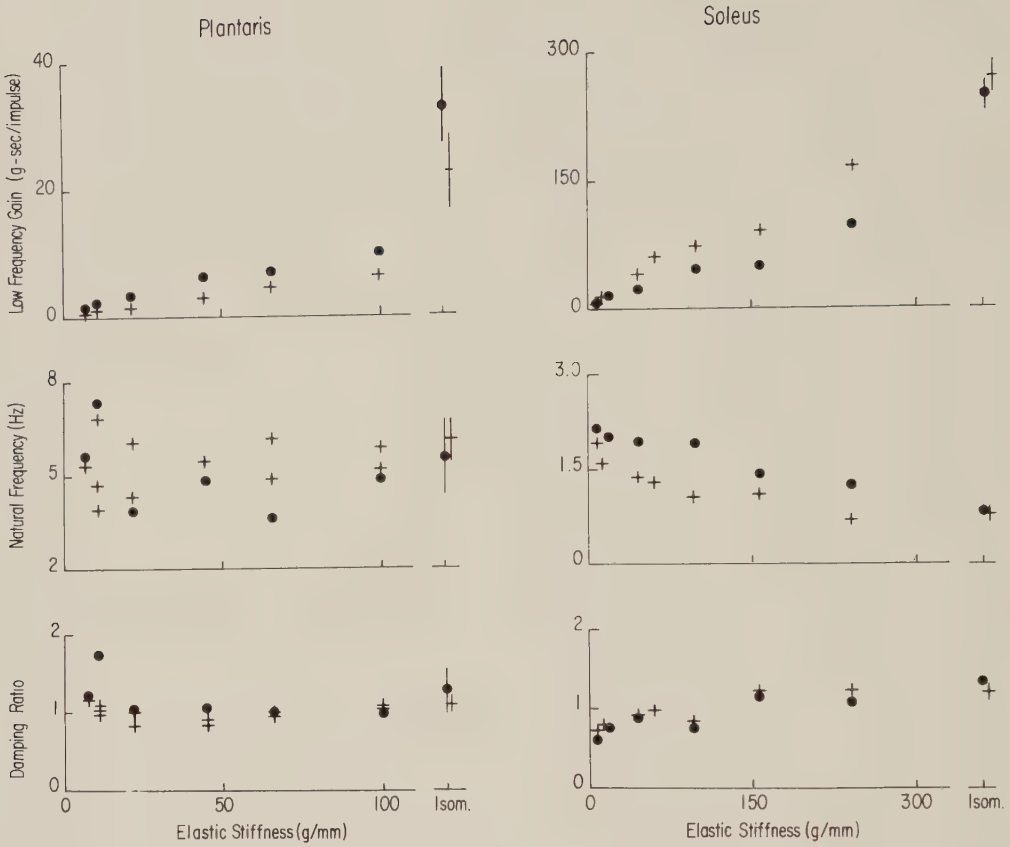

Fig. 5. Effect of the stiffness of an elastic load on the gain, natural frequency and damping ratio measured from the frequency response curves for plantaris and soleus muscles. Gain increases steadily with increasing stiffness in both muscles, but the natural frequency and the damping ratio are affected differently. The implications of these results are discussed in the text. The two types of symbols represent data from different experiments with each muscle. The vertical extent of the symbols for isometric conditions with plantaris indicate the S.D. of the values obtained from several runs. Note the different scales for the two muscles

Time constants can also be defined which are the inverse of the rate constants. The larger rate constant (smaller time constant) will determine the rising phase of a twitch while the smaller rate constant will determine the relaxation phase.

Figure 6A shows the values of these rate constants (left ordinate) or time constants (right ordinate) as a function of the stiffness of the external springs. Data obtained using a wide range of springs is shown and most springs were used more than once. The two rate constants computed from Eq. (1) vary in opposite directions, and in this experiment become equal at a stiffness of 30–40 g/mm. In some other experiments the equality of the rate constants occurred at somewhat higher stiffnesses (50–100 g/mm).

As pointed out above, a damping ratio of 1 occurs when both rate constants have the same value. Whenever the rate constants differ the damping ratio will be greater than 1, which explains the U-shaped damping curve seen in Fig. 5. Under several conditions in this experiment the best-fitting damping ratio was slightly less than 1. This occurred because the relaxation phase was relatively faster than expected for a critically damped second-order system. The rate constants for these conditions were set equal to the value given by Eq. (2).

This finding of two rate constants varying in the opposite directions with increasing stiffness would explain the relative constancy of the natural frequency (which depends on the product of the rate constants). Similar changes in the rate constants were observed when the length of the muscle was varied about the length which gave the largest twitch tension (Fig. 6B) or when the mean rate of stimulation was varied (Fig. 6C).

Soleus Muscle. Because the twitches of soleus were much longer (see Fig. 2), lower mean rates of stimulation (5 or 7/sec) were used so that the responses remained relatively unfused. The time course of the twitch was shorter at shorter lengths (Rack and Westbury, 1969) so some experiments were carried out at 10 mm below physiological maximum length.

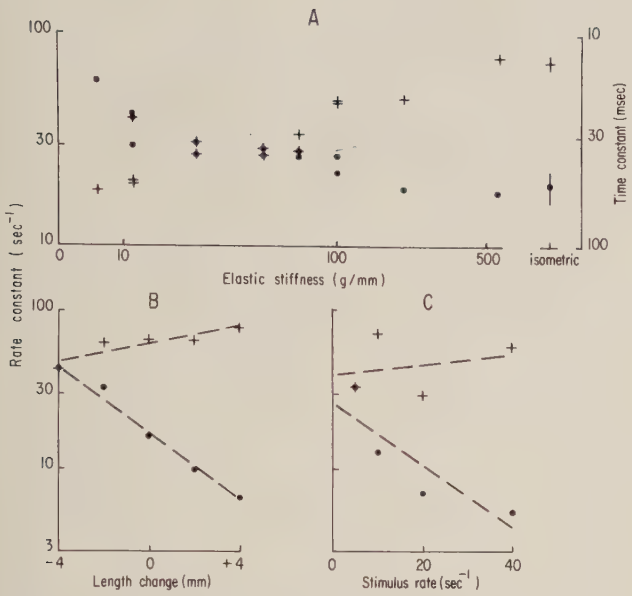

Fig. 6A–C. Changing either (A) the stiffness of springs in series with a muscle, (B) the length of the muscle from that which produces the largest twitch, or (C) the mean rate of stimulation affects the two rate constants. Isometric conditions were used for (B) and (C). The computed best-fitting straight lines on the semi-log plots in (B) and (C) have been drawn to indicate the trend of the data. Note that the lines of the two rate constants in (A) appear to cross. The corresponding values of time constants can be determined from the right-hand scale in (A). The data in the three graphs are from different plantaris muscles

As shown in Fig. 5 the low frequency gain of soleus muscle changed with elastic load in much the same way as for plantaris muscle. However, the damping ratio increased and the natural frequency decreased monotonically with the stiffness of the external springs. A U-shaped curve for the damping ratio was never observed. Note that for very compliant springs the best-fitting values of the damping ratio were near 0.6. With such low values the twitches should have been frankly oscillatory, but they were not. The reason stems from the shapes of the twitches (Fig. 2), which were not of the expected form for a linear second-order system. The computer program showed that the resultant frequency response curve was best fitted by a curve having a damping ratio less than 1. However, the fit was not as good and the values of coherence (a measure of linearity; Bendat and Piersol, 1966) were somewhat lower for soleus muscle. In other words, the non-linearities in soleus muscle were significant enough that a purely linear analysis begins to break down. The implications of these results will now be discussed.

Discussion

The magnitude of the response of a muscle, whether measured as gain in the frequency domain or twitch tension in the time domain, increased systematically with the stiffness of its elastic load. This result is expected from the classical force-velocity curve of Hill (1938). Hill's relationship is generally thought to arise from a non-linear viscous property of muscle, although it has been reinterpreted by Huxley (1957), who suggested that at higher contraction velocities, reached with weak springs for example, the fraction of bonds that could be formed and hence the force generated would be less. An additional factor is that a muscle will shorten against weak springs to lengths where it is able to develop rather less tension (Gordon *et al.*, 1966).

The shapes of the frequency response curves for plantaris muscle with elastic loads were well fitted by the responses expected for a simple second-order system, and are therefore consistent with there being two rate-limiting processes. The first and smaller rate constant under isometric conditions appears to be equivalent to Hill's rate constant for the decay of the active state (see also Jewell and Wilkie, 1960). This is now thought to involve the rate at which the sarcoplasmic reticulum can take up Ca ions (Julian, 1969; Connolly *et al.*, 1971; Stein and Wong, 1974). Because of its dependence on external series elasticity, the second rate constant is presumably a visco-elastic parameter involving the muscle's apparent viscosity, series elasticity and parallel elasticity. The elasticity of the muscle also appears to depend markedly on the state of the contractile elements (Grillner, 1972).

Nonetheless, in any simple mechanical model (see for example Bawa *et al.*, 1976) a visco-elastic rate constant should increase, other things remaining constant, when stiffer springs are added. Therefore, the rate constant which increases with stiffer springs and becomes the larger one under isometric conditions (Fig. 6A) can tentatively be assumed to be visco-elastic in nature. Why the other rate constant, which presumably depends on the active state, should have decreased when stiffer springs were used might seem obscure. One possible explanation is that although the initial length of the muscle was held constant, the muscle was allowed to shorten by greater amounts during its contractions when loaded with weaker springs.

The pre-stimulus length of a muscle is known to affect markedly the time course, as well as the magnitude, of its twitch (Rack and Westbury, 1969) and the parameters of its frequency response (Mannard and

Stein, 1973). The effect of changing muscle length alone is shown in Fig. 6B for comparison with the effect of changing elastic load. Increasing length decreases the value of one time constant sharply while producing a smaller increase in the other time constant. Increasing the length shifts the series elasticity of a muscle to a region of higher stiffness (Joyce and Rack, 1969; Grillner, 1972). Therefore, since a visco-elastic rate constant would be expected to increase with increasing length, the observed decrease in the one rate constant is presumably due to a slowing in the decay rate of the active state.

This hypothesis concerning the behaviour of the two rate constants is also consistent with the results obtained by varying the mean rate of stimulation (Fig. 6C). Increasing the rate of stimulation would be expected to load the pump responsible for the reuptake of Ca ions by the sarcoplasmic reticulum. This could slow the decay of the active state and decrease its measured rate constant. On the other hand, increasing the rate of stimulation and the tension produced isometrically would lead to further internal shortening against the muscle's series elasticity. The resulting stretching of the series elasticity would increase its stiffness (Joyce and Rack, 1969), which should increase the other rate constant.

Although the data are consistent with one rate constant depending on the muscle's visco-elasticity, they do not completely rule out the other possible rate-limiting steps mentioned in the Introduction. Indeed, the distinction between visco-elastic and contractile elements is now somewhat arbitrary. However, models involving simple contractile and visco-elastic elements have the advantage that predictions can be readily derived and checked experimentally. This is done in the following paper (Bawa *et al.*, 1976). Not only is the behaviour qualitatively consistent with the model, as indicated here, but quantitative predictions are also accurately fulfilled. This provides further evidence that one of the rate constants is visco-elastic in nature.

The generality of these conclusions is weakened by the differences observed between soleus and plantaris muscles. With elastic loads weaker than about 100 g/mm, the frequency response curves of soleus muscle were not well-fitted by a second-order model with two real time constants. When a second-order model was fitted, the damping ratios observed were less than 1, even though the twitches were not oscillatory. Rather, the twitch tension approached a steady level for a short period and then declined rapidly. The attainment of a steady level is consistent with the formation of stable bonds in this slow twitch muscle (Joyce *et al.*, 1969). When there are no longer a sufficient number of these bonds to maintain the tension, the muscle will begin to relax and be lengthened by the spring. More bonds will then be broken and the tension should fall rapidly, as observed. This "catch property" (Burke *et al.*, 1970) is an essential non-linearity which might warrant a fuller analysis.

The method of random stimulation can be used to determine non-linear as well as linear terms in a system (Marmarelis and Naka, 1972; French and Butz, 1973). However, it is not certain whether the much greater amount of computation required for non-linear analysis would add much insight into the nature of these non-linearities or in the functional role of these muscles for posture and movement. Therefore, the later papers in this series (Bawa *et al.*, 1976; Oğuztöreli and Stein, 1976) are restricted to linear models of muscle.

This study was supported in part by grants to Dr. Stein from the Medical Research Council of Canada and the Muscular Dystrophy Association of Canada. The authors thank Dr. A. S. French for his continuing development of the computer programs used here and Dr. T. R. Nichols for his assistance in the experiments with soleus muscle and his helpful comments on these manuscripts.

References

Aaron, S. L., Stein, R. B.: Comparison of an EMG-controlled prosthesis and the normal biceps brachii muscle. Amer. J. Phys. Med. in press (1976)

Ashley, C. C., Moisescu, D. G.: The mechanism of free calcium change in single muscle fibres during contraction. J. Physiol. (Lond.) **231**, 23—24 (1973)

Bawa, P., Mannard, A., Stein, R. B.: Predictions and experimental tests of a visco-elastic muscle model using elastic and inertial loads. Biol. Cybernetics **22**, 139—145 (1976)

Bendat, J. S., Piersol, A. G.: Measurement and analysis of random data. New York: John Wiley & Sons, Inc. 1966

Binkhorst, R. A.: The effect of training on some isometric contraction characteristics of a fast muscle. Pflügers Arch. ges. Physiol. **309**, 193—202 (1969)

Burke, R. E., Rudomin, P., Zajac, F. E.: Catch properties of single mammalian motor units. Science **168**, 122—124 (1970)

Connolly, R., Gough, W., Winegrad, S.: Characteristics of the isometric twitch of skeletal muscle immediately after a tetanus. J. gen. Physiol. **57**, 697—709 (1971)

French, A. S.: Automated spectral analysis of neurophysiological data using intermediate magnetic tape storage. Comput. Progr. Biomed. **3**, 45—47 (1973)

French, A. S., Butz, E. G.: Measuring the Wiener kernels of a non-linear system using the fast Fourier transform algorithm. Int. J. Control **17**, 529—539 (1973)

Gordon, A. M., Huxley, A. F., Julian, F. J.: The variation in isometric tension with sarcomere length in vertebrate muscle fibres. J. Physiol. (Lond.) **184**, 170—192 (1966)

Grillner, S.: The role of muscle stiffness in meeting the changing postural and locomotor requirements for force development by the ankle extensors. Acta physiol. scand. **86**, 92—108 (1972)

Henneman, E., Olson, C. B.: Relations between structure and function in the design of skeletal muscles. J. Neurophysiol. **28**, 581—598 (1965)

Hill, A. V.: The heat of shortening and the dynamic constants of muscle. Proc. roy. Soc. (Lond.) B **126**, 136—195 (1938)

Hill, A. V.: The effects of series compliance on the tension developed in the muscle twitch. Proc. roy. Soc. (Lond.) B **138**, 325—329 (1951)

Houk, J. C., Cornew, R. W., Stark, L.: A model of adaptation in amphibian spindle receptors. J. theor. Biol. **12**, 195—215 (1966)

Huxley, A. F.: Muscle structure and theories of contraction. Progr. Biophys. **7**, 255—318 (1957)

Huxley, A. F.: A note suggesting that the cross-bridge attachment during muscle contraction may take place in two steps. Proc. roy. Soc. (Lond.) B **183**, 83—86 (1973)

Huxley, A. F., Simmons, R. M.: Mechanical properties of the cross-bridges of frog striated muscle. J. Physiol. (Lond.) **218**, 59—60 (1971)

Jewell, B. R., Wilkie, D. R.: The mechanical properties of relaxing muscle. J. Physiol. (Lond.) **152**, 30—47 (1960)

Joyce, G. C., Rack, P. M. H.: Isotonic lengthening and shortening movements of cat soleus muscle. J. Physiol. (Lond.) **204**, 475—491 (1969)

Joyce, G. C., Rack, P. M. H., Westbury, D. R.: The mechanical properties of cat soleus muscle during controlled lengthening and shortening movements. J. Physiol. (Lond.) **204**, 461—474 (1969)

Julian, F. J.: Activation in a skeletal muscle contraction model with a modification for insect fibrillar muscle. Biophys. J. **9**, 547—570 (1969)

Mannard, A., Stein, R. B.: Determination of the frequency response of isometric soleus muscle in the cat using random nerve stimulation. J. Physiol. (Lond.) **229**, 275—296 (1973)

Marmarelis, P. Z., Naka, K.: White noise analysis of a neuron chain: an application of the Wiener theory. Science **175**, 1276—1278 (1972)

Milsum, H. H.: Biological Control Systems Analysis. New York: McGraw-Hill 1966

Nichols, T. R., Houk, J. C.: Reflex compensation for variations in the mechanical properties of a muscle. Science **181**, 182—184 (1973)

Podolsky, R. J., Nolan, A. C., Zaveler, S. A.: Cross-bridge properties derived from muscle isotonic velocity transients. Proc. nat. Acad. Sci. (Wash.) **64**, 504—511 (1969)

Rack, P. M. H., Westbury, D. R.: The effects of length and stimulus rate on tension in the isometric cat soleus muscle. J. Physiol. (Lond.) **204**, 443—460 (1969)

Stein, R. B., Wong, E. Y-M.: Analysis of models for the activation and contraction of muscle. J. theor. Biol. **46**, 307—327 (1974)

Stein, R. B., Oğuztöreli, M. N.: Tremor and other oscillations in neuromuscular systems. Biol. Cybernetics **22**, 147—157 (1976)

Weber, A., Murray, J. M.: Molecular control mechanisms in muscle contraction. Physiol. Rev. **53**, 612—673 (1973)

Wong, E. Y-M.: Theoretical and experimental studies on frog skeletal muscle. M. Sc. Thesis, University of Alberta, Edmonton, Canada (1972)

Prof. R. B. Stein
Dept. of Physiology
The University of Alberta
Edmonton, Canada T6G 2H7

Biol. Cybernetics 22, 139—145 (1976)
© by Springer-Verlag 1976

Predictions and Experimental Tests of a Visco-Elastic Muscle Model Using Elastic and Inertial Loads

P. Bawa*, A. Mannard**, and R. B. Stein
Department of Physiology, University of Alberta, Edmonton, Canada

Received: September 5, 1975

Abstract

A simple, linear visco-elastic model of muscle is described which contains five parameters: a series and a parallel elasticity, a viscosity, and a magnitude and rate constant for the decay of the active state. The effects of adding springs in series with a muscle are predicted. The responses to random stimulus trains can be used to evaluate the parameters of the model. The effects of applying inertial loads to the muscle can also be predicted. These predictions are in good agreement with experimental observations on plantaris muscle of the cat. For example, damped oscillations of the predicted frequencies can be observed for various inertial loads. The gain of the frequency response falls off sharply (as the fourth power of frequency) at higher frequencies. However, responses to lower frequency signals, including most of the frequencies important for cyclic movements, are only slightly affected by a wide variation in inertial load.

Introduction

In the preceding paper (Bawa *et al.*, 1976) we showed that when a muscle is contracting against elastic loads, as well as under isometric conditions (Mannard and Stein, 1973), the forces generated are well described by those expected for a simple, second-order system. By varying the elastic load, the length of the muscle, and the stimulation rate, one of the two rate constants of the second-order system appeared to be visco-elastic in nature, whereas the second corresponded in classical terms (Hill, 1938) to the decay of the active state. As a result we thought it worthwhile to develop the predictions of a muscle model in sufficient detail that the experimental results could be tested quantitatively against the model. Once the parameters are determined, the model can also be used to predict the responses to other types of loads, e.g. inertial loads.

The effects of inertial loads on a muscle's performance are of interest for two reasons. Firstly, in normal contractions muscles work, not only against the elasticity of antagonistic muscles, but they must also move inertial loads which vary widely during normal movements. For example, during the swing phase of locomotion the calf muscles extend the ankle before the foot strikes the ground. The foot represents a relatively small inertial load. However, during the stance phase, the muscles again extend the ankle after initially giving under the weight of the body, but now the inertial load consists of a substantial fraction of the animal's weight, rather than the foot alone. Thus, to understand normal movements it is important to analyse how muscles respond to changes in inertial load.

Secondly, Partridge (1966, 1967) has suggested that muscles have remarkable abilities to compensate for variations in inertial loads. When he varied the inertial load of the triceps surae muscles (soleus + gastrocnemius muscles) by a factor of 28, he found that the movements of the muscles during low frequency sinusoidal inputs was hardly affected. Partridge (1967) argued that 'from basic Newtonian considerations, it is obvious that for the movement amplitude to remain constant, the force amplitude at the test frequency must have increased in proportion to the load inertia. The implication of this basic mechanical relationship is the rather dramatic conclusion that the force delivered by the muscle to the load, at the signal frequency, must have varied by almost 10000 times depending on the load impedance'. Partridge then went on to suggest that to explain these results 'the length-tension relationship in muscle forms a functional non-neural servo-feedback. These signal handling characteristics of muscle make it more nearly a "position servo" than a "force motor".'

Our experimental results with inertial loads are consistent with those of Partridge, but our analysis shows that his assumption of a non-neural feedback is unnecessary. From our muscle model, which does not include any internal feedback pathways, we are able to predict that the movements in response to low frequen-

* Graduate student of the Medical Research Council of Canada.

** Present address: Department of Physiology, McGill University, Montreal, Quebec, Canada. Formerly a Post-doctoral Fellow of the Muscular Dystrophy Association of Canada.

cies of stimulation should be nearly independent of inertial load, as observed experimentally. Furthermore, our model is able to predict the responses to higher frequencies, including the damped oscillations which result with larger inertial loads. Irrespective of their interpretation, these results do add support to the idea demonstrated by Partridge (1966) that muscles are well designed to produce a given pattern of movement, despite the wide variations in inertial load that they normally encounter.

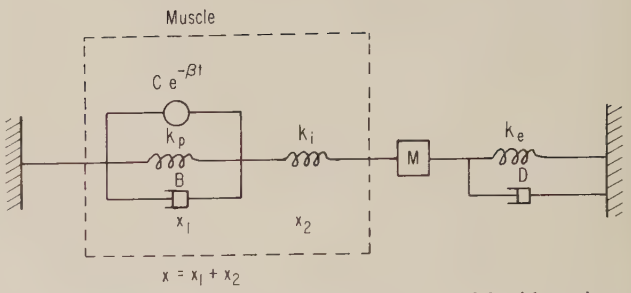

Fig. 1. Schematic representation of a muscle model with various types of external loads. The meaning of the parameters is discussed in the text

Theoretical Predictions

Figure 1 shows a simple visco-elastic model of muscle such as proposed by Houk *et al.* (1966) based on Hill's (1938) model of muscle. This model contains an internal series elastic element of stiffness k_i, and a parallel elastic element of stiffness k_p. It also contains an active state element which produces a contractile force C each time a stimulus is received. The force decays exponentially with a rate constant β. This model is actually simpler than Hill's original model in that the non-linear force velocity relation he found has been represented by a linear dashpot with viscosity B. A linear dashpot will not be adequate to describe very high shortening velocities. However, our results (Bawa *et al.*, 1976) indicate that the *linear* aspects of muscle can be described by three parameters. This muscle model already contains five parameters so it is worthwhile to consider its properties carefully before adding further complexity. Also included in Fig. 1 are an external elastic element of stiffness k_e, a mass M and a dashpot of viscosity D. The element k_e simulates the stiffness of antagonist muscles against which contraction always takes place, and the mass M corresponds to both gravitational and inertial masses against which the muscle contracts. There will always be some damping in the external system which is specified by the parameter D.

Equations of Motion. If x_1 and x_2 represent changes in length of the parallel and series elastic elements respectively during a twitch contraction, two equations of motion can be written for the forces which must balance at the two central nodes of Fig. 1

$$k_p x_1 + B\dot{x}_1 + Ce^{-\beta t} = k_i x_2 , \tag{1}$$

$$k_i x_2 + k_e x + D\dot{x} + M\ddot{x} = 0 \tag{2}$$

where $x = x_1 + x_2$ is the total displacement of the muscle and derivatives are represented by dots over the appropriate symbols. Substituting in Eq. (1) for

$$x_1 = x - x_2 = x + \frac{1}{k_i}(k_e x + D\dot{x} + M\ddot{x}) \tag{3}$$

and rearranging gives an equation for the displacement of the muscle

$$\ddot{x}[MB] + \dot{x}[M(k_i + k_p) + DB] + \dot{x}[D(k_i + k_p) + B(k_i + k_e)] + x[k_p k_i + k_p k_e + k_i k_e] = -k_i C e^{-\beta t} . \tag{4}$$

Taking Laplace transforms we have

$$X(s) = \frac{-k_i C}{(s+\beta)\{MBs^3 + [M(k_i + k_p) + DB]s^2 + [D(k_i + k_p) + B(k_i + k_e)]s + k_p k_i + k_p k_e + k_i k_e\}} \tag{5}$$

where transformed variables are functions of s; e.g. $X(s) = \int_0^\infty x e^{-st} dt$. The force measured by a transducer in series with the external spring (see Methods, Bawa *et al.*, 1976) will simply be the force g generated in the spring.

$$g = -k_e x . \tag{6}$$

Taking Laplace transforms of Eq. (6) and substituting from Eq. (5) gives

$$G(s) = \frac{k_e k_i C}{(s+\beta)\{MBs^3 + [M(k_i + k_p) + DB]s^2 + [D(k_i + k_p) + B(k_i + k_e)]s + k_p k_i + k_p k_e + k_i k_e\}} . \tag{7}$$

Equation (7) is a formidable expression, and before considering the whole expression we will discuss some simplifications. The most important simplification occurs when the mass M and external damping D are negligible. This corresponds to the situation of a pure elastic load studied experimentally in the previous paper.

Elastic Loading. If $M = 0$ and $D = 0$ Eq. (7) reduces to a simple second-order equation which represents the transfer function of the muscle with elastic loads

$$G(s) = \frac{k_i k_e C}{(s+\beta)\{B(k_i + k_e)s + k_p(k_i + k_e) + k_i k_e\}} . \tag{8}$$

One rate constant which we will denote by α depends on the external spring. From Eq. (8)

$$\alpha = \frac{1}{B}\left(k_p + \frac{k_i k_e}{k_i + k_e}\right) . \tag{9}$$

If k_e is varied α should reach simple lower and upper limits:

$$\lim_{k_e \to 0} \alpha = \frac{k_p + k_e}{B}, \tag{10}$$

$$\lim_{k_e \to \infty} \alpha = \frac{k_p + k_i}{B}. \tag{11}$$

By plotting α vs. k_e, the slope for weak springs will give the value of $1/B$, according to Eq. (10) and from the intercept one can obtain the value of k_p. The value of k_i can then be determined from Eq. (11). Thus, using Eqs. (10) and (11) the parameters k_i, k_p, and B can be determined. One further point that can be noted from Eq. (9) is that as $k_e \to k_i$

$$\lim_{k_e \to k_i} \alpha = \frac{k_p + \frac{1}{2}k_i}{B} \tag{12}$$

which is the midway point in the transition from the lower to the upper limits.

The second rate constant is the parameter β for the decay of the active state. The final parameter C can be determined from the limit of $G(s)$ as $s \to 0$

$$\lim_{s \to 0} G(s) = \frac{k_i k_e C}{\beta\{k_p k_i + k_e(k_p + k_i)\}}. \tag{13}$$

We will call this quantity G_0 in line with previous work (Mannard and Stein, 1973). From it C can be determined using any value of k_e. For example, under isometric conditions

$$\lim_{k_e \to \infty} G_0 = \frac{k_i C}{(k_p + k_i)\beta_\infty} \tag{14}$$

where β_∞ indicates the high stiffness limit of the rate constant β. This notation is used because β changes systematically with the stiffness of springs placed in series with muscle (Bawa *et al.*, 1976).

Equation (13) can also be used to obtain an independent estimate of the effective stiffness of the muscle. This is done by plotting $1/(G_0\beta)$ vs. $1/k_e$. After rearranging Eq. (13) one obtains

$$\frac{1}{G_0\beta} = \frac{1}{C}\left(\frac{k_p + k_i}{k_i} + \frac{k_p}{k_e}\right). \tag{15}$$

The ratio of the slope to the intercept of such a plot is $k_p k_i/(k_p + k_i)$. This ratio gives the effective stiffness k of the muscle model since the model contains two springs in series, and

$$\frac{1}{k} = \frac{1}{k_i} + \frac{1}{k_p}$$

or

$$k = \frac{k_p k_i}{k_p + k_i}. \tag{16}$$

The value of k obtained experimentally from Eq. (15) will be compared with that obtained from the values of k_i and k_p from Eqs. (10) and (11).

The high frequency limit of Eq. (8) is also readily derived. Indeed, one can show that in terms of the quantities already considered

$$\lim_{s \to \infty} G(s) = G_0 \alpha\beta/s^2. \tag{17}$$

Since the quantities G_0, α, and β have been considered separately, the high frequency limit does not provide new data for evaluating parameters of the model.

Inertial Loads. Having considered the reduced system of Eq. (8) in some detail, we now turn to the more complex system with inertial and viscous loading. The low and high frequency limits are readily derived. In fact, the low frequency limit is identical to Eq. (13). *The presence of inertial or viscous loads should not change the steady-state response or the response to sufficiently slowly-changing inputs.* Hence, non-neural feedback is not required for compensation of these loads in contrast to the suggestion by Partridge (1967) which was quoted in the Introduction. In Partridge's (1966) experimental study k_e was small and the amplitude of movement was measured. Under these conditions according to Eq. (5)

$$\lim_{k_e \to 0} X(0) = \frac{-C}{\beta k_p} \tag{18}$$

which shows that the low frequency amplitude is also independent of the mass. The high frequency limit of either Eqs. (5) or (7) does depend on mass M. For example,

$$\lim_{s \to \infty} G(s) = \frac{k_e k_i C}{MBs^4}. \tag{19}$$

It is very difficult to move the mass at high frequencies and the response declines as the fourth power of frequency. The force actually generated by the muscle (as opposed to the signal measured by a length transducer or a force transducer in series with the external spring) declines as the square of frequency at high frequencies. This force f is, using Eq. (2)

$$f = k_i x_2 = -(k_e x + D\dot{x} + M\ddot{x}). \tag{20}$$

Taking Laplace transforms and substituting from Eq. (5) gives

$$F(s) = \frac{k_i C(Ms^2 + Ds + k_e)}{(s+\beta)\{MBs^3 + [M(k_i + k_p) + DB]s^2 + [D(k_i + k_p) + B(k_i + k_e)]s + k_p k_i + k_p k_e + k_i k_e\}}. \tag{21}$$

The limit of Eq. (21) as $s \to \infty$ is simply

$$\lim_{s \to \infty} F(s) = \frac{k_i C}{B s^2}. \tag{22}$$

Equation (22) is identical to the limit of Eq. (8) as $s \to \infty$ and $k_e \to \infty$; i.e. the isometric condition at high frequencies. Since the mass cannot readily be moved at high frequencies, the force generated by the muscle approaches its isometric value. At low frequencies much less force is required to move a mass. If under Partridge's experimental conditions the external damping D and elasticity k_e were negligible even at low frequencies, then the force produced by the muscle at low frequencies would be proportional to the mass and to the square of the frequency according to Eq. (21), as he suggested.

The higher order and the increased number of parameters in Eqs. (5), (7), and (21) makes it difficult to describe all possible types of behaviour at intermediate frequencies. However, certain general properties can be determined. An analysis, which includes the mechanical properties of the muscle and the properties of sensory feedback pathways, is contained in the last of this series of papers (Stein and Oğuztöreli, 1976).

We will now turn to comparisons with experimental data. The parameters of the muscle can be determined using elastic loads as indicated above. Then, the effects of varying the inertial or other types of load can be computed for example from Eq. (7) and compared with experiment.

Results

Elastic Loads. Equation (10) predicts that for weak springs the rate constant α should be proportional to k_e. This prediction is tested in Fig. 2. The linear correlation coefficient is 0.77 and no obvious deviation from linearity is observed. The best-fitting straight line has a slope of 0.24 ± 0.06 (mean $\pm$ S.E.), which indicates that the parameter B for the viscosity of the muscle has a value of 4.1 g-sec/mm. The intercept has a value of 21.5 ± 2.0 (mean $\pm$ S.E.) which would give a value for the parallel elasticity, $k_p = 90$ g/mm [see Eq. (10)]. The isometric value of α was 74.4 ± 2.4 (mean $\pm$ S.E.) which from Eq. (11) indicates a series elasticity $k_i = 220$ g/mm.

The effective stiffness of the muscle can also be determined once k_i and k_p are known, and is 63 g/mm [see Eq. (16)]. As indicated in the theoretical section an independent measure of muscular stiffness can be obtained from the low frequency gain G_0 and the rate constant β. A plot of $1/(G_0\beta)$ vs. $1/k_e$ should give a straight line, and the ratio of the slope to the intercept of that line should give the muscular stiffness. Figure 3

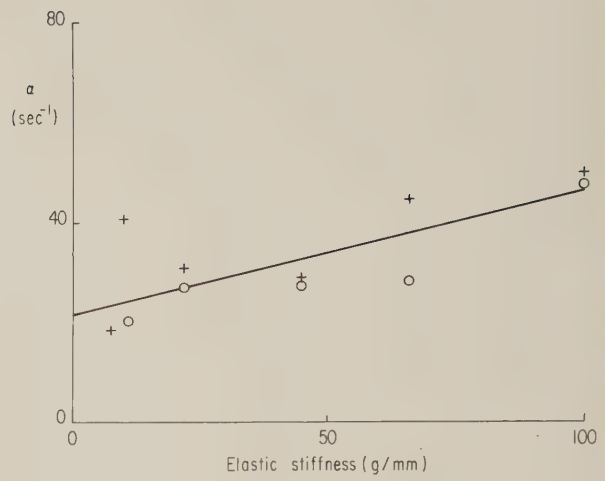

Fig. 2. The effect of varying the stiffness of springs in series with a plantaris muscle on the visco-elastic rate constant (α). Values were obtained before (+) and after (0) studying the effects of inertial loads. The rate constants were somewhat smaller in the later series, but the best-fitting straight line has been computed using all the data

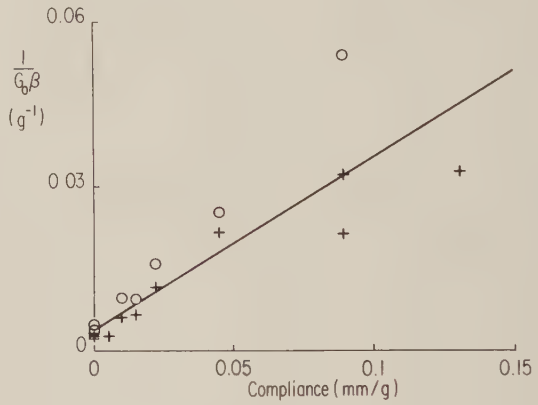

Fig. 3. Effect of varying the compliance ($1/k_e$) of a series spring on the inverse of the product of the low frequency gain (G_0) and active state rate constant (β). Same muscle as in Fig. 2. The gain declined somewhat between the earlier (+) and later (0) series, but again a single best-fitting straight line has been computed for all the data

Table 1. Values of experimentally determined parameters for a visco-elastic model of plantaris muscle in the cat. The values give the means and S.E. of the mean for at least eight experiments. The effective stiffness k of the muscle could be determined in two ways as indicated in the Theoretical section. Values are given in conventional units of grams weight, and after conversion to standard MKS units (see Methods, Bawa *et al.*, 1976)

Parameter	Mean	S.E. of Mean	Units	Corresponding MKS Values	Units
k (from α)	79	19	g/mm	774	N/m
k (from $G_0\beta$)	47	11	g/mm	461	N/m
k_i	380	84	g/mm	3724	N/m
k_p	103	26	g/mm	1010	N/m
B	6.4	1.0	g-sec/mm	63	N-sec/m
C	999	362	g	9.8	N

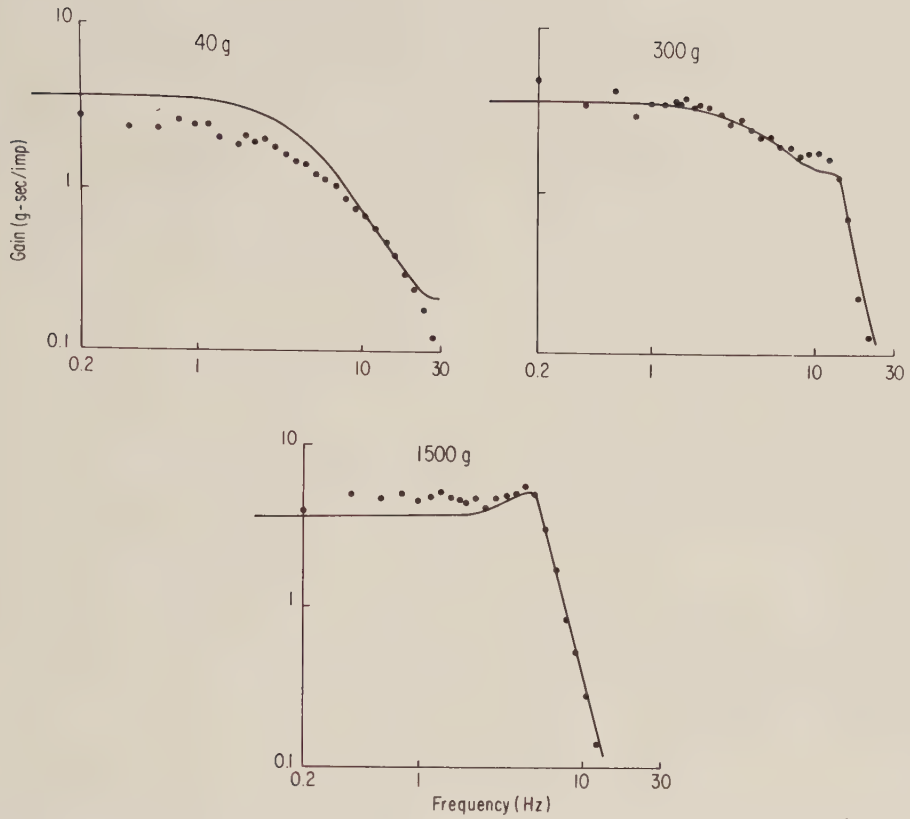

Fig. 4. Comparison of experimental data (·) with predictions (continuous lines) for the effect of adding inertial loads corresponding to the masses indicated. The muscle was also contracting against an elastic load of stiffness 66 g/mm in each part of this Fig. Further explanation in the text

shows such a plot from two series of experimental runs on one plantaris muscle. In between the two sets of runs inertial loads were tested (see below). Because of the large number of stimuli applied and the time elapsed the twitch tensions were smaller for the second set of data (0) compared to the first set (+). However, a straight line has been fitted to all the data, and the ratio of the slope to the intercept is 66 g/mm, which is very close to the value of 63 g/mm obtained independently from the rate constant α (see above).

From the low frequency gain the value of the peak active state tension C can also be obtained from Eq. (14). The value obtained was 300 g which was somewhat higher than the average isometric twitch tension, as one would expect. Higher values of C were obtained in other experiments in which larger animals and fewer stimuli were applied. In Table 1 the values of the parameters determined from a number of experiments are listed.

Inertial Loads. Having determined the parameters of the model, predictions for the responses with inertial loading can be made from Eq. (7) with no undetermined constants. Comparison of experimental results with predictions are shown in Fig. 4 for the gain of the frequency response using an elastic load of 66 g/mm and three different inertial loads. The shapes of the experimental and theoretical curves are in excellent agreement. Small peaks are observed between 10 and 15 Hz for an inertial mass of 300 g and at about 5 Hz for the inertial mass of 1500 g. The predicted peak for the inertial mass of 40 g is above 30 Hz, and would be very small in amplitude compared to the low frequency gain.

For comparison the twitch contractions are shown in Fig. 5 under the same loading conditions. Note the damped oscillations with periods of 70 msec (14 Hz) and 180 msec (5.6 Hz) with inertial masses of 300 and 1500 g respectively. These oscillations result from the interaction of the inertial mass with the elasticity of the muscle and the external spring. The oscillations are damped by the viscosity of the muscle and the external pulley.

The low frequency gains in Fig. 4 differ somewhat from their predicted values. With small inertial masses the data tended to lie below the predicted line whereas with the largest inertial mass, the data tended to lie above the predicted values, when deviations were

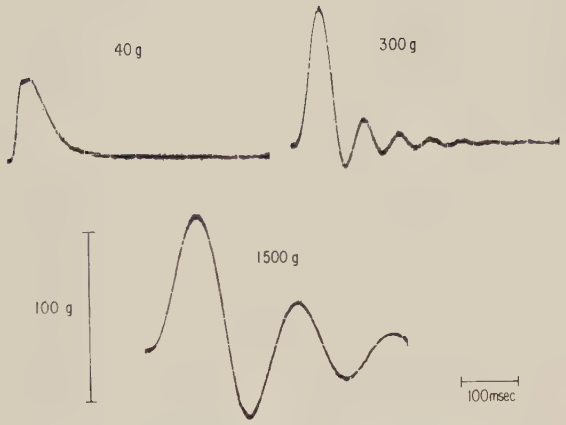

Fig. 5. Effect of inertial load on the twitch of plantaris muscle. Note the damped oscillations which occur with the larger inertial masses indicated on the Fig. The muscle was also contracting against an elastic load of 66 g/mm in each part of this Figure

seen. The reasons for these discrepancies, which were observed consistently, are uncertain. They might arise from the static friction of the pulley which was not included in the analysis. This friction would be less important with the larger forces that are generated against the larger inertial masses. Alternatively, the discrepancies could arise from some non-linearity in muscle which has been ignored by this linear analysis. This remains a topic for future investigation.

Discussion

The results presented here show the substantial predictive power of a simple, linear model of muscle which in many respects goes back to the model introduced by A. V. Hill in 1938. We have used the model to predict the responses of muscle to random stimulus trains under a variety of elastic and inertial loads. Springs in series with the muscle markedly affect the force output of the muscle, whereas inertial loads, as pointed out by Partridge (1966, 1967) have virtually no effect on the low frequency responses. The responses do fall off sharply at high frequencies and the upper frequency limits are progressively reduced with increasing inertial masses. For example, in Fig. 4 the response with an inertial mass of 1500 g declined to 0.1 g-sec/impulse at 14 Hz, compared to 30 Hz with an inertial mass of 40 g. However, even with the largest inertial mass used which is probably close to the upper limit normally experienced by the muscle, as calculated from values given by Grillner (1972), the response was still large up to 6 Hz. The range from 0 to 6 Hz includes the major frequency components of most movements. Thus, to the extent that our results apply to the normal, asynchronous pattern of activation, muscles appear to generate the forces required to produce most normal movements demanded by the nervous system despite wide variations in inertial loads. This ability follows, not from any special internal feedback or other mechanisms for inertial compensation, but rather from a simple model in which the visco-elastic and active state elements limit the response at low frequencies, and inertial masses within physiological limits only affect the response to higher frequencies.

Higher frequency components will be present when brief external disturbances or single electrical stimuli are applied. With the intermediate mass of 300 g damped oscillations in the twitch were observed which were close to the tremor frequency of cat muscles (Lippold, Redfearn and Vučo, 1958). This observation does *not* imply that physiological tremor is normally caused by muscle properties, but it does highlight the fact that muscle properties must be carefully studied before ascribing other causes to the generation of tremor (see also Stein and Oğuztöreli, 1976).

Methods were also developed whereby all the parameters of the model could be evaluated experimentally. We already noted that the values of active state tension produced in response to a stimulus were consistent with the twitch tension, although both were much smaller after 10000 or more stimuli than would be produced by a fresh muscle. The effective stiffness of the muscle was measured in two ways which produced consistent values (Table 1).

The overall stiffness of the muscle could be further subdivided into a series and a parallel elastic component and a viscous element. The magnitudes of these components have not been measured for plantaris muscle using conventional methods. Values are available in the literature for soleus muscle (Rack and Westbury, 1969; Joyce *et al.*, 1969; Grillner, 1972), but the non-linearities present in this muscle (Bawa *et al.*, 1976) prevented a full analysis with linear methods. Nonetheless, certain characteristic differences were noted between the two muscles under isometric conditions. The natural frequency of soleus was only 1 Hz, rather than 5 Hz for plantaris (Mannard and Stein, 1973), while the damping ratio was similar for the two muscles. This suggests that both rate constants were reduced, i.e., the active state decays more slowly in soleus muscle and the visco-elastic rate constant is less. This second rate constant depends on the ratio of the stiffness of the muscle to its viscosity [Eq. (11)]. Joyce and Rack (1969) measured the series stiffness of soleus muscle using small length changes and obtained values which from their Fig. 9 varied between 250 and 600 g/mm for the tensions studied here (200–500 g). Their values are in good agreement with our results for plantaris muscle (Table 1). This implies that the lower

visco-elastic rate constant for soleus may arise from a larger viscosity, although the magnitudes of the viscous components are not well studied for either muscle. To verify this implication would require further experimental work using methods such as those of Joyce *et al.* (1969) and Joyce and Rack (1969).

This study was supported in part by grants to Dr. Stein from the Medical Research Council of Canada and the Muscular Dystrophy Association of Canada.

References

Bawa, P., Mannard, A., Stein, R. B.: Effects of elastic loads on contractions of cat muscles. Biol. Cybernetics **22**, 129—137 (1976)

Grillner, S.: A role for muscle stiffness in meeting the changing postural and locomotor requirements for force development by the ankle extensors. Acta physiol. scand. **86**, 92—108 (1972)

Hill, A. V.: The heat of shortening and the dynamic constants of muscle. Proc. roy. Soc. (Lond.) B **126**, 136—195 (1938)

Houk, J. C., Cornew, R. E., Stark, L.: The model of adaptation in amphibian spindle receptors. J. theor. Biol. **12**, 196—215 (1966)

Joyce, G. C., Rack, P. M. H.: Isotonic lengthening and shortening movements of cat soleus muscle. J. Physiol. (Lond.) **204**, 475—491 (1969)

Joyce, G. C., Rack, P. M. H., Westbury, D. R.: The mechanical properties of cat soleus muscle during controlled lengthening and shortening movements. J. Physiol. (Lond.) **204**, 461—474 (1969)

Lippold, O. C. J., Redfearn, J. W. T., Vučo, J.: The effect of sinusoidal stretching on the activity of stretch receptors in voluntary muscle and their reflex responses. J. Physiol. (Lond.) **144**, 373—386 (1958)

Mannard, A., Stein, R. B.: Determinations of the frequency response of isometric soleus muscle in the cat using random nerve stimulation. J. Physiol. (Lond.) **229**, 275—296 (1973)

Partridge, L. D.: Signal-handling characteristics of load-moving skeletal muscle. Amer. J. Physiol. **210**, 1178—1191 (1966)

Partridge, L. D.: Intrinsic feedback factors producing inertial compensation in muscle. Biophys. J. **7**, 853—863 (1967)

Rack, P. M. H., Westbury, D. R.: The effects of length and stimulus rate on tension in the isometric cat soleus muscle. J. Physiol. (Lond.) **204**, 443—460 (1969)

Stein, R. B., Oğuztöreli, M. N.: Tremor and other oscillations in neuromuscular systems. Biol. Cybernetics **22**, 147—157 (1976)

Prof. R. B. Stein
Dept. of Physiology
University of Alberta
Edmonton, Canada T6G 2H7

Biol. Cybernetics 22, 147—157 (1976)
© by Springer-Verlag 1976

Tremor and Other Oscillations in Neuromuscular Systems

R. B. Stein and M. N. Oğuztöreli

Departments of Physiology and Mathematics University of Alberta, Edmonton, Canada

Received: September 5, 1975

Abstract

A model has been analyzed which is based on recent experimental evidence concerning the properties of muscles and the sensory feedback pathways from muscles. Damped oscillations can arise in the absence of sensory feedback due to the interaction of a muscle with inertial loads. These mechanical oscillations can have a wide range of frequencies depending on the inertial and elastic loads that are attached to the muscle. Small amounts of sensory feedback will tend to reduce deviations from a steady muscle length, but larger amounts of feedback can produce oscillations. The frequency of these reflex oscillations is determined by the properties of the muscle and feedback pathway, and is rather independent of load. If the strength of the sensory feedback is sufficient, either the mechanical oscillations or the reflex oscillations or both can grow, rather than decay, with time. The growth of these oscillations is limited by saturation non-linearities in the muscle receptors and the muscle itself, so that the oscillations approach a steady amplitude and frequency. Using typical properties of muscles and spinal reflex pathways, the frequency of reflex oscillations will be within the range 8–12 Hz found for physiological tremor. With the longer latency found for supraspinal reflexes, oscillations will occur in the range 4–6 Hz which is characteristic of Parkinson's and cerebellar diseases. The role of longer latency reflexes in the generation of these tremors is discussed.

Introduction

The reflex mechanisms which stabilize a limb during a maintained posture may also be responsible for physiological tremor (Lippold, 1970). This possibility arises from the fact that there are substantial delays in the feedback from muscle so that at certain frequencies (8–12 Hz) the feedback is sufficiently delayed that it adds to the next phase of the movement, rather than resisting the phase that produced it. However, the finding that there are centers in the brain (i.e. the inferior olive) which tend to produce oscillations at about 10 Hz (Armstrong, 1974) casts some doubt on the hypothesis that physiological tremor at 10 Hz has a reflex origin. Oscillations in the inferior olive become much more prominent, even in the absence of sensory feedback, after administration of drugs which enhance tremor (Llinás and Volkind, 1973).

Recent work has indicated that the important reflex in the maintenance of posture may not be the traditional spinal stretch reflex. During the course of evolution other, more powerful and flexible reflexes have developed which involve higher centres such as motor cortex (Phillips, 1969; Melvill Jones and Watt, 1971; Evarts and Tanji, 1974; Milner-Brown *et al.*, 1975). These "longer loop reflexes" have greater delays and hence may produce oscillations at lower frequencies. Interestingly, in Parkinsonian patients, who typically show a prominent tremor at 4–6 Hz, these long loop reflexes are greatly enhanced, particularly at rest (Lee and Tatton, 1975). At the same time there is strong evidence for the central generation of Parkinsonian tremor (Lamarre and Cordeau, 1967).

To summarize the current state of knowledge, in both physiological and pathological types of tremor there is some indication that the oscillations are centrally generated within the nervous system. However, there are also sensory feedback pathways which can cause some types of oscillation, although the nature of the reflexes (spinal or supraspinal) and the extent of reflex involvement is uncertain. This uncertainty arises to some extent from the difficulty in doing experiments which assess quantitatively and critically the role of these reflexes.

We thought it might be important to consider from a theoretical viewpoint the conditions under which reflexes, interacting with skeletal muscles, can give rise to oscillations. There are also substantial difficulties in dealing with this problem in a general mathematical way, so we have restricted our analysis here to specific examples which could be compared with experimental results. We have also restricted our attention to the peripheral factors involved in oscillatory movements, because there is not yet sufficient information about central pattern generators in mammalian systems to warrant a detailed theoretical study, although a number of general models have been proposed for small invertebrate systems (e.g. Wilson, 1966; Stein *et al.*, 1974; Perkel and Mulloney,

1974). This paper deals with the more biological implications of such an analysis. The more mathematical aspects will appear elsewhere (Oğuztöreli and Stein, 1975).

The results are organized in the following way: first, we consider qualitatively a block diagram of reflex pathways, and the simplifications such a block diagram necessarily entails. Secondly, we consider the mechanical component (muscle and load) of the diagram in more detail. Thirdly, we consider the interaction of mechanical and reflex factors in the generation of tremor, and finally we consider the nonlinearities that limit the magnitude of these oscillations.

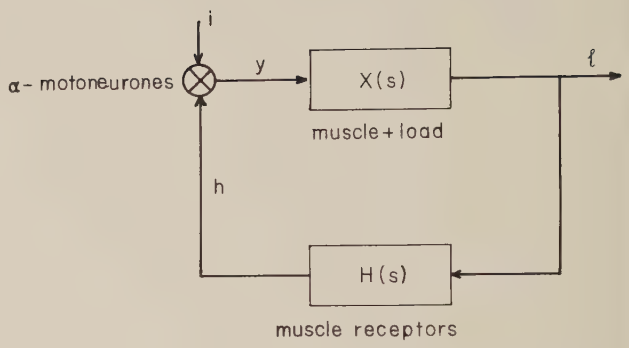

Fig. 1. Block diagram of a feedback pathway involving the properties of a muscle and its load $X(s)$ and the dynamics of the muscle receptors and their associated reflex pathways, $H(s)$. Motoneurones sum central inputs i and sensory feedback h to provide an input y to the muscle. The output of the muscle is considered here as length l

Results

The tremor one observes in a normal limb depends on muscle properties (Lippold, 1970) and can be greatly modified by changing the load against which a muscle is working (Joyce and Rack, 1974). Therefore, any adequate model must contain a description of muscle properties and the effects of loads on these properties, as shown in Fig. 1. In addition, sensory feedback via one or more pathways can modify motoneuronal activity and must be included in a model of reflex oscillations. Thus, the block diagram of Fig. 1 contains the bare essentials of a model for reflex oscillations. It is greatly simplified in that:

1) higher centres are not considered except insofar as they supply inputs, for example in the production of voluntary movements, or to the extent that they are involved in longer sensory feedback pathways which eventually impinge on α-motoneurones.

2) There are several types of sensory receptors, and these have various reflex connections. Furthermore, the properties of both primary and secondary muscle spindle afferents are under control of higher centres through the γ-motoneurones (Matthews, 1972). These complexities are all lumped into a single box, but in a theoretical study the effect of changing the gain and form of this feedback can be investigated to evaluate possible errors. The results will be valid for conditions where the "γ-bias" remains constant, but a more complex model would be necessary to account for voluntary movements in which inputs to γ- as well as α-motoneurones are changing continuously with time (Houk, 1972).

3) The α-motoneurones are considered as a simple summing point. Poppele and Terzuolo (1968) showed that they do not modify the dynamics of a reflex, at least for frequency components up to 6 Hz. To the extent that this is not valid at other frequencies, the dynamic properties of the α-motoneurones could be included in the form of the sensory feedback transfer function $H(s)$.

4) The properties of the components have been specified in Fig. 1 by transfer functions such as $H(s)$, where s is the Laplace variable. This assumes that one can use *linear* techniques such as the Laplace transformation. The assumption of linearity should be valid for small oscillations, such as in physiological tremor, but non-linearities will be considered in later sections for larger oscillations.

Despite its simplifications a block diagram of this sort is often included in texts (Houk and Henneman, 1974) and review articles (Stein, 1974) dealing with motor control, but it is only in recent years that the relevant transfer functions have been measured experimentally. Using these measured values the implications of this model can now be accurately assessed.

1. Oscillations Arising from the Interaction of a Muscle with its Load

Under *isometric* conditions the forces produced by muscles in frogs (Wong, 1972), cats (Mannard and Stein, 1973) and man (Aaron and Stein, 1976) in response to randomly applied stimulus trains, are well fitted by the transfer function of a linear, second-order system, namely

$$G(s) = \frac{G_1}{(s+\alpha)(s+\beta)} \tag{1.1}$$

where G_1 is a constant. The two real rate constants α and β represent two processes which are rate-limiting in the generation of force by a muscle. Recent work (Stein and Wong, 1974; Bawa *et al.*, 1976a) indicates that one of these processes corresponds to the decay

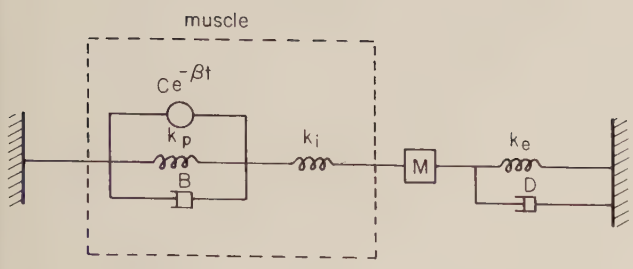

Fig. 2. Schematic representation of a muscle with various types of external loads (from Bawa *et al.*, 1976b). An "active state" element produces a contractile force C which decays with rate constant β following a stimulus. The muscle contains a viscous element B and parallel (k_p) and internal (k_i) series elastic elements which interact with external loads which may consist of a mass M, a spring k_e and a dashpot D

of the active state in A. V. Hill's (1938) terminology. The second rate constant α increases when elastic loads of increasing stiffness are placed in series with a muscle. This increase would be expected if the rate constant α were visco-elastic in nature. The model shown in Fig. 2 for a muscle working against an external elastic load (k_e), an inertial load (M) and a viscous load (D) was therefore proposed (Stein and Wong, 1974) and tested experimentally (Bawa *et al.*, 1976b). When only a pure *elastic* load (a spring) is present, the transfer function remains of second-order. The rate constant α is given by Bawa *et al.* (1976a)

$$\alpha = \frac{1}{B}\left\{k_p + \frac{k_i k_e}{k_i + k_e}\right\} \tag{1.2}$$

and

$$G_1 = \frac{k_i k_e C}{B(k_i + k_e)}. \tag{1.3}$$

The force generated by the muscle to a synchronous volley of nerve impulses (the twitch response) should be given by

$$g(t) = \frac{G_1}{\beta - \alpha}(e^{-\alpha t} - e^{-\beta t}) \tag{1.4}$$

if the muscle behaves linearly and $\alpha \neq \beta$. If $\alpha = \beta$ Eq. (1.4) becomes

$$g(t) = G_1 t e^{-\alpha t} \tag{1.5}$$

Equations (1.4) and (1.5) are well-known functions which are illustrated in Fig. 3. To obtain these equations, we assumed that the volley of nerve impulses can be treated mathematically as a Dirac δ-function. The function $g(t)$ is then referred to as the *impulse response*, which is the inverse Laplace transform of the transfer function (Milsum, 1966) and can be found in any table of Laplace transforms (e.g. Selby, 1969).

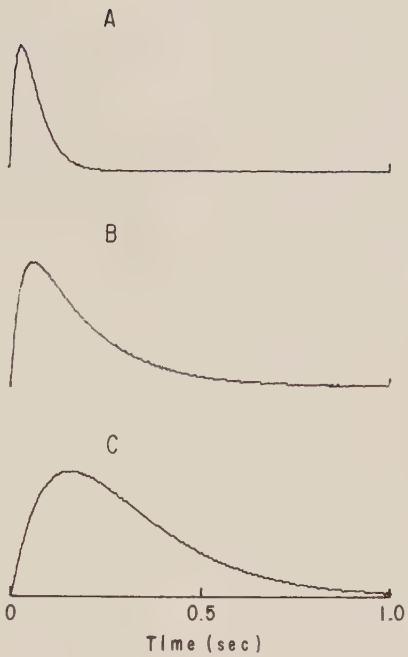

Fig. 3. Impulse responses (twitches) for second-order systems. In A) $\beta = 30\,\text{sec}^{-1}$ and $\alpha = 34\,\text{sec}^{-1}$, which corresponds to the values measured in the experiment shown in Fig. 5 of Bawa *et al.* (1976b) for a plantaris muscle contracting against an elastic load of 66 g/mm. In C) $\beta = 6\,\text{sec}^{-1}$ and $\alpha = 7\,\text{sec}^{-1}$ which corresponds more to the values for a slow muscle (soleus) under similar conditions. Part B) shows a hypothetical situation in which α and β are quite different ($\beta = 6$, $\alpha = 34$) so that the twitch has a fast rising phase and slow decay phase. The twitch heights have been set to the same value in each part for ease of comparison

With elastic loads, the length of the muscle and the force it generates are linearly related and the displacement of a muscle (assuming it is initially at a position $x = 0$), will be given by

$$x(t) = \frac{-X_1}{(\beta - \alpha)}(e^{-\alpha t} - e^{-\beta t}) \tag{1.6}$$

when $\alpha \neq \beta$

$$x(t) = -X_1 t e^{-\alpha t} \tag{1.7}$$

when $\alpha = \beta$. In either case $X_1 = G_1/k_e$ (Bawa *et al.*, 1976b).

Notice that the muscle will shorten as it develops contractile force so that a minus sign is required in Eqs. (1.6) and (1.7). Alternatively, as has been done in the Figs., muscle shortening, rather than extension, can be treated as a positive quantity. A negative sign is then required for the effect of the sensory feedback from a shortening muscle onto motoneurones. In either case, the block diagram of Fig. 1 represents a negative feedback system, the simplest example of which is the classical, monosynaptic stretch reflex.

Another important point, which arises from these equations and is illustrated in Fig. 3, is that *the muscle will not generate oscillations on its own when contracting against elastic loads.* It will, of course, respond in an oscillatory fashion if it receives oscillatory inputs and in the absence of sensory feedback, the shortening for any arbitrary input $i(t)$ can be predicted using well-known properties of linear systems.

In general a muscle will contract, not against a pure elastic load, but against loads which include viscous and inertial elements. These elements include other muscles, the limb itself, and any load the limb may be supporting. As may be understood intuitively from Fig. 2, the interaction of the muscle, considered as a second-order system, working against an external mass-spring system, which is also of second-order, will produce a fourth-order system. The transfer function $X(s)$ between nerve impulses as an input and muscle length as an output is then given by Eq. (5), (Bawa *et al.*, 1976b)

$$X(s)=\frac{-X_1}{(s+\beta)(s^3+as^2+bs+c)} \tag{1.8}$$

where, in terms of the model of Fig. 2,

$$a=\frac{k_i+k_p}{B}+\frac{D}{M}, \tag{1.9}$$

$$b=\frac{D(k_i+k_p)+B(k_i+k_e)}{MB}, \tag{1.10}$$

$$c=\frac{k_pk_i+k_pk_e+k_ek_i}{MB}, \tag{1.11}$$

$$X_1=\frac{k_iC}{MB}. \tag{1.12}$$

Since the quantities a, b and c are all positive, it follows easily (D'Azzo and Houpis, 1966) that the responses will always be stable, i.e. they will not grow indefinitely with time. The roots of the cubic expression in Eq. (1.8) can be determined by standard procedures (see Appendix). There must be at least one real root, but there may also be a pair of roots which are complex conjugates and will give rise to damped oscillatory solutions. The conditions for oscillatory solutions can be given in terms of the parameters a, b, and c (Selby, 1969).

Finally, the inverse Laplace transform of Eq. (1.8) can be found from a standard table, which gives the predicted impulse response (the muscle twitch). Numerical results using procedures described in the Appendix are shown in Fig. 4 for conditions identical to those studied experimentally by Bawa *et al.* (1976b). The parameters of the model in Fig. 2 had been determined experimentally using elastic loads and used to predict the responses for various inertial loads. The good agreement between the experimental and theoretical results is apparent, although the computed solutions were often somewhat more or less damped than the experimental curves. In general, as the mass is increased the frequency of oscillation declines and the rate at which the oscillation dies away decreases. This is shown systematically in Fig. 5 where the frequency of oscillation is plotted as a function of mass M and external elasticity k_e. The frequency of oscillation was determined after computing the roots of the cubic factor in Eq. (1.8) as described in the Appendix.

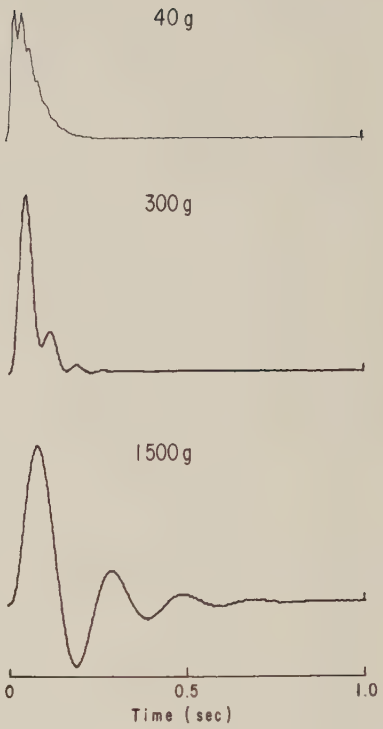

Fig. 4. The effect of mass (values indicated above) on the computed twitch for a plantaris muscle. The masses are indicated on the Fig. for comparison with the experimental results of Fig. 5 of Bawa *et al.* (1976b). The values of the parameters which were used in the calculations were those measured independently in that experiment using elastic loads: $k_i=220$ g/mm, $k_p=90$ g/mm, $k_e=66$ g/mm, $B=4.1$ g-sec/mm, $D=0.05$ g-sec/mm, $\beta=30\,\text{sec}^{-1}$ (see Fig. 2 for the definition of the parameters)

It is important to understand the basis of these oscillations. They arise from the mechanical system in series with the muscle in Fig. 2, not from the muscle itself. A mass M and a spring k_e constitute an oscillatory system with a natural frequency equal to $\sqrt{k_e/M}$. For comparison, the lower solid lines in both parts of Fig. 5 give the expected responses for a

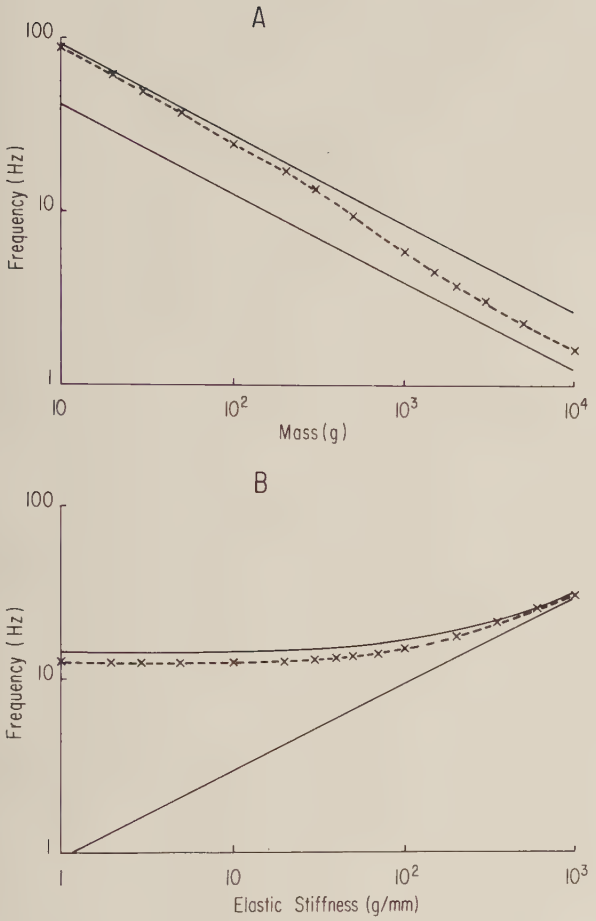

Fig. 5. Frequency of mechanical oscillations arising from the interaction of a mass and an external spring with a muscle, as a function of A) the size of the mass or B) the stiffness of the spring. The data points were computed for the same conditions as Fig. 4 and are plotted on double logarithmic coordinates. The solid lines give two simple approximations which are mentioned in the text and considered further in the Appendix. They serve as upper and lower bounds for the values in this Fig. For all points in A) $k_e =$ 66 g/mm and for all points in B) $M = 300$ g

mass-spring system. Note that the added stiffness of the muscle tends to increase the frequency of oscillation. Also shown in Fig. 5 are the expected results if the natural frequency ω were given by

$$\omega = \sqrt{(k_e + k_i)/M} \,. \tag{1.13}$$

The rationale behind this equation is given in the Appendix. It provides an upper bound on the frequencies of oscillation in this Fig. The rate at which the oscillations decay away is not shown in Fig. 5, but the rate may be either increased or decreased by the presence of the muscle.

As the external stiffness is increased the two approximations converge (Fig. 5B) and the frequency of oscillation approaches that of a simple mass-spring system. This was observed experimentally by Joyce and Rack (1974). A final point to note is that oscillations of a wide range of frequencies can be produced from the interaction of a muscle with its load. This possible source of oscillations must be eliminated before concluding that oscillations in the body arise from reflex mechanisms or from central pattern generators.

2. Oscillations in a Linear Reflex Model

Muscle receptors are well-known to respond to the length l and velocity $\dot{l}$ of a muscle, and the transfer function will be assumed to be (Matthews and Stein, 1969)

$$H(s) = H(s+\gamma)e^{-st_0} \tag{2.1}$$

where t_0 represents all the time delays around the feedback loop. The parameter γ has the dimensions of a rate constant ($\sec^{-1}$). Its value gives the frequency in radians/sec at which the length response and the velocity response of the muscle receptors are equal (Matthews and Stein, 1969). More complex transfer functions have also been derived (Poppele and Bowman, 1970) for the cat and for human muscle spindles (Poppele and Kennedy, 1974), but these will not be considered here. We will also assume, as mentioned in the Introduction, that the muscle receptors determine the dynamics of the feedback loop. This point has recently been verified with human subjects during normal voluntary contractions (Bawa and Stein, in preparation).

The advantage of these particular assumptions is that we can then write for the feedback h as a function of time

$$h(t) = H_1[\gamma l(t-t_0) + \dot{l}(t-t_0)] \,. \tag{2.2}$$

Equation (2.2) is easily obtained from Eq. (2.1) using the properties of Laplace transforms and the notation shown in Fig. 1. This feedback will sum with other inputs to the motoneurones which will give an output $y(t)$, where from Fig. 1

$$y(t) = i(t) + h(t) \,. \tag{2.3}$$

Then, using the standard techniques of linear analysis, the length of the muscle is given by

$$L(s) = Y(s)X(s) \tag{2.4}$$

or

$$l(t) = \int_0^t y(t)x(t-u)\mathrm{d}u \tag{2.5}$$

where $x(t)$ is obtained by taking the inverse Laplace transform of an Eq. such as (1.8). In order to compare

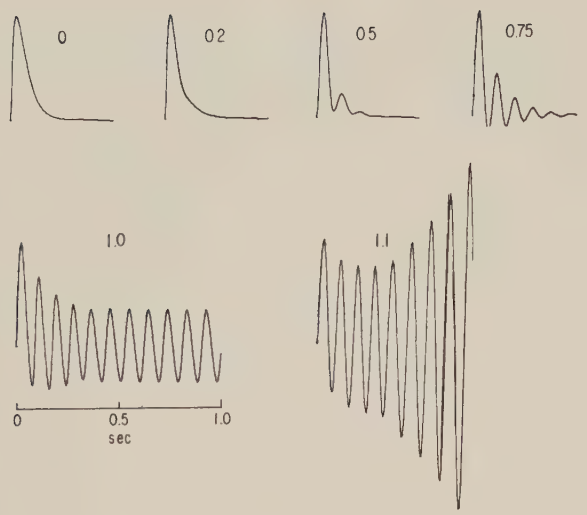

Fig. 6. The effect of increasing sensory feedback on the response to a stimulus pulse. The parameters are the same as those used in Fig. 3 for plantaris muscle (i.e. no added mass, and hence no mechanical oscillations). The delay around the feedback loop was 30 msec in all parts of the Fig., and the gain of the feedback pathway is indicated on each part, relative to that which produced periodic solutions. The form of the damped oscillations is similar to those observed experimentally (Bawa and Stein, in preparation) for human soleus muscle, although the frequency is higher here because of the differences in muscle speed and delay. See also Lippold (1970) and Joyce and Rack (1974) who show responses of human muscles to brief perturbations

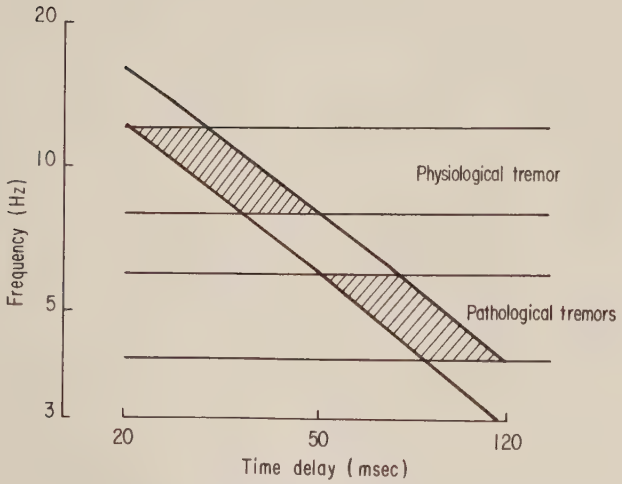

Fig. 7. The frequency of reflex oscillations for different delays in the reflex pathway. The frequencies were calculated for two values of rate constants (see Fig. 3) corresponding to a fast muscle (plantaris, upper line) and a slow muscle (soleus, lower line). Note that for delays (from sensory stimulus to onset of contraction) in the range corresponding to spinal reflexes (20–50 msec) the frequencies are in the range of physiological tremor (8–12 Hz), while for the longer latencies of supraspinal reflexes (50–120 msec) the frequencies are in the range found in Parkinson's disease and cerebellar disorders (4–6 Hz). Both axes are logarithmic

our results with those obtained previously with no feedback ($H_1 = 0$), we will again consider a synchronous volley as our input, which corresponds to letting $i(t)$ be a Dirac delta function. Combining Eqs. (2.2), (2.3), and (2.5) and assuming $i(t)$ is a delta function, we have

$$l(t) = x(t) + H_1 \int_0^t [\gamma l(u - t_0) + \dot{l}(u - t_0)] x(t - u) \mathrm{d}u \,. \quad (2.6)$$

If we assume that $l(t) = 0$ and $\dot{l}(t) = 0$ for $-t_0 < t \leqq 0$ the response will be independent of feedback in the interval $0 < t \leqq t_0$. The values computed for $l(t)$ in this interval can then be used to compute $l(t)$ in the interval $t_0 < t < 2t_0$. This process can be repeated as often as required to predict the responses for various feedback parameters. Figure 6 shows computed results for various values of feedback gain H_1, assuming that $\gamma = 10\ \mathrm{sec}^{-1}$, which corresponds to a corner frequency of about 1.6 Hz (Matthews and Stein, 1969), and $t_0 = 30$ msec (Grillner, 1972). Note that for low values of feedback gain the feedback tends to shorten the twitch response. As feedback gain is increased this shortening becomes more prominent but damped oscillations are also observed. Eventually, with sufficiently high gains, these oscillations increase, rather than decay, with time. The system is then unstable in that the responses to brief inputs do not decay away with time, but continue to increase. This increase will eventually be limited by non-linearities in the system, as will be described later.

The frequency of reflex oscillations is quite independent of feedback gain over the range illustrated (the frequency is between 11 and 12 Hz in all parts of Fig. 6). The frequency of reflex oscillations does depend markedly on the value of the time delay, t_0. Figure 7 shows the effect of increasing the delay in the range from 20 to 120 msec. The shorter values correspond to the traditional spinal stretch reflexes (when conduction delays, synaptic delays and excitation-contraction coupling delays are included). The larger values correspond to longer loop reflexes which probably involve motor cortex. These larger values appear to be the important reflexes functionally (Melvill Jones and Watt, 1971) in normal voluntary movement. Keeping everything else constant, it can be seen from Fig. 7 that increasing the delay from a spinal value (20–50 msec) to a cortical value (50–120 msec) would reduce the frequency of oscillation from that of physiological tremor (8–12 Hz; Lippold, 1970) to that of Parkinson's disease or cerebellar disease (4–6 Hz; Lamarre and Cordeau, 1967). This result, together with the finding that these longer reflex pathways are hyperactive in Parkinsonian patients, even at rest (Lee and Tatton, 1975), led us to consider whether these longer latency pathways

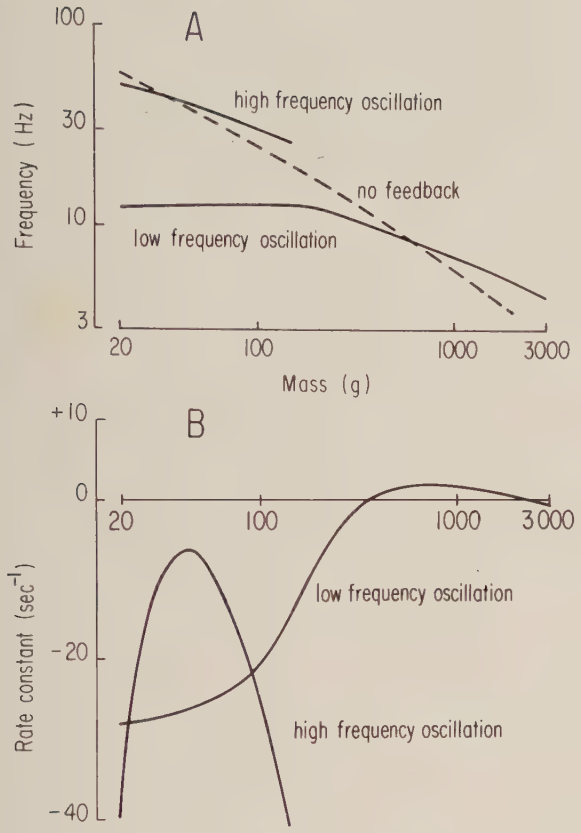

Fig. 8. Interaction of mechanical and reflex oscillations as a function of the mass loading a muscle. The interrupted line in A) shows the frequency of the purely mechanical oscillations which occur in the absence of sensory feedback (see Fig. 5). In the presence of sensory feedback and small masses two sets of oscillations are observed: one at a high frequency near the frequency of the mechanical oscillations mentioned above and a second set of oscillations of reflex origin (with a frequency near 12 Hz). These two types of oscillation change exponentially with the rate constant p shown in B). Positive values of p indicate exponentially growing oscillations and negative values indicate exponentially decaying oscillations. Growing oscillations occur most readily with masses for which the mechanical and the reflex oscillations have approximately the same frequency. The scales for frequency and mass are logarithmic

could be responsible for the Parkinsonian tremor. This topic will be treated in detail in the Discussion.

The reflex oscillations can also interact with the mechanical oscillations, as shown in Fig. 8, and observed experimentally by Joyce and Rack (1974) with human subjects working against various loads. Depending on the reflex gain, both oscillations may be damped or one or both may tend to grow with time. Mathematically, the oscillations were studied by solving for the roots of a transcendental equation (see Methods). A real root r corresponds to an exponential solution e^{rt} while a pair of complex conjugate roots, $r=p\pm qj$, corresponds to an oscillatory solution e^{pt} sin qt. If p is positive, the oscillation will grow, and if p is negative, it will decay. The boundary between these two regions ($p=0$) corresponds to a maintained periodic solution.

Figure 8 shows computed results using a level of gain at which periodic solutions will occur with masses of approximately 360 g or 2400 g. With masses between these values the oscillations will slowly grow with a rate constant of up to $p=2\,\text{sec}^{-1}$. For masses outside this range, the oscillations decay. With masses between 20 and 140 g two frequencies of oscillation are observed which decay with time constants greater than 25 msec ($p<-40\,\text{sec}^{-1}$). One corresponds to the frequency of mechanical oscillation and the other to the frequency of reflex oscillations discussed in preceding sections. The parameters are identical to those used in Fig. 5A with the exception that sensory feedback (with a delay of 25 msec) has been included. The results from Fig. 5A are superimposed on the new results so that they can be compared. Note that the range of masses where growing oscillations are observed corresponds to the region where the frequencies of the reflex and the mechanical oscillations are approximately the same. In principle a feedback system with time delays can give rise to an infinite number of independent oscillatory solutions (Levin, 1964; Oğuztöreli, 1966), but in practice other oscillations than the mechanical and the primary reflex oscillation appear to be of high frequency and to be damped out very quickly.

3. Non-linear Oscillations

The final topic to be considered before discussing these results is the nature of the non-linearities which limit the extent of oscillations. Although muscles behave remarkably linearly when random impulse trains are applied at a given mean rate of stimulation (Mannard and Stein, 1973), the force produced as the mean rate of stimulation is increased is generally a sigmoid function. The maximum or tetanic tension that a muscle can produce at a given length is an obvious saturation non-linearity. Similarly, muscle receptors have a limited range of firing rates which is bounded by zero (no firing) and a maximum value which depends on the refractory periods of the neuron. Muscle spindle afferents also show a high sensitivity for small fluctuations about a mean length and a smaller sensitivity for larger fluctuations (Matthews and Stein, 1969) so a sigmoid function again seems appropriate. A commonly used sigmoid function in

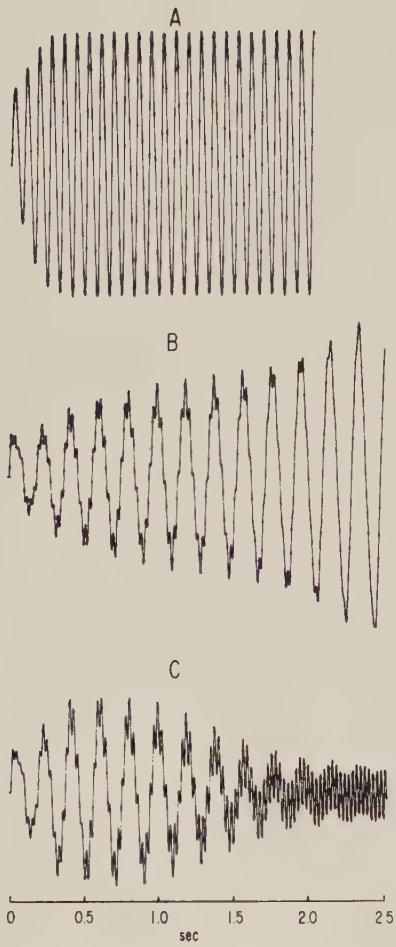

Fig. 9. With non-linear sensory feedback oscillations can grow with time until reaching a stable limit cycle. The parameters in A) are identical to those shown in Fig. 6 except for the inclusion of non-linear sensory feedback and higher gain than illustrated in that Fig. The parameters in B) and C) are identical to those shown in Fig. 4 except that sensory feedback has been included with a reflex delay of 75 msec, and a sufficient gain to produce growing oscillations. Initially, both the slow reflex oscillations (5.7 Hz) grow and the fast mechanical oscillations (38 Hz) grow but B) at one gain level the mechanical oscillations die out while C) at a 25% higher value of gain (H_1) the reflex oscillations eventually decay

neural modelling studies is (Cowan, 1970; Stein *et al.*, 1974).

$$f(z)=(1+e^{-z})^{-1} \tag{3.1}$$

which is bounded between 0 and 1 for all values of some variable z. This function, if substituted for a muscle receptor, would produce a continuous tendency for muscle shortening (because it always has a positive value) which could only be counteracted by a steady negative input, $i(t)$. There is a further justification for including such a negative input in that the region of high sensitivity for muscle spindles is automatically reset about any steady operating point by fusimotor activity (Brown *et al.*, 1969). The maximum sensitivity of the sigmoid function of Eq. (3.1) occurs about $z=0$, but even here it is only 1/4 (i.e. $df(0)/dz=1/4$). To overcome these difficulties, we can let

$$y(t)=h(t)+i(t)$$

$$y(t)=\frac{K}{1+\exp\{-H_1[\gamma l(t-t_0)+\dot{l}(t-t_0)]\}}+i(t). \tag{3.2}$$

If $K=4$, $i(t)=-K/2+\delta(t)$ and $\delta(t)$ is a Dirac delta function, a direct comparison with the previous linear example is possible. The length $l=0$ will then always be a steady-state solution about which the effect of delta function perturbations can be studied. It is easily shown that an equivalent form of Eq. (3.2) is

$$y(t)=\frac{K}{2}\tanh\left\{\frac{H_1}{2}[\gamma l(t-t_0)+\dot{l}(t-t_0)]\right\}+\delta(t) \tag{3.3}$$

where $\tanh(z)$ is the hyperbolic tangent function. Computed solutions are shown in Fig. 9, using techniques described in the Appendix. The numerical values are identical to those of Fig. 6, and the results agree for moderate values of H_1. However, for large values of H_1 the oscillations are bounded and continue indefinitely at a constant amplitude. A proof that the oscillations will always be bounded is included elsewhere (Oğuztöreli and Stein, 1975). The frequency of these maintained non-linear oscillations is not markedly different from the oscillations calculated for the linear model of Fig. 6. Thus, the saturation non-linearities found in muscle receptors (or in muscles themselves) will limit the magnitude of the oscillations but not change their frequency very much. Also shown in Fig. 9 is an example with two distinct oscillations. A small mass of 40 g was used which produces high frequency oscillations which are superimposed on a lower frequency, reflex oscillation (reflex delay = 75 msec). At one level of gain (Fig. 9B) the reflex oscillation becomes dominant, while with a somewhat higher level of gain the mechanical oscillation dominates. We have not observed two maintained, non-linear oscillations, although conditions may exist where this is possible. However, the switching of one type of oscillation to another is interesting, since it is well known that Parkinsonian tremor subsides, and may be replaced by physiological tremor during voluntary movements which generally involve changes in reflex gain. The implications of these results for physiological and pathological tremors will now be discussed.

Discussion

The results presented here distinguish clearly between two types of oscillation: those arising from the interaction of a muscle with its load (mechanical oscillations), and those arising from high gain in a reflex pathway (reflex oscillations). The frequency of the first type of oscillation depends strongly on load whereas that of the reflex oscillations does not. A pure muscle-load oscillation must decay with time in the absence of oscillatory inputs whereas, with the addition of a reflex pathway, maintained and growing oscillations can result. These differences were well demonstrated experimentally in a recent study by Joyce and Rack (1974) on normal human subjects.

We have shown that the traditional spinal reflexes have the right properties to generate the normal physiological tremor for fast or slow muscles (Fig. 7), in line with the suggestions of Lippold (1970) and Joyce and Rack (1974). However, the recent work mentioned in the Introduction, which suggests that the inferior olive can generate rhythms of the appropriate frequency centrally, means that the mechanisms responsible for physiological tremor require further experimental study.

The evidence for the central generation of tremor is stronger in certain pathological states. For example, Joffroy and Lamarre (1971) showed that the 4–6 Hz tremor (in monkeys with lesions intended to mimic Parkinson's disease) was still present after the dorsal roots had been cut and sensory feedback had thereby been eliminated. Also, rhythmic activity at 4–6 Hz could still be recorded from various places in the nervous system after movement had been abolished by curarization (Lamarre and Cordeau, 1967). However, there is also good evidence that the gain of longer loop reflexes is very high in Parkinsonian patients, even at rest (Lee and Tatton, 1975), although the high gain appears to be associated more with the rigidity, rather than the tremor, in this disease. We have shown here that these longer loop reflexes do have the right properties to generate or add to the ongoing tremor at 4–6 Hz. Even if the tremor is generated in the ventro-lateral thalamus (Lamarre and Cordeau, 1967), the high gain of these reflexes may be responsible for the expression of this rhythm through thalamo-cortical pathways. Therefore, a careful experimental study of the interaction of reflex and central mechanisms in these patients would be highly desirable.

This work should provide a firmer theoretical basis for evaluating the various possibilities experimentally.

This study was supported by grants from the National Research Council of Canada (to M.N.O.) and the Medical Research Council of Canada (to R.B.S.). We thank Mrs. M. Willard from the Department of Mathematics, University of Alberta, for valuable assistance in computer programming. Drs. W. Tatton and R. G. Lee of the University of Calgary have kindly given us access to much unpublished data on reflexes and tremor in normal human subjects and Parkinsonian patients. Miss P. Bawa and Dr. T. R. Nichols made helpful suggestions on this manuscript.

Appendix

The mechanical response of a muscle working against an inertial load depends strongly on the cubic polynomial in Eq. (1.8). In general, the roots of the polynomial are a complex function of the parameters of the muscle and load. However, in a special case of interest the polynomial can be factored easily. If $k_i \ll k_e$ (the internal series stiffness of the muscle is small compared to the stiffness of the external load), the cubic polynomial becomes

$$\left(s+\frac{k_i+k_p}{B}\right)\left(s^2+\frac{D}{M}s+\frac{k_i+k_e}{M}\right) \tag{4.1}$$

as can easily be verified by multiplying the factors and comparing the result with Eqs. (1.8)–(1.11). The correct expressions are obtained for the coefficients a and b of the cubic polynomial in Eq. (1.8), but

$$c=\frac{k_pk_i+k_pk_e+k_ek_i+k_i^2}{MB} \tag{4.2}$$

which is greater than the value in Eq. (1.11) to the extent that k_i is non-negligible with respect to k_e. It can also be shown that (4.1) will hold for all k_e if $k_i \ll k_p$, although normally the series elasticity of a muscle is larger, not smaller, than the parallel elasticity.

A common form for a quadratic term (D'Azzo and Houpis, 1966) is

$$s^2+2\zeta\omega_n s+\omega_n^2 \tag{4.3}$$

where

$$\omega_n=\sqrt{\frac{k_i+k_e}{M}} \tag{4.4}$$

is the natural frequency and

$$\zeta=\frac{D}{2\sqrt{M(k_e+k_i)}} \tag{4.5}$$

is the damping ratio of a second-order system. Because of the difference between Eqs. (4.2) and (1.11), Eq. (4.4) will tend to overestimate the natural frequency and Eq. (4.5) will underestimate the damping ratio.

If k_i can be neglected with respect to k_e the muscle is effectively decoupled from its load. The left hand factor in (4.1) depends only on muscle properties and the right hand factor only on the properties of the load. Equation (4.4) becomes

$$\omega_n=\sqrt{\frac{k_e}{M}} \tag{4.6}$$

which is the natural frequency of the load alone. Equations (4.4) and (4.6) have been plotted in Fig. 5. Under these conditions they tend to overestimate (4.4) or underestimate (4.6) the actual frequency of oscillation.

More generally, where the transfer function is of fourth-order, as in Eq. (1.8), it is often simplest to obtain the impulse response from the transfer function numerically. To do this we computed the frequency response function by substituting $s=j\omega$, where $j=\sqrt{-1}$ and ω is a frequency in radians/sec. From the frequency response, the impulse response $x(t)$ can be obtained in an inverse Fourier transform. This transform can be carried out on a small computer efficiently using the fast Fourier transform algorithm (the program used is part of a spectral analysis package described by French and Holden, 1971). If the Fourier transform was done after multiplying the frequency response by $j\omega$, $\dot{x}(t)$ could be obtained because of the relation between the transforms of a function and its derivatives. The impulse response $x(t)$ or $\dot{x}(t)$ was then used to compute the length $l(t)$ in the presence of sensory feedback by numerical integration of the convolution integral of Eq. (2.5). Either the linear form for $y(t)$ from Eqs. (2.2) and (2.3) or the non-linear form from Eq. (3.2) was used in this integration.

Computation of the Time Course of the Responses. The convolution integral (2.5) can be rewritten

$$l(t)=x(t)+\int_0^t h(u)x(t-u)\mathrm{d}u \tag{5.1}$$

where

$$h(u)=H_1[\gamma l(u-t_0)+\dot{l}(u-t_0)] \tag{5.2}$$

from Eq. (2.6) for the linear case, and

$$h(u)=\frac{K}{2}\tanh\left\{\frac{H_1}{2}[\gamma l(u-t_0)+\dot{l}(u-t_0)]\right\} \tag{5.3}$$

from Eq. (3.3) for the non-linear case. Differentiating Eq. (5.1) gives

$$\dot{l}(t)=\dot{x}(t)+\int_0^t h(u)\dot{x}(t-u)\mathrm{d}u \tag{5.4}$$

with the initial conditions $h(t)=l(t)=\dot{l}(t)=0$ for $-t_0<t\leqq 0$. The function $\dot{x}(t)$ for $t>0$ was calculated and stored as indicated above. In the interval above $0<t\leqq t_0$, Eq. (5.4) reduces to

$$\dot{l}(t)=\dot{x}(t)\,, \tag{5.5}$$

Also,

$$l(t)=\int_0^t \dot{l}(u)\mathrm{d}u \tag{5.6}$$

can be easily calculated. From Eqs. (5.5) and (5.6) $h(t)$ can be calculated and stored for the interval $0<t\leqq t_0$.

For $t>t_0$ 1) $\dot{l}(t)$ was calculated step by step from Eq. (5.4), 2) $l(t)$ was calculated from Eq. (5.6), 3) $h(t)$ was calculated from Eq. (5.2) or (5.3), depending on whether the linear or the non-linear case was being considered, and 4) the value of $l(t)$ was plotted and printed out. $h(t)$ was stored for later use and was also printed out. In practise a time interval $\Delta t=5$ msec was used in calculating the convolution integral of Eq. (5.4), and the integral was truncated after $n=t/\Delta t$ steps, where n varied between 60 and 500.

Computation of Roots. Equation (5.1) and (5.2) involve the operations of differentiation, differencing and integration. One operation, namely integration, can be eliminated using standard methods (Oğuztöreli, 1966). The result in this case is a fourth-order differential-difference equation.

$$l^{\mathrm{IV}}(t)+C_3\ddot{l}(t)+C_2\dot{l}(t)+C_1\dot{l}(t)+C_0 l(t)=-X_1H_1[\gamma l(t-t_0)+\dot{l}(t-t_0)]\,. \tag{6.1}$$

Details of this procedure and the constants C_3, C_2, C_1, and C_0 are given elsewhere (Oğuztöreli and Stein, 1975). It can then be shown that for small deviations about $l=0$, Eq. (6.1) can be transformed using the substitution

$$l(t)=\mathrm{e}^{rt} \tag{6.2}$$

which gives the transcendental Eq.

$$\lambda(r+\gamma)\mathrm{e}^{-t_0r}+r^4+C_3r^3+C_2r^2+C_1r+C_0=0\,. \tag{6.3}$$

The roots of Eq. (6.3) can be obtained using a standard FORTRAN routine for the IBM 360 computer system. Similarly, routines are available for computing the roots of cubic polynomials, such as in Eq. (1.8). From Eq. (6.2) it is clear that a real root of Eq. (6.3) corresponds to an exponentially increasing (if r is positive) or decreasing (if r is negative) solution of the original equation. A pair of complex conjugate roots $r=p\pm jq$ corresponds to an oscillatory solution of the form

$$x(t)=\mathrm{e}^{pt}\sin qt\,. \tag{6.4}$$

Further details of the programming may be obtained from either of the authors.

References

Aaron, S.L., Stein, R.B.: Comparison of an EMG controlled prosthesis and the normal human biceps brachii muscle. Amer. J. phys. Med. in press (1976)

Armstrong, D.M.: Functional significance of connections of the inferior olive. Physiol. Rev. **54**, 358—417 (1974)

Bawa, P., Mannard, A., Stein, R.B.: Effects of elastic loads on the contractions of cat muscles. Biol. Cybernetics **22**, 129—137 (1976a)

Bawa, P., Mannard, A., Stein, R.B.: Predictions and experimental tests of a visco-elastic muscle model using elastic and inertial loads. Biol. Cybernetics **22**, 139—145 (1976b)

Brown, M.C., Goodwin, G.M., Matthews, P.B.C.: After-effects of fusimotor stimulation on the response of muscle spindle primary afferent endings. J. Physiol. (Lond.) **205**, 677—694 (1969)

Cowan, J.D.: A statistical mechanics of nervous activity. In: Some mathematical questions in biology. (ed. M.Gerstenhaber) pp. 1—58, Providence, R.I.: American Mathematical Society 1970

D'Azzo, J.J., Houpis, D.H.: Feedback control system analysis and synthesis. New York: McGraw-Hill 1966

Evarts, E.V., Tanji, J.: Gating of motor cortex reflexes by prior instruction. Brain Res. **71**, 479—494 (1974)

French, A.S., Holden, A.V.: Frequency domain analysis of neurophysiological data. Comp. Prog. Biomed. **1**, 219—234 (1971)

Grillner, S.: A role for muscle stiffness in meeting the changing postural and locomotor requirements for force development by the ankle extensors. Acta physiol. scand. **86**, 92—108 (1972)

Hill, A.V.: The heat of shortening and the dynamic constants of muscle. Proc. Roy. Soc. (Lond.) B**126**, 136—195 (1938)

Houk, J.C.: The phylogeny of muscular control configurations. In: Drischel, H., Dettmar, P. (Eds.): "Biocybernetics IV" pp. 125—144, Jena: VEB Gustav Fischer 1972

Houk, J., Henneman, E.: Feedback control of muscle: introductory concepts. In: Mountcastle, V.B. (Eds.): Medical physiology, 13th Edn, pp. 608—616. St. Louis: C.V. Mosby Co. 1974

Joffroy, A.J., Lamarre, Y.: Rhythmic unit firing in the precentral cortex in relation with postural tremor in a deafferented limb. Brain Res. **27**, 386—389 (1971)

Joyce, G.C., Rack, P.M.H.: The effects of load and force on tremor at the normal human elbow joint. J. Physiol. (Lond.) **240**, 375—396 (1974)

Lamarre, Y., Cordeau, J.P.: Étude du méchanisme physiopathologique responsable, chez le singe, d'un tremblement expérimental de type parkinsonian. Actual. Neurophysiol. **7**, 141—166 (1967)

Lee, R.G., Tatton, W.G.: Motor responses to sudden limb displacements in primates with specific CNS lesions and in human patients with motor system disorders. Canad. J. Neurol. Sci. **2**, 285—293 (1975)

Levin, B. Ja.: Distributions of zeros of entire functions. Providence. Amer. Math. Soc. 1964

Lippold, O. C. J.: Oscillation in the stretch reflex arc and the origin of the rhythmical 8–12 c/s components of physiological tremor. J. Physiol. (Lond.) **206**, 359—382 (1970)

Llinás, R., Volkind, R. A.: The olivo-cerebellar system: functional properties as revealed by harmaline-induced tremor. Exp. Brain Res. **18**, 69—87 (1973)

Mannard, A., Stein, R. B.: Determination of the frequency response of isometric soleus muscle in the cat using random nerve stimulation. J. Physiol. (Lond.) **229**, 275—296 (1973)

Matthews, P. B. C.: Mammalian muscle receptors and their central actions. London: Arnold 1972

Matthews, P. B. C., Stein, R. B.: The sensitivity of muscle spindle afferents to small sinusoidal changes in length. J. Physiol. (Lond.) **200**, 723—743 (1969)

Melvill Jones, G., Watt, D. G. D.: Observations on the control of stepping and hopping movements in man. J. Physiol. (Lond.) **219**, 709—727 (1971)

Milner-Brown, H. S., Stein, R. B., Lee, R. G.: Synchronization of human motor units: possible roles of exercise and supraspinal reflexes. Electroenceph. clin. Neurophysiol. **38**, 245—254 (1975)

Milsum, J. H.: Biological control systems analysis. New York: McGraw-Hill 1966

Oğuztöreli, M. N.: Time-lag control systems. New York-London: Academic Press 1966

Oğuztöreli, M. N., Stein, R. B.: An analysis of oscillations in neuromuscular systems. J. math. Biol., **2**, 87—105 (1975)

Perkel, D. H., Mulloney, B.: Motor pattern production in reciprocally inhibitory neurons exhibiting post-inhibitory rebound. Science **185**, 181—183 (1974)

Phillips, C. G.: Motor apparatus of the baboon's hand. Proc. roy. Soc. (Lond.) B**173**, 141—174 (1969)

Poppele, R. E., Bowman, R. J.: Quantitative description of linear behavior of mammalian muscle spindles. J. Neurophysiol. **33**, 59—72 (1970)

Poppele, R. E., Kennedy, W. R.: Comparison between behavior of human and cat muscle spindles recorded *in vitro*. Brain Res. **75**, 316—319 (1974)

Poppele, R. E., Terzuolo, C. A.: Myotatic reflex: its input-output relation. Science **159**, 743—745 (1968)

Selby, S. M.: C. R. C. Standard mathematical tables, 17th ed. Cleveland: Chemical Rubber Co. 1969

Stein, R. B.: The peripheral control of movement. Physiol. Rev. **54**, 215—243 (1974)

Stein, R. B., Leung, K. V., Mangeron, D., Oğuztöreli, M. N.: Improved neuronal models for studying neural networks. Kybernetik **15**, 1—9 (1974)

Stein, R. B., Leung, K. V., Oğuztöreli, M. N., Williams, D. W.: Properties of small neural networks. Kybernetik **14**, 223—230 (1974)

Stein, R. B., Wong, E. Y.-M.: Analysis of models for the activation and contraction of muscle. J. theor. Biol. **46**, 307—327 (1974)

Wong, E. Y.-M.: Theoretical and experimental studies on frog skeletal muscle. M.Sc. Thesis, Department of Physiology, University of Alberta 1972

Prof. R. B. Stein
Dept. of Physiology
University of Alberta
Edmonton, Canada T6G 2H7

Biol. Cybernetics 22, 159—168 (1976)
© by Springer-Verlag 1976

Associative Recall of Images

T. Kohonen, E. Reuhkala, K. Mäkisara, and L. Vainio
Department of Technical Physics, Helsinki University of Technology, Otaniemi, Finland

Received: November 2, 1975

Abstract

Orthogonal projection operations in a linear vector space are shown to have a close relation to the processes by which optimal associative recall of patterned information can be implemented. Two association schemes, the autoassociative mapping and the associative encoding, are introduced. The latter has a bearing on pattern recognition, especially in the recognition of an optical image from a small fragment of it. Analytical expressions for the quality of the recollections are derived, and computerized demonstrations of associative recall with 3024-element optical images are presented. Some preprocessing principles of the images are studied, whereby the two-dimensional Laplacian is found very effective. This finding may have some connection to lateral inhibition effects occurring in biological visual systems.

1. Introduction

The classical concept of associative memory, with relation to information processing, may be understood in many divergent ways (Anderson and Bower, 1973; Longuet-Higgins *et al.*, 1970; Parhami, 1973). Although in the most abstract sense, associative memory is a system of structured relations (Anderson and Bower, 1973), the basic action in the associative recall of a stored item always takes the form of a process which contains a set of input signals or elements, together called the *key*, and some sorts of outcome which constitute the *recollection*. In many papers published on associative memory, no distinction is made between two basic types of associative recall that we would like to call *autoassociative* and *heteroassociative*, respectively. In autoassociative recall, an item is recalled from its fraction, that is, the recollection comprises a set of data elements of which a fraction is used as the key; in heteroassociative recall, arbitrary keys can be paired with arbitrary responses which may also be recalled from fragmentary keys. If this distinction is made, it is possible to recognize many familiar psychological effects, for instance, classical conditioning, stimulus-response relations, and recall of optical images or other stimulus patterns from their fragments, as different forms of the same basic process.

In a series of recent articles (for references, cf. Kohonen and Oja, 1975) it was suggested how elementary forms of spatially distributed associative memory might be implemented in adaptive networks of neuron-like elements. It was demonstrated, too, that orthogonalizing filters which have an important role in this paper may be formed adaptively in neutral networks with recurrent connections (ibid.). In this work no attention is given to possible biological implementations, although the mappings discussed here bear direct relations to such systems. The purpose of the present paper is to demonstrate the existence of associative mappings which provide all data elements with optimal weights, and are accordingly very suitable for the encoding of patterned information, such as optical images. There has been a need for such a theory because in some other models, for instance, in the holographic schemes, background noise amounts high (cf., e.g., Willshaw, 1971). Comparative analysis of noise problems is not included here, however.

2. Autoassociative Mapping

This section discusses a basic mathematical process in which the autoassociative recall of patterns is implemented as an orthogonal projection operation in a linear vector space. It has the property of correcting and standardizing incomplete key patterns towards "memorized" reference patterns, and may result in practical applications, such as the correction of broken fonts in character reading, the filtering of noisy messages, and so on.

2.1. Orthogonal Projections

Patterns composed of n real-valued elements are here represented as vectors in the Euclidean space R^n.

Let there be m discrete patterns denoted by $a_1, a_2, \ldots, a_m \in R^n$ which span a subspace $\mathscr{L} \subset R^n$. An arbitrary vector $a \in R^n$ can be uniquely decomposed into the sum of two vectors $\hat{a} \in \mathscr{L}$, whereby $\hat{a}$ is the orthogonal projection of a on the space $\mathscr{L}$, and $\tilde{a}$ orthogonal to $\hat{a}$. In connection with associative recall, the a_k, $k=1, 2, \ldots, m$ are understood as the "memorized" or *reference patterns*, and a is an arbitrary pattern used as the *key*. It can be stated that $\hat{a}$ is the best linear combination of the a_k that approximates a in the sense of least squares; let us denote

$$\hat{a} = \sum_{k=1}^{m} c_k a_k \tag{1}$$

with c_k being numerical constants. It might be expected that under certain circumstances, one of the terms in $\hat{a}$, say $c_r a_r$, will predominate. This usually occurs when the key a bears a close correlation with the reference pattern a_r. In this case, it is said that a_r is recalled associatively; the other terms in the linear mixture represent noise, with no content of any components other than cross-talk arising from the other reference patterns.

The classical method for the computation of orthogonal projections is the Gram-Schmidt process; for the subspace $\mathscr{L}$ spanned by the a_k, a new orthogonal vector basis is defined by the recursion

$$\tilde{a}_1 = a_1 ,$$

$$\tilde{a}_k = a_k - \sum_{i=1}^{k-1} \frac{(a_k, \tilde{a}_i)}{\|\tilde{a}_i\|^2} \tilde{a}_i \quad (k=2, 3, \ldots, m) , \tag{2}$$

where $(a_k, \tilde{a}_i)$ is the inner product of a_k and $\tilde{a}_i$, and the sum must be taken only over such terms for which $\tilde{a}_i \neq 0$.

If a is now the key vector, the decomposition $a = \hat{a} + \tilde{a}$ which is unique results from the continuation of the above process one step further, $k = m+1$, whereby $\tilde{a} = \tilde{a}_{m+1}$, $\hat{a} = a - \tilde{a}_{m+1}$.

Some other orthogonalizing methods apply the concept of the *pseudoinverse* of a matrix (Albert, 1972).

2.2. The Standardizing Property of the Orthogonal Projection Operation

It can be shown that if the key a is a noisy version of one of the reference patterns a_r,

$$a = a_r + v ,$$

where v is a stochastic error, then in general, $\hat{a}$ is an improved approximation of a_r. This is shown analytically in a simple case in which v has a constant length $\|v\| = v_0$ and a direction that is uniformly distributed in R^n. It is a straightforward matter to generalize the result for the case in which v has an arbitrary radial distribution in R^n, for instance a symmetrical multivariate Gaussian one. The orthogonal projection of a_r on $\mathscr{L}$ is equal to a_r. However, it is shown in Appendix 1 that the projection $\hat{v}$ of v on $\mathscr{L}$ has a distribution with a variance that is m/n times the square of the norm of v, where m is the number of patterns, and n their dimensionality. In other words, the noise occurring in the key pattern is attenuated in the orthogonal projection operation if $m < n$: its standard deviation is

$$\mathrm{var}^{\frac{1}{2}}(\|\hat{a} - a_r\|) = \sqrt{\frac{m}{n}} \, \|a - a_r\| . \tag{3}$$

Sections 2.3.2 and 2.3.3 provide demonstrations of noise attenuation.

One of the central features of associative recall is that elements lacking from a data set that is otherwise complete can be recalled by the rest. The most basic case in the present study, consequently, is that in which a *masked* version of, say, a_r is used as the key a; in other words, a is obtained from a_r by setting a number of its elements equal to zero. The masked portion may be selected at random, whereby $(a_r - a)$ can be regarded as stochastic noise; its statistics, however, depend upon pattern a_r, and are as a result difficult to define. If it is tentatively assumed, again, that the noise attenuation factor is < 1, then $\hat{a}$ is an improved approximation of a_r, and it is said that autoassociative recall of the missing portion has taken place.

It should be noted that the noise attenuation analysis with the spherically symmetrical noise v was carried out with arbitrary a_k. If it is to be transferable, qualitatively at least, to the autoassociative recall from masked patterns, then for preference the a_k should have certain statistical properties; unless this is inherently due, the patterns may be preprocessed by simple means to attain some of these properties (see Section 3.3).

2.3. Demonstrations of Autoassociative Recall of Optical Images

2.3.1. Preparation and Handling of Data. Along with theoretical analysis, the objective of this work was that of demonstrating associative recall of optical images. The study was made feasible as a result of experimental facilities developed within our laboratory during the course of several years; the main features are described in Appendix 3. By the application of

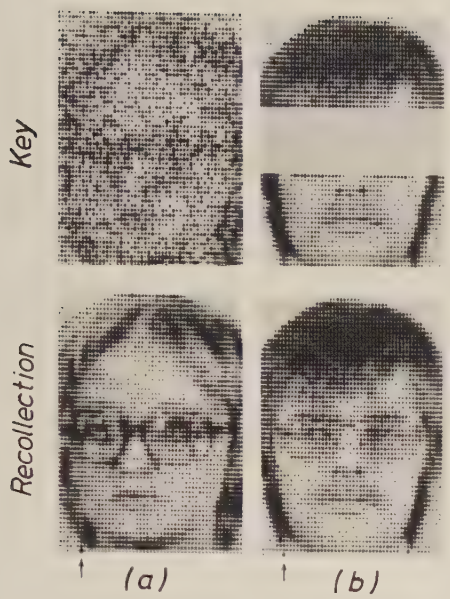

Fig. 1a and b. Standardizing property of the autoassociative mapping with 100 reference patterns. (a) Suppression of white noise superimposed on picture no. 8. The norm of the noise vector was 1.6 times the norm of the pattern vector. (b) Recall of picture No. 9 when a masked version of it was used as the key. (Arrows: see the text)

this system, a test pattern consisting of a few thousand picture elements, discretized to eight gray levels, could be prepared in digital form and transferred to the computer files in about one second. For this study, a rectangular point grid of 54 by 56 elements was chosen. The pictures were treated as 3024-component real pattern vectors. As the apparatus was designed to employ a line-printer as its on-line output device, the spacing of the points in the vertical direction is approximately 3/2 of the horizontal one. For this report, an alternative display method was chosen: by the courtesy of the typesetting company Foto-Set Oy, Helsinki, their phototype-setting machine was used for the preparation of reproductions of the eight-shade pictures, using oval dots with corresponding intensities. All of the test pictures were accepted as they were exposed, and none deliberately rejected from the experiment. Fifty pictures, Nos. 1 through 50, were real shots; the additional ones used in the analysis were mirror images of the originals: tests (see Fig. 4) indicated that they had a linear independence with respect to the originals that was sufficient for the experiment.

2.3.2. Demonstrations of the Standardizing Property and Autoassociative Recall. This section gives pictorial demonstrations of noise suppression and autoassociative recall. In the first one, Fig. 1a, the key was one of the original patterns, with white noise superimposed on all picture elements. The norm of the noise vector was 1.6 times that of the pattern, and the noise was derived from a uniform distribution. There is illustrated the corresponding recollection from a "memory" in which 100 reference patterns were stored, giving a conception of the noise suppression ability of this mapping.

Another experiment in which the key was derived from another pattern, by masking 25% of it, is shown in Fig. 1b.

Associative recall by keys with masking of 50% of the stored patterns (right half) is illustrated in the next series of pictures, Fig. 2. The recollections were multiplied by 2 in order to have as many shades in them as in the original images. The displayed images have a further feature to aid in the judgement of recollections: in the *recollections* only, the lowest row is in reality a "tag field" (see Section 3.2) with dots, counted from the left, that directly correspond to the magnitudes of the coefficients c_k of Eq. (1) in an eight-grade scale. (Actually, no more than only 54 first coefficients were displayed.) Consequently, if the recollection is of good quality, there should be only one intense point in the due position (indicated by an arrow). It should be noted that the lowest grade is also indicated by a tiny dot, although its value may be zero.

2.3.3. Experimental Verification of the Noise Attenuation Law. The noise attenuation, as defined in Eq. (3), was determined when the key was contaminated with white noise derived from a uniform distribution, and with white Gaussian noise, respectively, and represented in Fig. 3. The conclusion drawn from Fig. 3 is that the results of simulation bear reasonable agreement to the theoretical $(m/n)^{\frac{1}{2}}$-law in the case of spherically symmetrical noise (Gaussian), and the results given by the uniform noise, the projection of which is not spherically symmetric, differed only slightly from that.

3. Associative Encoding

If the purpose of associative recall is that of recognition of a stored item, associative mappings can be applied for the generation of characteristic *symbols*, *symbolic codes*, or *tags* for each pattern, according to which the stored items can be identified. This principle may have some bearing upon the way in which the central nervous system processes information; symbols are attached to patterns by simultaneous presentation.

Fig. 2. Autoassociative recall of images when their *right half* was masked off in the key. First row: Six samples of reference patterns. Second row: Recollections from a memory with ten stored patterns. Third row: Recollections from a memory in which 100 patterns were stored (Arrows: see the text)

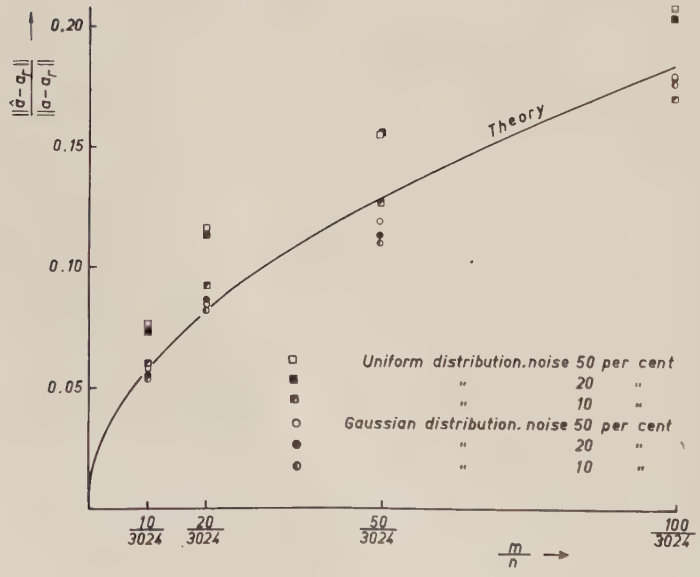

Fig. 3. Verification of the noise attenuation law. White noise was superimposed on a reference pattern, and its attenuation has been represented as a function of the ratio of the number of patterns to their dimensionality, m/n

3.1. Transformation of Patterns Into Symbolic Tags in a Linear Mapping

The simplest tags for patterns consist of unit vectors u_k, or orthonormal coordinate vectors in a Euclidean space R^m, with m the number of patterns. Unit vectors may be understood as representatives of a set of signals in which one signal is active and the others are inactive, respectively. A mapping has to be designed by which every pattern a_k is transformed into the corresponding unit vector u_k. Let us first consider linear transformations. The problem can be formulated as follows: What is the linear (matrix) operator M by which every u_k is obtained as

$$u_k = Ma_k \quad \forall k \in \{1, 2, \ldots, m\}? \tag{4}$$

Denoting

$$U = [u_1, u_2, \ldots, u_m], \; A = [a_1, a_2, \ldots, a_m], \tag{5}$$

Eq. (4) can be put into the form

$$MA = U. \tag{6}$$

A formal solution for M is obtained by means of the pseudoinverse matrix A^+ of A (Albert, 1972), whereby the least-square approximate reads (Kohonen and Ruohonen, 1973)

$$M = UA^+. \tag{7}$$

A convenient algorithm for the computation of UA^+ can be derived from the gradient projection method of Pyle (1967) in the case where exact solutions exist. A generalization of the gradient projection method for approximative solutions has been suggested by Oja (1975).

The operator M is used as follows: if a is an unknown pattern vector which is an approximation of a_r, $r \in \{1, 2, \ldots, m\}$, then $\hat{u} = Ma$ is expected to be an approximation of u_r. The pattern a may be identified as a_r if the largest component of $\hat{u}$ is found at its r:*th* position. To answer the question how this encoding scheme works if incomplete versions of the a_k are used as the keys, $\hat{u}$ is derived into a form which enables direct discernment of the quality of the recollection. If it is recalled that (Albert, 1972) $A^+ = A^+ AA^+$, then $\hat{u} = UA^+ a = UA^+ (AA^+ a)$. Now $AA^+ a = \hat{a}$, since AA^+ is the orthogonal projection operator on the space $\mathscr{L}$ (Albert, 1972). Then, from Eqs. (7), (1), and (4) it follows that

$$\hat{u} = M\hat{a} = \sum_{k=1}^{m} c_k (Ma_k) = \sum_{k=1}^{m} c_k u_k = [c_1, c_2, \ldots, c_m]^T \tag{8}$$

so that the elements of $\hat{u}$ *directly correspond to the relative intensities of the* a_k *in mixture* $\hat{a}$. Conversely, the statistical analysis carried out in Section 2.2 is now directly transferable to the optimal associative encoding problem.

3.2. Association of Symbolic Codes to Patterns by Autoassociative Encoding

It is to be noted that the transformation formalism of Section 3.1 does not necessarily presuppose that a signal-transforming system has the patterns a_k as its inputs and yields the codes u_k at its outputs. In a more natural association scheme, pairs of data sets (a_k, u_k) occur at the inputs of a memory system, whereby the a_k and u_k are memorized by their simultaneous presentation. In the simplest case, the output signals have a topographically similar arrangement. If the inputs are now excited by a pair of patterns (a, u), these signals are transformed into a pair of patterns $(\hat{a}, \hat{u})$ at the output.

In order to analyze autoassociative recall of symbolic codes, the a_k and u_k are first combined into a single vector $a'_k = [a_k^T, u_k^T]^T$ in which all elements are treated equally irrespective of their meaning. If this model has to bear any connection with biological memory, then a similar effect would be the convergence of signals of different modality in the same neural area. The autoassociative encoding is now applied to the augmented pattern vectors a'_k. For example, the Gram-Schmidt process may be carried out on the a'_k to yield the new base vectors $\tilde{a}'_k$. If, during recall, a pictorial pattern a is used as the key, the key vector attains the form $a' = [a^T, 0]^T$. The orthogonal projection $\hat{a}'$ of a' is then expected to contain the missing code; if a was an approximation of, say, a_r, then the recollection in the code part $\hat{u}$ is expected to be an approximation of the unit vector u_r that was associated with a_r.

Actually, the mapping of a into $\hat{u}$ differs slightly from that introduced in Section 3.1: however, if the dimensionality of the a_k is much larger than 1, the error introduced is insignificant, which can be deduced in the following way. Note that u_k takes the form $[0, \ldots, 1, \ldots, 0]^T$, i.e., only one element is nonzero; if, during recall, a is an approximation of a_r then $a' = [a^T, 0]^T$ is an approximation of $[a_r^T, u_r^T]^T$, in which only one more differing element due to u_r is present. If the elements of a_r are of the order of unity, a relative error in the square of the norm of a no larger than of the order of $1/n$ is induced by this approximation. In the processing of images, as a rule n is of the order of several thousands.

Note that in the autoassociative scheme, other symbolic codes or patterns in addition to unit vectors may be used, too.

3.3. Preprocessing of Patterns for Increased Orthogonality

It has become evident that the inherent orthogonality of the stored patterns is a good indicator of the quality of recall and noise attenuation. If the patterns were derived from statistical distributions, and if the picture elements were uncorrelated, the patterns, especially with a large dimensionality, might be rather orthogonal. In practice, however, natural patterns do not have this property except in some special cases, characterized by the following properties: 1. The elements of the a_k have zero mean. 2. The fraction of nonzero elements to zero elements in the a_k is small.

It is always possible to preprocess the patterns before application of memorization mappings. Different kinds of spatial differentiation (cf. Appendix 2) are operations which in general increase the orthogonality. These include, e.g.,

— Formation of the absolute value of the two-dimensional gradient of the patterns, which strongly enhances the border-lines and suppresses plain areas.

— Operation of the patterns by the two-dimensional Laplacian which makes the borders bipolar, and suppresses plain areas.

The effect of different preprocessing methods has been compared in Fig. 4 which indicates the relative norms of the $\tilde{a}_k$ in the Gram-Schmidt process; for good orthogonality, these values should decrease as slowly as possible with successive values of k. It can be seen that the Laplacian is superior to all of the other preprocessing methods discussed.

3.4. Noise Attenuation in Masked Images

Since two pictures may be regarded similar, although one is obtained from the other after multiplication by a constant factor, it may be better to define the noise attenuation characteristics of the mappings in terms of angles between representation vectors than in terms of Euclidean distances. So, the angle between the recollection and a reference pattern ought to be smaller than the angle between the key pattern and the respective reference pattern. Thus the noise attenuation is hereupon defined as

$$K = \frac{arc\ cos\,[(\hat{a}, a_r)\|\hat{a}\|^{-1}\|a_r\|^{-1}]}{arc\ cos\,[(a, a_r)\|a\|^{-1}\|a_r\|^{-1}]}. \tag{9}$$

The noise attenuation factor K was determined with different values of m for test patterns preprocessed by subtraction of the mean, by taking the absolute value of the gradient, and by operation with the Laplacian, respectively. Picture elements were masked off at the right-hand edge to correspond to a noise of 10, 20, and 50%, respectively. The qualitative conclusions drawn from the simulations represented in Fig. 5 are that the factor K may be approximately expressed as constant times $(m/n)^{\frac{1}{2}}$ where the constant depends on the fraction masked off.

3.5. Recognition Experiments

Results obtained from experiments in which images were recognized from their fragments are listed in Table 1. The experiments were conducted by means of autoassociative encoding. Masks were used cor-

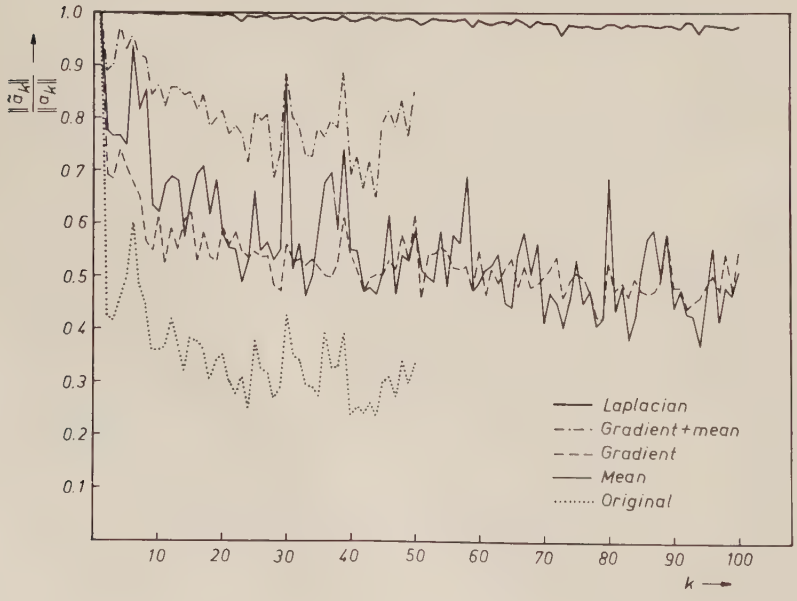

Fig. 4. Norms of successive base vectors obtained in the Gram-Schmidt orthogonalization of photographic images. Original = images were orthogonalized as such. Mean = the mean of the picture elements was subtracted before orthogonalization, Gradient = the absolute value of the gradient was taken. Gradient + mean = after taking the gradient, the mean of it was subtracted. Laplacian = the images were preprocessed by the Laplacian before orthogonalization

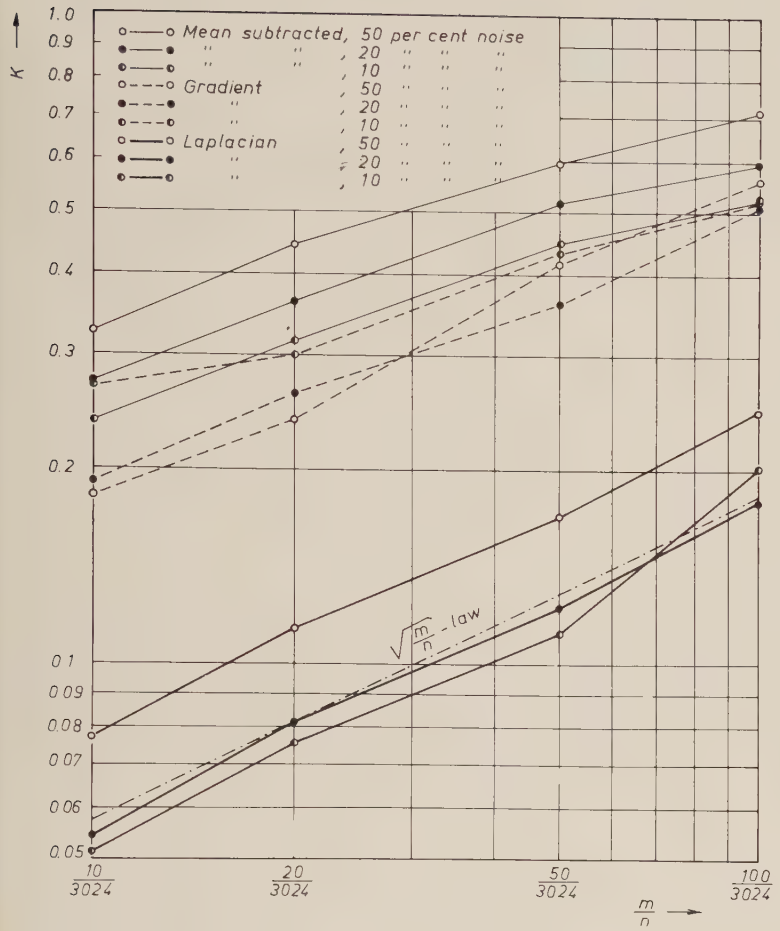

Fig. 5. The noise attenuation factor K defined in Eq. (9) vs. m/n was computed for masked images used as the keys. The difference from the reference patterns due to defects was 10, 20, and 50%, respectively. They were preprocessed by subtraction of the mean, by taking the gradient, and by operation by the Laplacian, respectively

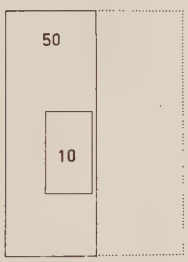

Fig. 6. Fractions (10 and 50%, respectively) of the picture elements used in the keys

responding to fractions of 10 and 50%, respectively, of the picture elements selected for the key, as defined in Fig. 6. The recognition was based upon comparison of the coefficients c_k [Eq. (8)]. It was reasoned that a good criterion for correct recognition was the ratio of c_r, corresponding to the correct image, to the next largest c_k. These numbers are represented in Table 1. It is deducible from the results that recognition of images on the basis of the c_k works well far above the limit where optical recollections are badly degraded.

Although our present experimental program was restricted to about 100 images due to the available memory capacity, it is possible to deduce from Figs. 4 and 5 and Table 1 along with other simulations performed with smaller patterns, that correct recognition from, say, 10% fractions of the images may be possible with more than one thousand stored pictures of this size.

3.6. More Involved Methods for Associative Encoding

Linear encoding methods, which are based upon the comparison of patterns in vector spaces by application of the Euclidean distance measure, may in themselves possess interest in many applications. However, if the number of images m is of the same order of magnitude as their dimensionality n, the nonexistence of solutions to equations $\forall k, u_k = Ma_k$ may introduce a problem. In this case, it is possible artificially to enlarge the dimensionality by preprocessing, or transformation of the primary patterns before they are addressed. In a recent article, Poggio (1975)

Table 1. Ratio of c_r to the next largest $c_{k'}$ (Mean: the mean of the picture elements was subtracted from all elements. Laplacian: the picture and the key were preprocessed by the Laplacian)

Pattern no.	10 reference patterns				100 reference patterns			
	Key 50%		Key 10%		Key 50%		Key 10%	
	Mean	Laplacian	Mean	Laplacian	Mean	Laplacian	Mean	Laplacian
1	9.92	23.79	1.73	5.32	4.93	16.14	1.25	5.19
2	3.16	22.02	1.54	7.01	4.10	19.75	1.24	5.14
3	7.00	63.40	1.62	22.67	4.47	18.95	1.79	7.36
4	8.92	25.89	2.75	9.82	5.82	20.42	2.37	5.64
5	19.53	20.43	1.32	8.93	3.90	15.00	1.30	3.93
6	5.69	58.58	6.10	23.39	8.80	24.47	3.41	6.89
7	4.71	45.85	1.25	6.98	3.89	18.70	1.87	6.19
8	5.54	35.37	2.17	20.26	3.76	12.62	2.37	6.35
9	5.26	21.34	1.93	4.73	6.18	9.36	2.10	4.13
10	7.06	31.89	1.22	25.39	3.73	15.44	1.14	5.65
Average	7.68	34.86	2.16	13.45	4.96	17.08	1.88	5.65

was concerned with an equivalent problem formulated as follows: Between a set of column vectors $\{x^j\}$ which represents a set of input patterns, and another set of column vectors $\{y^j\}$ which corresponds to the set of output patterns associated with the x^j by pairs, there is to be found a transformation T by which every y^j is obtained from the corresponding x^j, either exactly, or approximately in the sense of least squares, as $y^j = T(x^j)$. It should be noted that in a special case, the y^j can be identified with the unit vectors u_k. Poggio takes into consideration polynomial transforms of the type

$$P_k(X) = L_0 + L_1(X) + L_2(X, X) + \ldots + L_k(X, \ldots, X), \quad (9)$$

in which X is a matrix with the x^j as its columns, and L_q, $q = 0 \ldots k$, is a product form of degree q. [Linear transforms were introduced for the same purpose by Kohonen and Ruohonen (1973).] The expression $P_k(X)$ is written explicitly as

$$(P_k(X))_{ij} = (L_0)_{ij} + \sum_{\alpha_1} (L_1)_{i\alpha_1} X_{\alpha_1 j} + \ldots + \sum_{\alpha_1 \ldots \alpha_k} (L_k)_{i,\alpha_1 \ldots \alpha_k} X_{\alpha_1 j} \ldots X_{\alpha_k j}. \quad (10)$$

Poggio then denotes by Y a matrix with the y^j as its columns, and proceeds to devise recursive, corrective processes for the determination of a $P_k(X)$, such that it approximates Y in the sense of least squares.

It is also demonstrable that the basic task, the determination of $P_k(X)$, can be completed more directly, and that the procedure need not be restricted to polynomial forms. Let us define a preprocessing transformation which takes the matrix X into another matrix F with columns $f^j = f(x^j)$. The f^j may be arbitrary vector functions of the x^j, and column vectors of the following form: $[1, X_{1j}, X_{2j}, \ldots, X_{1j} X_{2j}, X_{1j} X_{3j}, \ldots]^T$, occurring in the $P_k(X)$, are special cases of the f^j. The problem is now reduced to determination of a linear form LF which approximates Y in the sense of least squares. Here L is a matrix, for which we have the least-squares solution

$$\hat{L} = Y F^+ \quad (11)$$

in which F^+ is the pseudoinverse of F. Fast recursive algorithms for the computation of $\hat{L}$ are derivable from Cline's lemma (Kohonen, 1974), or the Gram-Schmidt orthogonalization process is applicable direct to the column vectors f^j.

Preprocessing is a standard procedure in pattern-recognition techniques. [For a review, see Andrews (1972).] Furthermore, it may be a commonplace principle in biological sensory systems (cf. Lettvin *et al.*, 1959).

4. Conclusion

It has been demonstrated that a formalism based on optimal linear mappings is of use in the recognition of optical images from their fragments or noisy versions, particularly if the dimensionality of the images is much larger than their number. The analysis of noise tolerance has been rendered practicable by the application of classical results of linear algebra. Moreover, some basic transformations of the pictures, of which mention can be made of operation by the two-dimensional Laplacian, were shown significantly to increase the number of recognizable pictures. As is pointed out in Appendix 2, application of the Laplacian is equivalent to computation of the "source density" of the pictures, whereby it is assumed that

the picture itself represents the potential created by this source density in the sense of Poisson's differential equation. The discrete formulation of Laplacian may have a close bearing upon the lateral signal couplings that occur, for instance, in the biological visual systems.

Appendix 1

Statistics of the Orthogonal Projection of a Spherically Distributed Random Vector

Let $v \in R^n$ be a random vector which, for simplicity, is assumed to have constant length $\|v\| = v_0$ and a direction that has a uniform distribution in R^n. The basic problem is that of determining the distribution of its orthogonal projection v on an m-dimensional Euclidean subspace $\mathscr{L}_m \subset R^n$. It is a straightforward matter to generalize the result for the case in which v has an arbitrary radial distribution. The radial, normalized distribution of v can be written

$$f(\varrho) = S_n^{-1}(v_0)\,\delta(\varrho - v_0)\,, \tag{A1-1}$$

where ϱ is the radial coordinate in R^n, $S_n(v_0)$ is the surface area of an n-dimensional hypersphere with radius v_0, and $\delta(\cdot)$ is the Dirac delta function.

Instead of direct computation of the distribution of the projection $\hat{v} \in \mathscr{L}_m$ which is spherically symmetrical and equivalent to the mass distribution of the projection of the spherical shell defined by $f(\varrho)$, it is equivalent, and simpler, first to compute the mass distribution of the projection of the corresponding homogeneous sphere with radius v_0, and then to differentiate the result with respect to v_0. Denoting $v = \hat{v} + \tilde{v}$, where $\hat{v} \in \mathscr{L}_m$ and $\tilde{v} \perp \hat{v}$, and

$$\|\hat{v}\| = \varrho_m\,,\ \|\tilde{v}\| = \varrho_{n-m}$$

it follows from the orthogonality of $\hat{v}$ and $\tilde{v}$ that

$$v_0^2 = \varrho_m^2 + \varrho_{n-m}^2\,. \tag{A1-2}$$

Primarily we are interested in the mass projection of the homogenous sphere as a function of ϱ_m. This can be understood as the projection on $\mathscr{L}_m$ of all points in R^n which lie inside the original hypersphere and have the coordinate $\hat{v}$. These points are confined in an $(n\text{-}m)$-dimensional homogeneous hypersphere with radius ϱ_{n-m} defined by Eq. (A1-2). The volume of an N-dimensional sphere with radius ϱ is (cf., e. g., Mayer and Goeppert-Mayer, 1940)

$$V_N = \frac{\pi^{N/2}}{\left(\frac{1}{2}N\right)!}\varrho^N \quad \text{for } N \text{ even}\,,$$

$$V_N = \frac{2^N \pi^{(N-1)/2}\left(\frac{1}{2}N - \frac{1}{2}\right)!}{N!}\varrho^N \quad \text{for } N \text{ odd}\,, \tag{A1-3}$$

or, in general, of the form $V_N(\varrho) = \alpha_N \varrho^N$ where α_N is a numerical constant.

The *unnormalized* expression for the mass distribution of the projection is now

$$\mu(\varrho_m) = (v_0^2 - \varrho_m^2)^{\frac{n-m}{2}} \tag{A1-4}$$

from which the required distribution of $\hat{v}$, denoted by $p(\varrho_m)$, is obtained as

$$p(\varrho_m) = \frac{d\mu(\varrho_m)}{dv_0} = (n-m)\,v_0\,(v_0^2 - \varrho_m^2)^{\frac{n-m-2}{2}}\,. \tag{A1-5}$$

The variance of this distribution is

$$\mathrm{var}(\varrho_m) = \frac{\int_0^{v_0} \varrho_m^2 (v_0^2 - \varrho_m^2)^{\frac{n-m-2}{2}} (\varrho_m)^{m-1}\, d\varrho_m}{\int_0^{v_0} (v_0^2 - \varrho_m^2)^{\frac{n-m-2}{2}} (\varrho_m)^{m-1}\, d\varrho_m}$$

$$= v_0^2 \frac{\int_0^1 t^{m+1}(1-t^2)^{\frac{n-m-2}{2}}\, dt}{\int_0^1 t^{m-1}(1-t^2)^{\frac{n-m-2}{2}}\, dt}\,, \tag{A1-6}$$

where $t = \varrho_m / v_0$. From the definition of the *beta function*,

$$B(a,b) = 2\int_0^1 t^{2a-1}(1-t^2)^{b-1}\, dt \tag{A1-7}$$

it then follows that

$$\mathrm{var}(\varrho_m) = \frac{B\left(\frac{m+2}{2}, \frac{n-m}{2}\right) v_0^2}{B\left(\frac{m}{2}, \frac{n-m}{2}\right)}\,. \tag{A1-8}$$

By application of the following formulae (Gradstejn and Ryshik, 1963)

$$B(a,b) = \frac{\Gamma(a)\Gamma(b)}{\Gamma(a+b)}\,, \tag{A1-9}$$

$$\Gamma(a+1) = a\Gamma(a) \qquad (a>0)\,, \tag{A1-10}$$

where $\Gamma(\cdot)$ is the gamma function, there is finally obtained

$$\mathrm{var}(\varrho_m) = \frac{m v_0^2}{n}\,, \tag{A1-11}$$

whereby the standard deviation of $\|\hat{v}\| = \varrho_m$ is

$$\mathrm{var}^{\frac{1}{2}}(\|\hat{v}\|) = \sqrt{\frac{m}{n}}\, v_0\,. \tag{A1-12}$$

Appendix 2

Increasing Orthogonality by Spatial Differentiation of the Patterns

If an arbitrarily selected portion of one picture should á priori be as orthogonal as possible with respect to the same portion in other pictures, it can be reasoned intuitively that the chances of this occurring are higher if only high spatial frequencies occur in the pictures. Functionals which suppress the low frequencies, and thus increase orthogonality, are the spatial derivatives, of which the two of lowest order are the two-dimensional gradient and the two-dimensional Laplacian. Since gradient is a vector entity, it is more convenient to use its absolute value.

The method of differences in a rectangular grid with unity spacing in which the primary pattern is defined, enables computation of the absolute value of the *gradient*, for instance by the following formula: denoting the primary picture elements in the grid by $\xi_{i,j}$, where i is the horizontal and j the vertical index, respectively, and the corresponding picture elements of the transformed picture by $\eta_{i,j}$, respectively, the first differences yield

$$\eta_{i,j} = \sqrt{C^2 + D^2}\,, \tag{A2-1}$$

where $C = \frac{1}{2}(\xi_{i+1,j} - \xi_{i-1,j})$ and $D = \frac{1}{2}(\xi_{i,j+1} - \xi_{i,j-1})$.

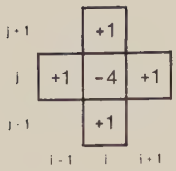

Fig. 7. Grid function

Diagonal differences, or differences averaged over a larger portion of the grid, might also be used.

The *Laplacian* is obtained by the second differences, whereby

$$\eta'_{i,j} = -4\xi_{i,j} + \xi_{i,j+1} + \xi_{i,j-1} + \xi_{i+1,j} + \xi_{i-1,j}. \quad \text{(A2-2)}$$

Another means of description of the Laplacian of Eq. (A2-2) is by regarding it as the two-dimensional *convolution* of the primary picture with the 5-point grid function defined in Fig. 7. Note that the absolute value of gradient and the Laplacian are operators which are circularly symmetrical in polar coordinates, i.e., they do not favour any direction in lines or edges. Consequently the grid function of Fig. 7 can be regarded as a rectangular representation of an annular penumbra around the point (i, j). It may not be too far-reaching a comparison to recall that such penumbrae occur in the biological visual systems where the excitatory receptive fields are surrounded by inhibitory penumbrae. These penumbrae of the visual system are, at least partly, considered as being due to local (short-range) lateral inhibitory effects of the neural networks.

Let the two-dimensional radius vector of the image plane be r, and $\xi(r)$ denote the original picture "field" and $\eta(r)$ the transformed one, respectively. If the grid were regarded continuous, then

$$\eta(r) = \nabla^2 \xi(r) \quad \text{(A2-3)}$$

is the Poisson differential equation that would give the *source density* $\eta(r)$ corresponding to the *scalar potential* $\xi(r)$ it creates. Thus application of the Laplacian in the preprocessing is equivalent to computation of the source density of an image which is then stored.

If the transformed pictures were stored in an autoassociative memory, recollections obtained by fragmentary cues could be operated by the inverse transform, for reconstruction of the original images. It is generally known that the Poisson differential equation has a solution for the potential if the source density is known: note, also, that if the original and the transformed grid point values are denoted by the vectors Ξ and H, respectively, a linear relation exist between them, $\Xi = TH$, where T is a matrix found from Eq. (A2-2). This vector-matrix equation has the best approximative solution $\hat{H} = T^+ \Xi$, where T^+ is the pseudoinverse of T.

Appendix 3

The Facilities Used in the Simulations

All the simulation experiments were carried out on a Nova 1220 minicomputer system provided with a fast hardware floating-point multiplication unit, a disk cassette memory, standard peripherals, and a nonstandard optical input system of our construction (Laine, 1974; Tuominen, 1973). The latter receives the video signal (CCIR type G) from an ordinary *tv*-camera and transforms it into a digital matrix array of maximum size 256 by 256 picture elements. In this demonstration, the frame was 54 by 56 points, discretized to eight gray levels. Digitalization was implemented by a special microprogrammed processor, so an 3024-element integer array representing an image could be prepared and transferred to the master computer in about one second. The size of the core memory was 32 K words, and in addition to system programs, normally only two pattern vectors could be buffered in it at a time.

The simulation programs were run under the Real Time Disk Operating System for the Nova computers, and the primary programming language was Algol. The most critical parts of the programs, for instance, the programs supporting the optical input system, and interfacing with the multiplication unit were coded in the assembly language. The average effective time for a multiplication operation including the overhead time was 120 μ sec. Of this, 70% was spent to data transfers between the disk and core memories and to the latency times. It has been estimated that by extensive alterations of the parallel operations and the use of a faster disk memory, an improvement in speed of about three times of the present could be achieved.

The total computing time can be estimated in terms of multiplication operations, being approximately $m^2 n$ multiplications for the orthogonalization (storage of all patterns), and $2mn$ multiplications for the recall of one pattern. Here n is the dimensionality (3024), and m is the number of pictures stored. For the present, the size of our demonstrations was bounded by the core and disk memories.

References

Albert, A.: Regression and the Moore-Penrose pseudoinverse. New York: Academic Press 1972

Anderson, J. R., Bower, G. H.: Human associative memory. Washington, D.C.: Winston & Sons 1973

Andrews, H.C.: Introduction to mathematical techniques in pattern recognition. New York: Wiley 1972

Gradstejn, I. S., Ryshik, I.: Tablitsij integralov, summ, rjadov i proizvedennyj. Moscow: F.M. 1963

Kohonen, T.: An adaptive associative memory principle. IEEE Trans. Comp. C-**23**, 444—445 (1974)

Kohonen, T., Oja, E.: Fast adaptive formation of orthogonalizing filters and associative memory in recurrent networks of neuron-like elements. Biol. Cybernetics **21**, 85—95 (1976)

Kohonen, T., Ruohonen, M.: Representation of associated data by matrix operators. IEEE Trans. Comp. C-**22**, 701—702 (1973)

Laine, H.: Lic. Techn. Thesis, Helsinki University of Technology, 1974

Lettvin, Y.J., Maturana, H., McCullogh, W.S., Pitts, W.H.: What the frog's eye tells the frog's brain. Proc. IRE **47**, 1940—1951 (1959)

Longuet-Higgins, H.C., Willshaw, D.J., Buneman, O.P.: Theories of associative recall. Quart. Rev. Biophys. **3**, 223—244 (1970)

Mayer, J.E., Goeppert-Mayer, M.: Statistical mechanics. New York: Wiley 1940

Oja, E.: Lic. Techn. Thesis, Helsinki University of Technology, 1975

Parhami, B.: Associative memories and processors: An overview and selected bibliography. Proc. IEEE **61**, 722—730 (1973)

Poggio, T.: On optimal nonlinear associative recall. Biol. Cybernetics **19**, 201—209 (1975)

Pyle, L.: Generalized inverse computations using the gradient projection method. J. Ass. Comp. Mach. **11**, 422—428 (1964)

Tuominen, J.: M.Sc. Thesis, Helsinki University of Technology, 1973

Willshaw, D.: Ph.D. Thesis, University of Edinburgh, 1971

Prof. Dr. Teuvo Kohonen
Department of Technical Physics
Helsinki University of Technology
SF-02150 Espoo 15, Finland

Biol. Cybernetics 22, 169—180 (1976)
© by Springer-Verlag 1976

Visual Perception: A Dynamic Theory

Erich Harth
Physics Department, Syracuse University
Syracuse, New York, USA

Received: November 21, 1975

Abstract

Perception is generally thought to occur centrally in the nervous system as a result of information which flows unidirectionally through a hierarchy of sensory processors. Such a view is in conflict with recent experimental evidence for a centrifugal control capable of enhancing particular features of the sensory input. Certain phenomena in human perception, resembling order-disorder transitions in physics, also suggest the existence of a positive feedback mechanism in the sensory pathway. A mechanism of perception is proposed in which unstructured feedback can accomplish the desired feature-specific enhancement of the input. The principle used here – the *Alopex principle* – is one that was devised in this laboratory for the experimental determination of visual receptive fields. The biological requirements for the operation of the principle are discussed, and a possible site in the thalamic relay nuclei is suggested.

1. Introduction

One of the functions brains perform with singular ease is the recognition of patterns of sensory input. The neuronal circuits which accomplish this task are often referred to as *feature extractors*. I shall use this term without implying a particular mechanism, requiring only that the system is able to signal the appearance of a member of a given class of events within its sensory space.

In all brains we can distinguish between *afferent* and *efferent* neural pathways. On the afferent side relay chains lead from the various sensory systems, where contact is made with the physical world, toward higher and higher cognitive centers of the brain. The efferent paths *descend* and converge on the body's muscles and glands which they control. It is interesting to note that on the efferent side we find many examples of *feature generators* which can be viewed as mirror images of the feature extractors mentioned above. Here specific, often unstructured activity can trigger stored repertories involving coordinated activity of widely separated muscle groups. In extreme examples a single so-called *command neuron* can cause the release of a stored action program such as the defense reaction in crayfish (Wiersma, 1947). In another example a short burst of activity in a group of *trigger neurons* will elicit the swimming escape motion of the mollusc *Tritonia*, lasting for about a minute or more (Willows *et al.* 1973, a, b; Hoyle and Willows, 1973).

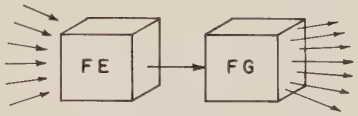

(corrected figure attached)

Fig. 1. Schematic showing a feature extractor (FE) coupled to a feature generator (FG)

The existence of feature detectors on the afferent side and feature generators on the efferent side suggests a simple schema by which an animal may select an appropriate response to a situation reported by the senses. A feature extractor (FE in Fig. 1) converts a globally[1] detected event into activity on a line (L). This line is coupled to a *feature generator* (FG) which in turn produces a *global* motor output. In the mammalian brain this is sometimes called a *transcortical reflex arc*, although some investigators like to reserve the term *reflex* for simpler, unpatterned input-response pairs. Similar principles have been demonstrated in lower vertebrates and in invertebrates.

In the frog special "bug" detectors respond to the presence of small moving objects, while other fibers report large moving shapes. The first elicit prey catching behavior, the second cause flight (Lettvin *et al.*, 1959). The swimming escape of *Tritonia* mentioned before is triggered by skin contact with starfish, believed to be *Tritonia's* chief predator.

Feature detecting as well as feature generating systems may be either native or the result of learning. The mechanisms underlying their function are largely

[1] The word *global* here is to express the fact that the simultaneous response of many receptors, possibly extending over several modalities, is required for the recognition of the event, or that motor action is patterned, involving more than the momentary stimulation of a local muscle group.

obscure. A number of schemes have been proposed whereby networks of neuron-like systems can be trained to recognize certain classes of patterns. The best known of these is the *perceptron* described by Rosenblatt (1962). The potentialities and limitations of these relatively primitive devices are discussed by Minsky and Papert (1972). Although we do not yet know how nervous systems carry out these tasks, especially the recognition of *learned* patterns, there is no real mystery involved. The feeling is that, when we get to know more about the connectivities in the neural net and the nature of the plasticity, i.e. the physical or chemical changes that constitute learning, then the correct mechanisms will surely emerge. The same may be said of the mechanisms for pattern generation.

It would be tempting to view the entire nervous system as an intricate and adaptable servo network whose sole purpose it is to trigger a set of motor and endocrine responses appropriate to any set of circumstances perceived by the sensory system. This picture may be correct for invertebrate or lower vertebrate brains, but is probably a very inadequate description of the brains of most mammals. When applied to humans it leaves unaccounted for a large class of phenomena. Leaving aside the obvious and tantalizing question of what constitutes consciousness, we find that many processes in the human brain are not directly concerned with motor or glandular control, and may at times have relatively little to do with sensory input. We *think*. "Thought is an attribute that belongs to me; it alone is inseparable from my nature", said Descartes (1641). But even if we don't subscribe to his dualism, many of us have an uncomfortable feeling that we are much farther from understanding the mechanisms of thought than those of, say, feature extraction. Ryle (1971) has suggested that the mystery is in part due to the "polymorphous" quality, the many different activities that come under the heading of *thought*. He likens the question "What does thinking consist of?" with "What does working consistof?", without explaining, however, why the first question mystifies us while the second does not.

An important group of activities classified as *thought* certainly involve our ability and predilection to *simulate* sensory inputs and to sample the putative outcome of various action programs without carrying out any of them. The interplay of actions, and sensations resulting from actions, can be synthesized in our brain spontaneously or at will. "My mind is a vagabond" said Descartes, and in Monod's view it is this simulative function which "characterizes the unique properties of man's brain." (Monod, 1971).

Opinions differ regarding the nature of the response of the feature extractors. According to one view prevalent among neurophysiologists the message consists of localized activity along specific fibers, sometimes referred to as *labeled* lines. This view is supported by a growing body of experiments in which it has been demonstrated that single neurons in the visual cortex of mammals respond selectively to classes of visual input (for example, Hubel and Wiesel, 1962; 1968). Even more startling are the reports of single units in the inferotemporal cortex of monkeys showing highly specific receptive fields (Gross *et al.*, 1969). Extrapolating mainly from the data of Hubel and Wiesel, Konorski (1967) postulated the existence of single *gnostic units* "at the highest levels of afferent systems". Others believe that the *localizers* have been misled by their own tools. The technique of intracellular recording cannot easily be applied to more than one neuron at a time, hence, the *globalizers* or *holists* argue, undue significance has been attached to *unit activity* (Freeman, 1972). Instead, they believe, information is contained in a *global response*. The *labels*, if we wish to continue this metaphor, are attached to the spatial or temporal characteristics of neural activity of many, perhaps widely scattered neurons in the brain. This would account for experiments in which slow potential waveforms were shown to be different for different sensory stimuli, but relatively insensitive to location in the brain. (John, 1972; Spinelli and Pribram, 1974.)

It is likely that both points of view contain elements of truth. But, whether *local* or *global*, in both, the processes of feature extraction and sensory information processing in general, are thought to proceed *centripetally*, i.e. starting at the sensory interfaces and continuing through a hierarchy of cognitive centers. It is a further tacit assumption that the *higher* centers are associated with higher cognitive functions. The neural activities in these structures carry labels of greater complexity or abstraction.

If the nature of the central coding of real sensory events is obscure, we know even less about the mechanisms responsible for simulative functions. An economy of assumptions would suggest that the simulation of a sensory experience should be accomplished by producing central activity *resembling* that caused by the real event, the degree of resemblance determining the degree of realism of the simulation.

In this picture, then, what determines our sensations is the activity at the highest centers, while the more peripheral systems serve mostly to convey information up, and commands down the pipelines of afferent and efferent structures respectively. Along

the way there is of course filtering, cataloguing, indexing, and referencing to stored information. The resulting central activity takes the form of spatially or temporally *labeled* events involving single neurons or populations of scattered cells.

Several questions of principle may be raised against this view. The concept of a *label* suggests that the message appearing at this location is not an end in itself, but is *to be read* by someone, or something. A *homunculus* who scans the labels in the way a telephone operator scans a switchboard is surely a very unpalatable solution. But without him we face a most disconcerting openendedness in our relay chain, raising the question why all this information processing was undertaken in the first place.

A way out that has been suggested in the past, is to say, simply, that the distilled information that arrives, and is expressed as neural activity at the highest brain centers *is* our conscious sensation of the preceived (or simulated) event. Here the individual cell would function not as an indicator light but as a *sentient atom.*

A close look at a neuron shows how difficult it is to accept this alternative. Each neuron is a living cell with a well-defined boundary, its membrane, that is continuous over the cell body and over the most intricate arborizations of its dendrites and axon. This wall separates the cell from the *outside*, the interstitial fluid that fills the space between it and neighboring cells. With the exception of occasional tight junctions linking cell membrane to cell membrane, all external influences on a neuron, its nutrients as well as a host of chemical messengers, reach it by way of this bathing fluid. This is true also for the transmitter substances that cause the drastic electrical changes in membrane characteristics that are the coin of exchange in all informational transactions in the brain. Conversely, a neuron can affect the world outside its membrane wall only by secreting its chemical messages into the same interstitial fluid. No action *wholly* within the cell can have significance to the rest of the organism. Thus, the firing of a neuron is only significant because of the transmitter substance released at its terminals.

We started by following the flow of information up sensory pathways, assuming an ultimate destination where the filtered, fully interpreted and distilled information reaches its final expression in the meaningful blips of feature detecting neurons. The task of information processing is presumed to have been accomplished when, for example, the complex, shifting retinal patterns caused by a scene containing a half-hidden zebra, have produced activity in the cortical zebra detector.

But what we find at the end of this chain of processing, the *sentient atom* is merely another cell that knows nothing of zebras or grandmothers, having in its lifetime experienced nothing other than the cresting and waning of transmitter molecules streaming in across hundreds or thousands of synaptic gaps. To conceive of a neuron as being *conscious* of whatever physical event lies at the beginning of the long sensory relay chain responsible for its firing is like asserting it is the back of a turtle that holds up Atlas who holds up the world.

It would be even more difficult to conceive of a consciousness arrived at *by committee*, as suggested in the globalist's view. Our picture of the insular existence of the individual neuron suggests that, were the information distributed over many neurons, some other agency would have to put together all the scattered bits of information. We are back to what Ryle (1949) derisively called "the ghost in the machine".

The impasse of hierarchical and unidirectional processing of sensory information may now be summarized: The central message resulting from a perceived (or simulated) sensory event either leads to efferent messages, i.e. real or simulated motor responses, or it exits *unheard* through an open line, unless we accept the alternatives of sentient atoms or disembodied spectators.

The dilemma I have described here has, of course, been recognized before, and been expressed in many ways. It has led to the concept of *projection* described by Ruch (1965):

"The ultimate event in the sensory process occurs in the brain, but in no case are we aware of this. On the contrary, our sensations are projected either to the external world or to some peripheral organ in the body, i.e. the place where experience has taught us that the acting stimulus arises. Sound seems to come from the bell, light from the lamp, etc ... the *law of projection* is that stimulation of sensory pathways at any point central to the sense organ gives rise to a sensation which is projected to the periphery and not to the point of stimulation."

Ruch's *projection* has no physical basis. It is, according to him, a "psychchologic process which makes sensation seem to come from some layer of the body or from the external world." It is a way of taking the *central representations* back into the world of *sensata* from which they came. But it is not clear why this is done, nor what is accomplished by it. It is questionable whether the *sensation* of externality, the *sound coming from the bell*, really forces on us anything like the concept of projection. Does the person who wears spectacles have to project farther

because an additional link has been interposed between the object perceived and his central nervous system? And what about the captain of a submarine who observes an enemy ship through the periscope, or a sports fan watching his favorite team on television? Do they project to the ultimate objects of their interest, or just to their respective links with the external world, the ocular of the periscope and the phosphorescent screen of the picture tube?

Smythies (1956) maintains that this reaching back to the causes of perception cannot be achieved. It is "logically impossible", he says, "for the first and last members of a causal chain to be identical events." He quotes Bertrand Russell (1927):

"Whoever accepts the causal theory of perception is compelled to conclude that percepts are in our heads, for they come at the end of a causal chain of physical events leading, spatially, from the object to the brain of the percipient. We cannot suppose that, at the end of this process, the last effect suddenly jumps back to the starting point like a stretched rope when it snaps."

Apparently both Smythies and Russell failed to be aware of a simple engineering principle, the positive feedback loop. But more on that later.

Up to now we have intentionally presented an impoverished picture of the afferent side of the brain. True, the ascending pathways can be followed along series of hierarchical structures and a little way into the most central part of the mammalian brain, the cerebral neocortex. But the hierarchies are not always unequivocal. There are side branches and shortcuts and loops in the pathways that complicate the picture. Prominent among the major sensory feedback loops is the system involving the thalamic relay nuclei of the visual pathway, – the so-called lateral geniculate bodies (LBG), – and the visual cortex. Each LGB receives its inputs directly from the retinae via the optic nerves. From there the so-called *optic radiations* fan out to the primary visual cortex. At the same time return paths exist leading from the cortex back to the LGB (Guillery, 1967; Shkol'nik-Yarros, 1971). These connections appear to be precisely reciprocal and retinotopically organized.

Physiological effects of this organization have been observed in different experiments. Cortical stimulation was shown to produce both inhibitory and excitatory effects on LGB neurons (Iwama *et al.*, 1965; Suzuki and Kato, 1965; Angel *et al.*, 1967). Cooling of the cortex in monkeys (Hull, 1968) has produced a decrease in the LGB response to stimulation, and, applying similar techniques in cats, Kalil and Chase (1970) have shown that single LGB units show marked changes in background activity and response to photic stimulation when the visual cortex is reversibly *turned off* by cooling. These authors propose a simple model involving depolarizing corticofugal connections, both to the geniculate relay cells and the Golgi type II interneurons found in the LGB, in order to explain their data.

2. Corticofugal Control and Perceptual Hysteresis

More sweeping objections to the unidirectionality of sensory processing were voiced by Pribram (1974). As an alternative to the simple transcortical reflex arc he proposes that "a corticofugal efferent control system emanates from the temporal cortex downward to subcortical structures, there to influence by a parallel processing mechanism the visual input." He cites as evidence the fact that stimulation of the *suprasylvan gyrus* in cats has produced changes in visual receptive fields "as peripheral as the optic nerve, but the most clean-cut and systematic effects were shown at the lateral geniculate level."

These findings were followed up in awake monkeys. Here Pribram found that a "redundancy control mechanism" would shorten or lengthen the response in the striate cortex to brief flashes of light, depending on stimulation in the inferior temporal lobe or frontal cortex. However, the effects were present "only when monkeys were not attending to some other aspect of their environment." This points to an exclusivity in sensory processing that we shall stress further in connection with observations in human perception, notably the examples of the Necker cube and figure-ground reversal. The phenomenon also has its counterpart on the efferent side of the brain, the "singleness of action" referred to by Sherrington.

Finally, in a series of experiments Rothblat and Pribram (1972) have shown that transitions occur in the evoked potentials recorded in temporal lobe and striate cortex of monkeys as the criteria in a discrimination task are changed from *color* to *form*. The authors record activity immediately following the stimulus, and just preceeding and following the response. It is the "response locked" recording that shows the changes. Pribram concludes that a particular temporal lobe activity "throws a programmed filter or program tape into the visual system" (Pribram, 1974), and that this filter determines the input feature to which attention is drawn. While Deutsch and Deutsch (1963) postulated that attention is guided by a level of arousal which selects events above a certain level of significance, the filter theory suggests that "attention is truly selective of stimulus dimensions not just levels of significance." (Rothblat and Pribram, 1972).

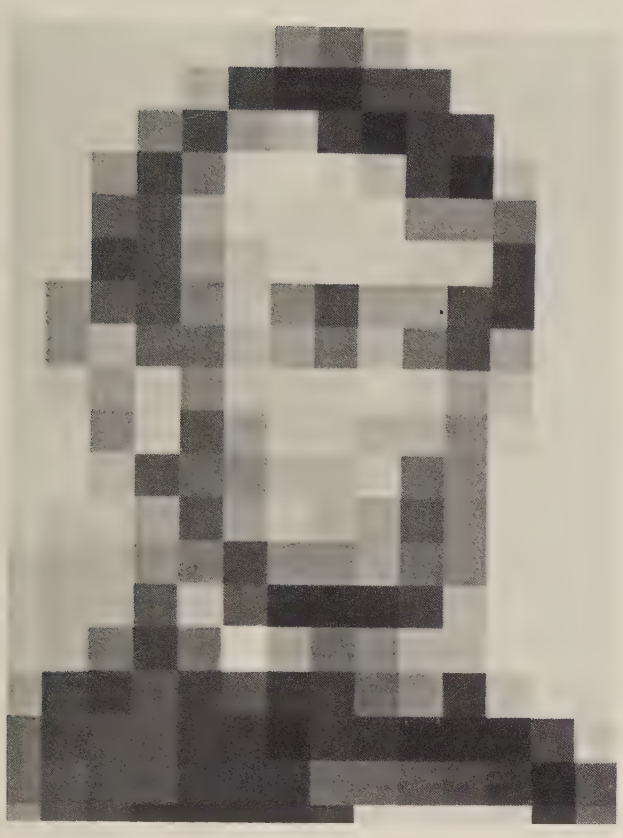

Fig. 2. Coarse-grained picture processed by a computer and displayed on a TV screen. This process was originated by L. D. Harmon while at Bell Laboratories. Each square in a 20×20 raster is assigned one of 16 gray intensity levels. Perception of the face ordinarily occurs when the picture is viewed from a distance of about 30 to 40 picture diameters. (Reproduced, with kind permission of the author and the publishers, from L. D. Harmon, Some aspects of recognition of human faces. In: Pattern Recognition in Biological and Technical Systems, Grüsser, O. J., Klinke, R. (Eds.) Berlin-Heidelberg-New York: Springer 1971)

The above example has demonstrated that the attention dependent activity is "response locked" rather than "stimulus locked". It thus takes time to develop. Szentágothai and Arbib (1974) have pointed to similar delays in human visual perception, which they describe as analogous to order-disorder transitions in physics. The random dot stereograms of Julesz (1971) provide striking examples of the sudden perceptual change upon recognition of form, and the locking-in on the perceived pattern. The resulting *hysteresis* effect was most clearly demonstrated by Fender and Julesz (1967) by projecting a single dot disparately into each eye. Binocular fusion is obtained initially when the disparity is below six minutes of arc, but, once fused, *breakaway* will occur only at much larger angles. When the disparity was changed cyclically a typical hysteresis curve was traced out.

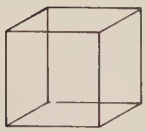

Fig. 3. Necker Cube. The orientation of the cube relative to the observer will spontaneously alternate between two possible states

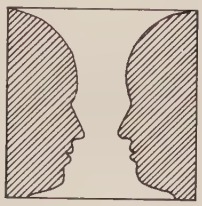

Fig. 4. Figure-ground reversal. As in Fig. 3. two interpretations are possible

Another example of perceptual hysteresis is seen when we vary the viewing distance for Fig. 2 (taken from Harmon, 1971). Recognition will occur at a certain minimum distance, and transition to *disorder* at a shorter distance, upon approaching.

An interesting special case of perception occurs when a stimulus pattern allows more than one interpretation. In the case of the Necker cube (Fig. 3) or the figure-ground reversal pattern shown in Fig. 4, perception switches spontaneously and abruptly back and forth between two *stationary* states. The perceptual states, moreover, are mutually exclusive. Thus, in Fig. 4, the vase and the pair of faces are never perceived simultaneously. This and the preceeding examples of visual perception are discussed by Szentágothai and Arbib (1974).

If we take seriously the metaphor of order-disorder transitions and hysteresis phenomena in perception, we are led to look for cooperative phenomena or positive feedback along the sensory pathways. Such effects were postulated by Cragg and Temperley (1954) for populations of central neurons. Hysteresis effects arising from cooperative phenomena were described by Harth *et al.* (1970), Anninos *et al.* (1970), Wilson and Cowan (1972), and Wong and Harth (1973) in populations of randomly connected model neurons. Also, Harth *et al.* (1975) have used these cooperative properties to explain the dynamics of a simple stereotyped neuromuscular control mechanism in the mollusc *Tritonia*. However, it is not easy to see how these principles by themselves could account for the phenomena described, particularly the high degree of specificity to stimulus types and the mutual exclusivity of alternative perceptions. If, instead, we invoke a

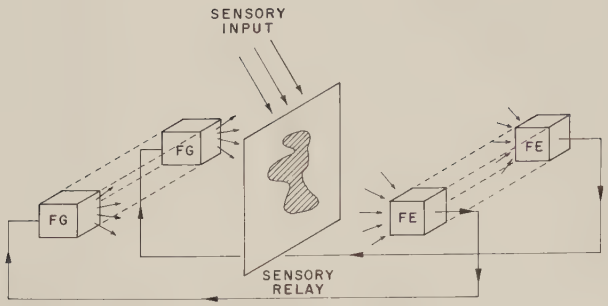

Fig. 5. Schematic showing a sensory relay nucleus receiving sensory afferents. The global pattern appearing at the relay nucleus is scanned by a set of feature extractors (FE) whose outputs trigger a set of matched feature generators (FG). These, in turn, act *globally* on the pattern appearing at the relay nucleus

positive feedback, then we are led again to something like Ruch's *projection*, but for quite different reasons. Also, we require a physical link with the input, not just a "psychologic process".

On the other hand, if positive feedback from the inferotemporal cortex to lower visual centers is to generate the pattern-specific *filters* postulated by Pribram, or account for the hysteresis effects in perception, then we must look for a mechanism which has the following properties: if a feature extractor at a given level of sensory processing shows some response, then, by centrifugal control, we wish to modify the neuronal firing pattern at a lower level in such a way as to produce a stronger response in the same feature detector. This positive feedback would then account for the phase transition and the *locking-in* of perception.

The structural requirements of such a device appear at first sight to be formidable. Referring back to the schematic of a feature extractor in Fig. 1, we could accomplish the task by coupling the output of a feature extractor to a feature generator whose global output, instead of acting on the motor system, is designed to modify the input to the feature extractor (Fig. 5). The two devices would have to be matched, that is to say, the feature generator must produce the kind of input pattern which the feature extractor is designed to detect. It would contain the *program tape* that Pribram wants to be switched back into the visual system. Thus, for an organism familiar with a large vocabulary of features, many such matched pairs would be required to achieve the ideal of an invertible transform in sensory processing (Fig. 5).

But such a scheme, apart from the heavy burden it would put on design, has no factual basis. There just does not exist the high degree of symmetry in neuronal pathways it would require.

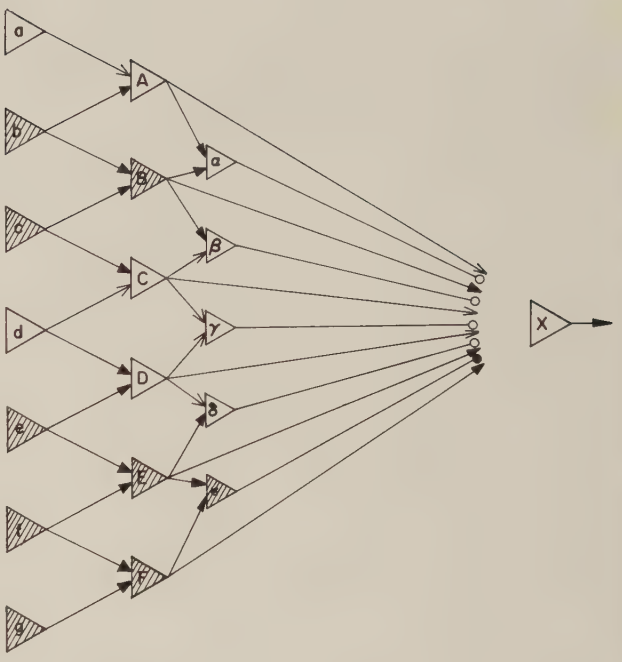

Fig. 6. Schematic of a feature extracting network. (a)–(g) are receptor cells forming a one dimensional "retina". *A–F* are excitatory, α–ε inhibitory interneurons. *X* is the output cell of the feature extractor. The firing thresholds are +1 for *X* and +2 for all interneurons. The PSPs are +1 at excitatory (arrows), and −2 at inhibitory synapses (circles). The device will detect objects of size two, but not in the presence of quadruples. A possible firing pattern is indicated by cross-hatching active neurons and showing active synapses as solid arrows and circles. *X* is seen to *detect* the presence of the pair (bc)

An even more serious objection has to do with the fact that the mapping caused by feature extractors is many-to-one, hence the inverse is undetermined. The classic example of this is Hubel and Wiesel's complex cell in the visual cortex which responds to a bar of light of specific spatial orientation, but whose location may vary within certain limits. Somewhat more abstractly, Fig. 6 shows the schematic of a simple network which is designed to detect "objects of size two" in the one-dimensional "retina" of receptors (a-g). Clearly many stimulus patterns can trigger the output cell *X* of the feature extractor, but the output of *X* would furnish no clue regarding the identity of the stimulus. Thus, a matching feature generator triggered by *X* could do no better than selecting randomly one of the stimuli capable of triggering *X*. This feedback, or *filter* may or may not match the current input.

We now wish to show that the requirements of a feature specific positive feedback in the sensory system can be met without the cumbersome and rather unlikely neuronal machinery depicted above.

The principle we shall invoke, moreover, will also be able to overcome the difficulty posed by the many-one mapping of feature extracting devices. In the remainder of this paper I shall define and demonstrate the existence of a general class of mechanisms which can achieve this goal. The prototype is a particular device designed and constructed in this laboratory for the purpose of obtaining receptive fields of single cells in the visual system (Harth and Tzanakou, 1974). The operating principles of this device will now be described briefly as an illustration and an existence proof of what I shall call the *Alopex principle*. It is not suggested that brain mechanisms resemble the algorithms used here, except perhaps in a very formal way. The principle may, however, play a significant role in perception. Some of the general requirements for a neuronal implementation of this principle, and some experiments that may provide evidence for or against such a supposition, are given at the end of this paper.

3. The Alopex Principle: A Generalized Feature Generator

When a single neuron anywhere in the visual pathway is monitored, its response is found generally to depend on the stimulus presented to one or both eyes. There is some dispute over what should properly be taken as a measure of the response. It is immaterial for the sake of this discussion whether an average firing frequency over a suitably chosen time interval is an adequate measure, or whether the temporal fine structure of the pulse train must be taken into account, as suggested, for example, by Chung *et al.* (1970). It suffices that responses can be numerically expressed or, at least, that for any two responses one can unequivocally be defined as the larger. For this discussion assume the response R to be a real positive number. In general R will depend on the distribution of light (both spatial and temporal) within a well circumscribed region of the visual field and be relatively independent of anything that happens outside that region. We call the region that effects R, the *receptive field* of that cell. The same term is also used to refer to the particular pattern of light (within that sensitive region) that produces maximal response. This last definition has come to dominate thinking, since it was discovered that cells in the visual cortex, in general, respond maximally to patterns more complex than the circular patches making up the receptive fields at the level of the mammalian retina and LGB.

The experimental determination of single cell receptive fields is fraught with difficulties. Apart from a somewhat fuzzy meaning of the term, it is in practice impossible to test systematically all possible patterns, including such parameters as color, motion, overall intensity, etc. Experimenters have to be satisfied with comparing responses to a few preselected simple patterns, varying one or two parameters at a time. Occasionally some very complex receptive fields are discovered, such as the *hand units* reported by Gross *et al.* (1969) in monkey inferotemporal cortex. But these are chance events, and nobody would suggest undertaking a systematic search for other similarly complex trigger features, if indeed they exist.

A method called Alopex[2] was proposed by Harth and Tzanakou (1974) which should be able to overcome some of the difficulties. It makes use of the weak cross correlations that must exist between local light intensity and the response to the global pattern. The idea rests on the assumption that the response to a stimulus pattern resembling an optimal stimulus will elicit responses which approach the corresponding maximum as this resemblance increases. The response thus forms a hypersurface in a multidimensional space that spans all the variables making up the pattern, and Alopex is a hill climbing algorithm.

The original algorithm proposed by Harth and Tzanakou was the following: Consider the visual field divided into small squares forming a square array of $N \times N$ such space elements. Let the n-th stimulus pattern be given by the vector $\boldsymbol{I}(n)$:

$$\boldsymbol{I}(n) = [I_1(n), \ldots I_{N^2}(n)] . \tag{1}$$

Here $I_j(n)$ is the light intensity at the j-th square element during the n-th stimulus pattern. These patterns are displayed consecutively on a TV or oscilloscope screen, and presented to the animal. The single cell response to the n-th stimulus, as recorded by a microelectrode, is called $R(n)$. The intensities $I_j(n)$ are made up of a *random* contribution $r_j(n)$ and a cumulative bias $b_j(n)$. The value of each $b_j(n)$ is increased or decreased at each iteration, depending on whether, in the preceding two iterations, a change in I_j was accompanied by a change in R in the same or opposite direction. This is expressed by

$$\boldsymbol{I}(n) = v(n)\,[\boldsymbol{b}(n) + \boldsymbol{r}(n)] \tag{2}$$

where

$$\boldsymbol{b}(n) = [b_1(n), \ldots, b_{N^2}(n)]$$

and

$$\boldsymbol{r}(n) = [r_1(n), \ldots, r_{N^2}(n)] .$$

[2] Acronym for Algorithmic Logic of Pattern Extracting Crosscorrelations

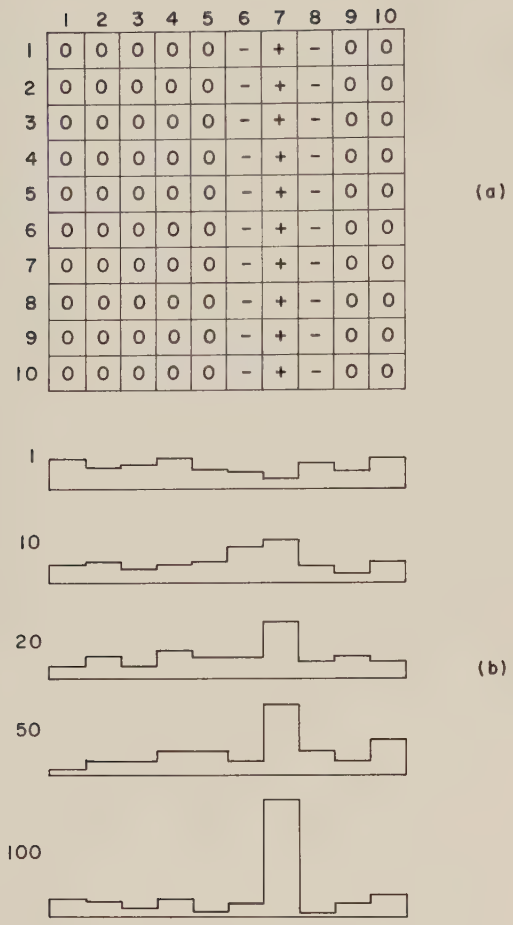

Fig. 7a and b. Performance of Alopex in computer simulation. In (a) a simple receptive field is pictured having an excitatory line (column 7) and inhibitory surround. In (b) the stimulus patterns are shown for various iterations (numbers on left). For ease of presentation the ordinates of the histograms show the column sums of stimulus intensities. The first pattern is random. Subsequent iterations show the progressive increase of stimulus intensities along column 7. (After Harth and Tzanakou, 1974)

For the first two iterations all bias values are identical, thus

$$b_j(0)=b_j(1)=b_0$$

for all j. The first two stimulus patterns are thus a mosaic of random light intensities. The factor $v(n)$ in Eq. (2) is a normalization which satisfies the condition

$$\sum_{j=1}^{N^2} I_j(n)=\text{const.}$$

The vector $\boldsymbol{I}(n)$ thus represents a constant amount of light flux. The components of $\boldsymbol{r}(n)$ in Eq. (2) are random numbers whose distribution may be chosen in many ways. The cumulative biases $\boldsymbol{b}(n)$ are given by

$$\boldsymbol{b}(n)=\boldsymbol{b}(n-1)+c[R(n-1) - R(n-2)]\cdot[\boldsymbol{I}(n-1)-\boldsymbol{I}(n-2)]\,. \tag{3}$$

The constant c in Eq. (3) determines the amplitudes of the bias corrections. Together with the range of random numbers $r_j(n)$ it is one of the critical parameters. Of course, many variants of these basic rules can be constructed.

Figure 7 shows the results of a computer simulation testing this algorithm. A simple linear receptive field is assumed in a 10×10 array in which the 7-th column is excitatory and columns 6 and 8 are inhibitory (Fig. 7a). The histograms in Fig. 7b show the light intensities (summed over vertical columns) for iterations 1, 10, 20, 50, and 100. The pattern, which is random in iteration 1, clearly converges to the assumed receptive field.

Complex receptive fields can be simulated by non-linear superposition of simple fields. In one series of simulation experiments a number of identically oriented *line detectors* were coupled to produce a complex field of the type described by Hubel and Wiesel (1962), in which a line of specified orientation but unspecified location is the trigger feature. Applying again the algorithms of Eq. (2) and (3) caused the illumination to converge on a single line in about the same number of iterations as for simple fields. But this time the location of the line depended on the starting values of the pseudorandom number sequences $\boldsymbol{r}(n)$. If these numbers were truly random the location of the pattern would be unpredictable from run to run. However, it was found that, by superimposing some additional bias in one column for a few iterations, the final pattern was shifted to that location, irrespective of the particular sequence $\boldsymbol{r}(n)$.

Following series of such computer simulations, the necessary electronic hardware was constructed and is now used for receptive field studies in this laboratory. Patterns are generated by a CRT display using 1024 field elements. The method may be extended also to include moving stimulus patterns.

4. Alopex: The Thinking Man's Filter?

The device described above has properties beyond those useful for determining visual receptive fields. Its most general aspect is the fact that, when coupled to a feature extractor, it can generate a pattern which approximates the optimal stimulus for that feature extractor. It is thus a generalized feature generator, matching its output automatically to the trigger features of its master. In the case of a complex feature

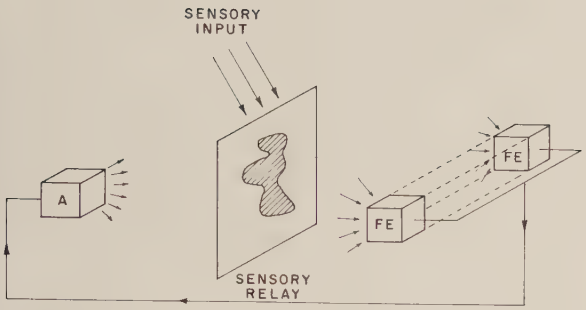

Fig. 8. Schematic of a sensory relay nucleus receiving sensory afferents and being scanned by feature extractors as in Fig. 5. The outputs of the feature extractors affect a single Alopex unit (A) which provides the global positive feedback to the relay nucleus

extractor having a many-one input-output relation, it has the remarkable property that, if a weak or partial stimulus is applied, it will reinforce that particular stimulus rather than others of the same class. We have seen for example that a *hint* of a line in a simulated *complex* line detector will cause Alopex to complete and reinforce that particular line. A similar property has recently been reported for human vision. Tynan and Sekuler (1975) have found that simple moving patterns such as sinusoidal gratings will produce the sensation of extensions of these patterns (phantoms) into regions where no such inputs exist.

It is evidently very tempting to invoke the Alopex principle to account for the sensory feedback that we were led to postulate. A block diagram of a sensory system having the desired dynamic properties and incorporating this principle is pictured in Fig. 8. This represents an enormous simplification over the diagram in Fig. 5. Here any number of feature extractors feed back to a single Alopex unit at a lower sensory level, perhaps on a single line.

The following would then be a model of perception: Sensory input causes some response in one of the feature extractors. By the Alopex principle this produces changes at the lower level which further enhance the response. This positive feedback gives the process the character of a phase transition and is responsible for the hysteresis. The mutual exclusivity in perception (as in the Necker cube and the example of figure-ground reversal) could be achieved for example by nonlinear addition of the outputs of the feature extractors. The problem is similar to that of building complex fields from simple fields, and was discussed by Harth and Tzanakou (1974).

The above model also offers an explanation for the lack of perception of one of Harmon's block pictures (Fig. 2) when viewed at close range. If we accept the premise of a positive feedback from a recognition device to an imperfect incident pattern, then the feedback which performs correcting or completing operations on the peripheral sensory space is able to accomplish this task only in the absence of strong direct sensory input contradicting such modifications. Thus, details cannot be filled in and smoothing operations cannot be carried out in the face of overwhelming sensory evidence that we are confronted with a collection of large, uniformly illuminated and sharply delineated squares. Only when the resolution is reduced (by viewing the picture from a greater distance) is a sufficient degree of local uncertainty reached that allows the kind of retouching by feedback that gives the picture a natural and recognizable appearance.

We may speculate on the possible role of the system pictured in Fig. 8 under conditions of no sensory input. If our theory is correct, then such processes as the sensory simulations we mentioned at the outset, or the more spectacular phenomena of dreaming and hallucinating, are not confined to the highest cortical levels, but must have strong representations at the level of lower order sensory neurons. The increased activity of LGB neurons during REM sleep reported by Sakakura (1968) is a bit of circumstantial evidence pointing in that direction. Sensory patterns could thus be created out of noise in the way receptive fields have emerged in our computer simulations. The dynamics of image successions would presumably be controlled at higher levels by such processes as accommodation and association.

5. Biological Prerequisites

We have, up to this point, attempted to show that the operation of what we called the *Alopex* principle on the afferent side of the nervous system would fulfill a number of requirements which emerge in studies of sensory physiology and perception. Unfortunately, in the past, desirability from the designer's point of view has not been a good guide in elucidating biological mechanisms. Biological and engineering solutions to a given problem are often discouragingly dissimilar, as expressed by the remark "airplanes don't flap their wings". Before investigating seriously whether Alopex – an engineering principle – may, in fact, be operating in some fashion in the brain, we should raise the question of plausibility and possible location of the mechanism.

One of the limitations of the process in experiments to determine visual receptive fields, is the time required for convergence. The response R in Eq. (3) is obtained by counting action potentials over preselected time

intervals following stimulus presentation. With firing frequencies of perhaps tens per second, a minimum of several seconds is required to obtain a statistically meaningful reading of R. In practice, because of adaptation, it may be necessary to use repeated presentation of the same stimulus, and integrate responses over a number of short counting gates. Habituation effects may further require the interpolation of waiting intervals or neutral patterns. Thus, the time for a single iteration in the process defined by Eq. (2) may become a minute or more. The number of iterations required for convergence is a quantity that is difficult to predict since no good stochastic theory of the process exists. With our algorithms, and using parameters which are certainly far from optimal, we generally observe that convergence occurred in fewer than 100 iterations (Harth and Tzanakou, 1974). Thus, the time for convergence on a single receptive field pattern could be of the order of an hour. Several methods to shorten this period are now being studied in this laboratory. In order to make plausible the operation of the same principle in the brain we must show that this period could be shortened to a matter of seconds.

Let us examine now whether some of the necessary ingredients for the process are available in the brain, and then come back to the question of timing. Assume that in some sensory relay we have a sheet of neurons that are a retinotopic representation of the visual field (Fig. 8). The activities of neurons on that sheet will be determined in part by the sensory afferents, in part by the feedback from the cortex. In addition, these neurons exhibit spontaneous activity which has all the aspects of a random contribution to their firing rate. The algorithm given by Eqs. (2) and (3) requires such a random component, as well as information on the rates of change of activity in the sensory relay. Such rates are available in the so-called *Y*-subsystem of neurons found in the visual system of cats (Enroth-Cugell and Robson, 1966; Stone and Hoffman, 1971). These cells give transient responses from *on-center* and *off-center* neurons (Brooks and Jung, 1973). They have large diameter axons and correspondingly high conduction velocities. Information concerning the rates of change of cortical responses, which are also needed, could be generated in a similar fashion. Thus, the measurements and computations which, in the electronic device, consume many seconds, could, in principle, be accomplished in the brain in a matter of tens of milliseconds, and the equivalent of 100 iterations, in seconds.

Finally, we may speculate on a likely location to which future search for empirical evidence of the mechanism may be directed. Pribram (1974) has singled out the LGB as that part of the visual system of cats showing most strikingly the effects of corticofugal control. It was pointed out by Szentágothai and Arbib (1974) that the thalamic relays of the auditory, the visual, and the somatosensory pathways, the *medial geniculate*, the *lateral geniculate*, and the *ventroposterolateral bodies*, posses a remarkable degree of structural similarity. All three consist of two cell types: 1) a thalamocortical *relay cell* which receives inputs from the specific sensory afferents and transmits its output to the appropriate sensory cortex; 2) a Golgi type II interneuron. The synaptic arrangement between these cells is also unique. The sensory afferents synapse with the relay cell as well as with interneuron dendrites which, in turn, form dendrodendritic synapses with the relay cell. These close *triadic* synapse structures are found in all three of the thalamic nuclei mentioned. In addition, both cell types receive inputs from cortical fibers.

Szentágothai and Arbib (1974) express puzzlement over these remarkable features in the relay nuclei. They further conjecture that

"... a large number of shaping mechanisms of the incoming sensory pattern by various types of inhibitory interactions could occur in this structural framework. Unfortunately, both neuron (relay and interneuron) types and the synaptic architecture appear to be rather stereotypic in all of the major subcortical sensory nuclei. Hence, the structure is not conducive to making deductions about specific mechanisms of more sophisticated or global feature-detection strategies."

I have shown that the Alopex principle makes possible a class of feature specific shaping mechanisms involving only stereotypic architecture. It remains to be seen whether the principle is operative in the brain, and by what mechanism. Meanwhile the thalamic sensory relay nuclei are probably the best locations where direct empirical evidence may be sought.

6. Summary and Conclusions

Sensory information processing involves the translation of sense data detected by sets of receptors into a code of neural activity, and the transmission of the resulting messages to neural structures generally located more centrally in the nervous system.

Evidence shows that, in the process of coding, particular features contained in the sense data are separated from the rest of the information, and reproducibly expressed in the activity of particular neurons or neuron groups. Such feature extractors

can act as the trigger mechanisms for eliciting motor responses appropriate to the appearance of the feature. Complex or learned features are often believed to be detected as a result of a hierarchy of structures, in which primitive features are combined to build greater and greater complexity.

I have argued that this picture leaves unaccounted for a number of problems concerned with perception and processes having to do with the simulation of sensory and motor activity in the brain. Evidence cited points to a positive feedback mechanism causing feature specific modification of neural activity at a lower level, resulting from responses of higher order feature extractors.

We have discussed briefly a class of mechanisms based on what was called the Alopex principle, which have the general property of feature enhancement when coupled to a feature extractor. It would be premature to speculate on how, in detail, the principle may be realized in the brain. But the necessary neural machinery appears to be available, and many design solutions exist.

It should not be too difficult to design experiments which could provide empirical support for the theory. Direct evidence would involve, for example, the detection at a sensory relay nucleus of neural activity characteristic of a particular sensory event, when that event is only *simulated*. Simulation could be accomplished by the occurrence of a different event – reported perhaps by a different modality – with which prior association has been made, or by direct stimulation of appropriate cortical centers.

In the traditional view the ultimate aim of sensory processing is the turning-on of certain central feature detectors. Instead, if the present theory is correct, perception (real or simulated) becomes a dynamic process, consisting of both central and peripheral neural events, with the first providing positive feedback to the second. The unidirectional flow of information toward hypothetical perception centers has thus been replaced by a process in which perception is accomplished by tuning the sensory input so as to produce a resonance with one or more feature detectors.

I will not pretend that all this has exorcized Ryle's ghost. *Sensation* is another ingredient in perception and is a more elusive process. Perhaps Morowitz (1969) has made a significant contribution by his suggestion that an observer has the ability of observing microstates of a system when he himself is the system under observation. Sensations are then hidden variables of the nervous system, accessible only to the owner of the brain.

Acknowledgements. I wish to thank the Aspen Center for Physics for its hospitality during the summers of 1974 and 1975 when part of this work was done. The research was supported by grants NS09773 and Ey01215 from the National Institutes of Health.

References

Angel, A., Magni, F., Strata, P.: The excitability of optic nerve terminals in the lateral geniculate nucleus after stimulation of visual cortex. Arch. ital. biol. **105**, 104—117 (1967)

Anninos, P. A., Beek, B., Csermely, T. J., Harth, E. M., Pertile, G.: Dynamics of neural structures. J. theor. Biol. **26**, 121—148 (1970)

Brooks, B., Jung, F.: Neuronal physiology and the visual cortex. In: Handbook of sensory physiology Vol. VII/3 Part B, pp. 325—440. Berlin-Heidelberg-New York: Springer 1973

Chung, S. H., Raymond, S. A., Lettvin, J. Y.: Multiple meaning in single visual units. Brain Behav. Evol. **3**, 72—101 (1970)

Cragg, B. G., Temperley, H. N. V.: The organization of neurones: a cooperative analogy. Clin. Neurophysiol. **6**, 85—92 (1954)

Descartes, R.: Mediationes de prima philosophia. Paris: C. Adam and P. Tannery 1641. English translation: Meditations on first philosophy. (transl. L. J. Lafleur) Indianapolis-New York: Bobbs-Merrill 1951

Deutsch, J. A., Deutsch, D.: Attention: Some theoretical considerations. Psychol. Rev. **70**, 80—90 (1963)

Enroth-Cugell, C., Robson, J. G.: The contrast sensitivity of retinal ganglion cells of the cat. J. Physiol. (Lond.) **187**, 517—552 (1966)

Fender, D., Julesz, B.: Extension of Panum's fusional area in binocularly stabilized vision. J. Opt. Soc. Amer. **57**, 819—830 (1967)

Freeman, W. J.: Waves, pulses and the theory of neural masses. In: Progress in theoretical biology, Vol 2. Rosen, R., Snell, F. M. (Eds) New York-London: Academic Press 1972

Gross, C. G., Bender, D. B., Rocha-Miranda, E. C.: Visual receptive fields in inferotemporal cortex of the monkey. Science **166**, 1303—1305 (1969)

Guillery, R. W.: Patterns of fiber degeneration in the dorsal lateral geniculate nucleus of the cat following lesions in the visual cortex. J. comp. Neurol. **130**, 197—222 (1967)

Harmon, L. D.: Some aspects of recognition of human faces. In: Pattern recognition in biological and technical systems. Grüsser, O. J., Klinke, R. (Eds.) Berlin-Heidelberg-New York: Springer 1971

Harth, E., Csermely, T. J., Beek, B., Lindsay, R. D.: Brain functions and neural dynamics. J. theor. Biol. **26**, 93—120 (1970)

Harth, E., Lewis, N. S., Csermely, T. J.: The escape of *Tritonia*: dynamics of a neuromuscular control mechanism. J. theor. Biol. **55**, (in press, 1975)

Harth, E., Tzanakou, E.: Alopex: A stochastic method for determining visual receptive fields. Vision Res. **14**, 1475—1482 (1974)

Hoyle, G., Willows, A. O. D.: The neuronal basis of behavior in *Tritonia*. II. Relationship of muscular contraction to nerve impulse pattern. J. Neurobiol. **4**, 239—254 (1973)

Hubel, D. H., Wiesel, T. N.: Receptive fields, binocular interaction and functional architecture in the cat's visual cortex. J. Physiol. (Lond.) **160**, 106—154 (1962)

Hubel, D. H., Wiesel, T. N.: Receptive fields and functional architecture of monkey striate cortex. J. Physiol. (Lond.) **195**, 215—243 (1968)

Hull, E.: Corticofugal influence in the macaque lateral geniculate nucleus. Vision Res. **8**, 1285—1298 (1968)

Iwama, K., Sakakura, H., Kasamatsu, T.: Presynaptic inhibition in the lateral geniculate body induced by stimulation of the cerebral cortex. Jap. J. Physiol. **15**, 310—322 (1965)

John, E. R.: Switchboard versus statistical theories of learning and memory. Science **177**, 850—864 (1972)

Julesz, B.: Foundations of cyclopean perception. p. 406. Chicago: University of Chicago Press 1971
Kalil, R. E., Chase, R.: Cortical influence on activity of lateral geniculate neurons in the cat. J. Neurophysiol. **33**, 459—475 (1970)
Konorski, J.: Integrative Activity of the Brain. Chicago-London: University of Chicago Press 1967
Lettvin, J. Y., Maturana, H. R., McCulloch, W. S., Pitts, W. H.: What the frog's eye tells the frog's brain. Proc. IRE **47**, 1940—1959 (1959)
Minsky, M., Papert, P.: Perceptrons. Cambridge, Mass.: MIT Press 1972
Monod, J.: Chance and necessity. p. 154. New York: A. A. Knopf 1971
Morowitz, H.: Energy flow in biology. New York: Academic Press 1968
Pribram, K. H.: How is it that sensing so much we can do so little? In: The neurosciences, third study program. pp. 249—261. Schmitt, F. O., Worden, F. G. (Eds.) Cambridge, Mass.: MIT Press 1974
Rosenblatt, F.: Principles of neurodynamics. Washington: Spartan Books 1962
Rothblatt, L., Pribram, K. H.: Selective attention: input filter or response selection: Brain Res. **39**, 427—436 (1972)
Ruch, T. C., Patton, H. D.: Physiology and biophysics. p. 1242. Philadelphia: Saunders 1965
Russell, B.: The analysis of matter. p. 408. New York: Dover 1954
Ryle, G.: The concept of mind, p. 334. London: Hutchinson 1949
Ryle, G.: Collected papers. Vol 2, p. 258. New York: Barnes and Noble 1971
Sakakura, H.: Spontaneous and evoked unitary activities of cat lateral geniculate neurons in sleep and wakefulness. Jap. J. Physiol. **18**, 23—42 (1968)
Shkol'nik-Yarros, E. G.: Neurons and interneuronal connections of the central visual system. New York-London: Plenum 1971
Smythies, J. R.: Analysis of perception. p. 21. London: Routledge and Kegan Paul 1956
Spinelli, N., Pribram, K. H.: quoted in Pribram 1974
Stone, J., Hoffmann, K. P.: Conduction velocity as a parameter in the organization of the afferent relay in the cat's lateral geniculate nucleus. Brain Res. **32**, 454—459 (1971)
Suzuki, H., Kato, E.: Cortically induced presynaptic inhibition in the cat's lateral geniculate body. Tohoku J. exp. Med. **86**, 277—289 (1965)
Szentágothai, J., Arbib, M. A.: Conceptual models of neural organization. Neurosci. Res. Bull. **12**, 307—510 (1974)
Tynan, P., Sekuler, R.: Moving visual phantoms: a new contour completion effect. Science **188**, 951 (1975)
Wiersma, C. A. G.: Giant nerve fiber system of the crayfish; a contribution to comparative physiology of synapse. J. Neurophysiol. **10**, 23—38 (1947)
Willows, A. O. D., Dorsett, D. A., Hoyle, G.: The neuronal basis of behavior in *Tritonia*. I. Functional organization of the central nervous system. J. Neurobiol. **4**, 207—237 (1973a)
Willows, A. O. D., Dorsett, D. A., Hoyle, G.: The neural basis of behavior in *Tritonia*. III. Neuronal mechanism of a fixed action pattern. J. Neurobiol. **4**, 255—285 (1973b)
Wilson, H. R., Cowan, J. D.: Excitatory and inhibitory interactions in localized populations of model neurons. Biophys. J. **12**, 1—24 (1972)
Wong, R., Harth, E.: Stationary states and transients in neural populations. J. theor. Biol. **40**, 77—106 (1973)

Prof. E. Harth
Syracuse University
Dept. of Physics
Syracuse, N.Y. 13210, USA

Verantwortlich für den Textteil: Prof. Dr. W. Reichardt, Max-Planck-Institut für biologische Kybernetik, Spemannstr. 38, D-7400 Tübingen. – Verantwortlich für den Anzeigenteil: L. Siegel, W. Pehla, Springer-Verlag, Kurfürstendamm 237, D-1000 Berlin 15, Fernsprecher: (030) 882 1031, Telex: 01-85411. – Springer-Verlag, Berlin · Heidelberg · New York. – Druck der Brühlschen Universitätsdruckerei, Gießen. – Printed in Germany
© by Springer-Verlag Berlin Heidelberg 1976

APPLIED MATHEMATICS AND OPTIMIZATION
an international journal

Managing Editors: A. V. Balakrishnan, Los Angeles · J. L. Lions, Rocquencourt
G. I. Marchuk, Novosibirsk · L. S. Pontryagin, Moscow

Subscription Information: 1976, Vol. 3 (4 issues). Sample copies upon request.

North America: 1976, $58.00, including postage
Send your order or request to: Springer-Verlag New York Inc.,
175 Fifth Avenue, New York, NY 10010

Rest of the World: 1976, DM 144,—, plus postage
Send your order or request to: Springer-Verlag 4021, Heidelberger Platz 3,
D-1000 Berlin 33

CONTENTS

Springer-Verlag
Berlin
Heidelberg
New York

The Study of Time II

Proceedings of the Second Conference of the International Society for the Study of Time, Lake Yamanaka, Japan

Edited by J. T. Fraser,
International Society for the Study of Time, Westport, Connecticut
and N. Lawrence, Williams College, Massachusetts

80 figures. 4 tables. VII, 486 pages
1975. Cloth DM 57,—; US $23.40
ISBN 3-540-07321-3

Springer-Verlag
Berlin
Heidelberg
New York

This volume contains the proceedings of the Second World Conference on the Study of Time, which took place in the summer of 1973. The range of the topics covered is very wide, extending from biological and physical questions, to philosophical topics, political philosophy and sociological questions. Contributions of a special session, Timekeepers and Time, conclude the volume; the articles in this section are devoted to historical topics, and include many attractive illustrations of old or unusual clocks.

CONTENTS

Previously published

The Study of Time

Proceedings of the First Conference of the International Society for the Study of Time, Oberwolfach (Black Forest), West Germany

Edited by J. T. Fraser, F. C. Haber, and G. H. Müller

65 figures. VIII, 550 pages. 1972
Cloth DM 77,—; US $31.60
ISBN 3-540-05824-9

Prices are subject to change without notice